ABSTRACT

MECHANICS OF BIOCELL LANDFILL SETTLEMENTS

by
Chamil Hiroshan Hettiarachchi

Prediction of landfill gas generation and settlements are of concerns in design and maintenance of biocell landfills. Accurate settlement prediction is essential for design of piping systems used for the delivery of re-circulated leachate and recovery of landfill gas. Landfill settlement is the result of change in overburden stresses and biodegradation of waste. Biodegradation-induced settlement results from the re-arrangement of waste skeleton in response to the decomposition of waste mass.

Current practice of landfill settlement modeling is predominantly empirical, thus most of the available techniques make no attempt to simulate the real mechanisms of waste settlement. Traditionally compressibility index is defined similar to that of clays, to explain the general settlement behavior of waste. Although a landfill is an interacting multiphase medium there is limited research to explain landfill gas generation and dissipation and moisture distribution as integral parts of the process of landfill settlements.

This dissertation describes a model which couples settlements of a biocell landfill with the generation and dissipation of landfill gases and distribution of moisture. The major mechanisms of waste settlement were identified as mechanical compression and biodegradation-induced strain. Mechanical compression was modeled with the help of laboratory simulations. To model the biodegradation-induced settlement, it was assumed that waste degradation obeys the first order reaction kinetics. The mass balance of the

landfill gas was used to link settlement with gas pressure. The Richards equation was used to simulate the distribution of moisture.

A computer program was written to numerically predict the settlements, gas pressure and volumetric moisture content in a biocell landfill using landfill geometry and waste properties. In the absence of a complete set of data, settlement and gas pressure components of the model were validated using data from two different landfills.

The model was then used to predict the settlement behavior of The City of Calgary Biocell Landfill. The model predicted higher strain values, when moisture as well as gas pressure were incorporated in to the simulation. Therefore, it was concluded that modeling settlement without taking gas pressure and moisture in to account, could underestimate the total settlement. The model was capable of predicting landfill density, and the density values predicted for twenty five years matched with those reported in literature.

MECHANICS OF BIOCELL LANDFILL SETTLEMENTS

by
Chamil Hiroshan Hettiarachchi

A Dissertation
Submitted to the Faculty of
New Jersey Institute of Technology
in Partial Fulfillment of the Requirements for the Degree of
Doctor of Philosophy in Civil Engineering

Department of Civil and Environmental Engineering

May 2005

APPROVAL PAGE

MECHANICS OF BIOCELL LANDFILL SETTLEMENTS

Chamil Hiroshan Hettiarachchi

Dr. Jay N. Meegoda, Dissertation Co-advisor — Date
Professor of Civil and Environmental Engineering, NJIT

Dr. J. Patrick A. Hettiaratchi, Dissertation Co-advisor — Date
Associate Professor of Civil Engineering, University of Calgary, Canada

Dr. Raj P. Khera, Committee Member — Date
Professor of Civil and Environmental Engineering, NJIT

Dr. Hsin-Neng Hsieh, Committee Member — Date
Professor of Civil and Environmental Engineering, NJIT

Dr. John Tavantzis, Committee Member — Date
Professor of Mathematics, NJIT

Dr. Issa S. Oweis, Committee Member — Date
Chief Engineer, Oweis Engineering, Morristown, NJ

APPROVAL PAGE
(Continued)

MECHANICS OF BIOCELL LANDFILL SETTLEMENTS

Chamil Hiroshan Hettiarachchi

Dr. Salah El-Hagger, Committee Member — Date
Professor of Energy and Environment, the American University in Cairo, Egypt

BIOGRAPHICAL SKETCH

Author: Chamil Hiroshan Hettiarachchi

Degree: Doctor of Philosophy

Date: May 2005

Undergraduate and Graduate Education:

- Doctor of Philosophy in Civil Engineering,
  New Jersey Institute of Technology, Newark, NJ, 2005

- Master of Engineering in Geotechnical Engineering,
  Asian Institute of Technology, Thailand, 2001

- Bachelor of Science of Engineering in Civil Engineering,
  University of Moratuwa, Sri Lanka, 1998

Major: Civil Engineering

Presentations and Publications:

Meegoda, J. N., Rowe, G. M., Jumikis, A., Bandara, N., Hettiarachchi, C. H., and Gephart, N. (in press, scheduled to be published in September 2005 issue). "Estimation of Surface Macrotexture in Hot Mix Asphalt Concrete Pavement Using Laser Texture Data," *ASTM Journal of Testing and Evaluation.*

Hettiarachchi, C. H., Tavantzis, J., Meegoda, J. N., and Hettiaratchi J. P. A. (2005). "A Numerical Model to Predict Settlements and Gas Generation in Bioreactor Landfills," *WasteEng'05: First International Conference on Engineering for Waste Treatment*, Albi, France.

Hettiarachchi, C. H., Meegoda J. N., and Hettiaratchi, J. P. A. (2005). "Towards a Fundamental Model to Predict the Settlements in Bioreactor Landfills," GeoFrontiers Conference (Geptechnical Special Publications No. 142), Austin, TX.

Hettiarachchi, C. H. (2005). "Mechanics of Biocell Landfill Settlements," *5th forum: Doctoral Student Research in Transportation Geotechnics, 84th Annual Transportation Research Board (TRB) Meeting*, Washington, DC.

Rowe, G. M., Meegoda, J. N., Jumikis, A., Sharrock, M. J., and Hettiarachchi, C. H. (2004). "NJTxtr -A Computer Program Based on LASER to Monitor Asphalt Segregation," *ASCE Journal of Construction Engineering and Management*, 130 (6), 924-934.

Hettiarachchi, C. H., Meegoda, J. N., and Hettiaratchi, J. P. A. (2004). "A Model Based on Mechanics to Predict Settlements in Bioreactor Landfills," *Proceedings of the Fifth International Conference on Case Histories in Geotechnical Engineering*, New York, NY.

Meegoda, J. N., Rowe, G. M., Jumikis, A., Bandara, N., Hettiarachchi, C. H., and Gephart, N. (2003). "Detection of Segregation Using LASER," *82nd Annual Transportation Research Board (TRB) Meeting*, Washington, DC.

Meegoda, J. N., Rowe, G. M., Hettiarachchi, C. H., Bandara, N., and Sharrock, M. J. (2002). "Correlation of Surface Texture, Segregation, and Measurement of Air Voids," *Project 2000-34, Final Report Submitted to New Jersey Department of Transportation*, New Jersey Institute of Technology, Newark, NJ.

Rowe, G. M., Meegoda, J. N., Jumikis, A., Sharrock, M. J., Bandara, N., and Hettiarachchi, C. H. (2002). "Detection of Segregation in Asphalt Pavement Materials Using the ARAN Profile System," *Pavement Evaluation 2002 Conference*, Roanoke, VA.

Hettiaratchi, J. P. A., Stein, V. B., Chandrakanthi, M., Pokhrel, D., Hettiarachchi, C. H., Perera, L. A. K., and Amatya, P. L. (2002). "Bioreactor Landfills: A Comprehensive Literature Review," *A Report Submitted to the Solid Waste Services Division of City of Calgary*, University of Calgary, Canada.

Hettiarachchi, C. H. (2001). "Numerical Analysis of Transient Heat Flow Coupled with Groundwater Flow," *MEng Thesis*, Asian Institute of Technology, Thailand.

This dissertation is dedicated to my mother, Sreema De Livera Kulatunga

and my father, Dayananda Hettiarachchi

ACKNOWLEDGMENT

I wish to express deepest gratitude to my advisors, Dr. Jay N. Meegoda and Dr. Patrick Hettiaratchi, for their advice, guidance and continuous support throughout the research which has been a rewarding experience to me. I thank the members of my doctoral dissertation committee: Dr. Raj P. Khera, Dr. Hsin-Neng Hsieh, Dr. John Tavantzis, Dr. Issa Oweis, and Dr. Salah El-Hagger for their valuable advice and constructive criticisms.

I also wish to express my gratitude to the Department of Civil and Environmental Engineering of New Jersey Institute of Technology for the financial assistance and support. The Department of Civil Engineering, University of Calgary, is greatly acknowledged for their financial assistance and support to continue my research in the summer months in Canada in 2002, 2003 and 2004.

I wish to thank my friends, Qian Wu and Vishal Gawarikar, for helping me in numerous ways to make my life at school comfortable. I also appreciate all the support and encouragement given by my fellow graduate students and staff in the Department of Civil and Environmental Engineering at NJIT as well as all the other friends whose names are not specifically mentioned.

A Special thanks to my loving wife, Mala, not only for the continuous moral support but also for sharing ideas and helping me in computer programming. Last, but not least, I extend my sincere gratitude to my beloved parents, my sister Manori, and my brother Mahesh for their inspirational support and love.

TABLE OF CONTENTS

TABLE OF CONTENTS
(Continued)

Chapter **Page**

TABLE OF CONTENTS
(Continued)

Chapter **Page**

TABLE OF CONTENTS
(Continued)

Chapter **Page**

TABLE OF CONTENTS
(Continued)

TABLE OF CONTENTS
(Continued)

Chapter **Page**

LIST OF TABLES

LIST OF FIGURES

LIST OF FIGURES
(Continued)

LIST OF FIGURES
(Continued)

LIST OF SYMBOLS

V	Total volume of waste layer (m^3)
V_s	Volume of solids (m^3)
V_w	Volume of liquids (m^3)
V_g	Volume of gas (m^3)
Z	Height of waste layer (m)
Z_s	Height of solid phase (m)
Z_w	Height of liquid phase (m)
Z_g	Height of gas phase (m)
δZ	Change in height (m)
Z_i	Initial height (m)
C_c^*	Compression ratio
C_c^*	Swelling ratio
σ'	Effective stress (kN/m^2)
$\delta\sigma'$	Difference in effective stress (kN/m^2)
ε	Strain (m/m)
$\delta\varepsilon$	Difference in strain (m/m)
M	Total mass of the waste layer (kg)
M_s	Mass of solids (kg)
M_{si}	Total initial mass of solids (kg)

M_{sj} Mass of the j^{th} solids group (kg)

M_w Mass of liquid phase (kg)

M_g Mass of gas (kg)

λ_j Decay constant of the j^{th} solids group (1/day)

f_{sj} Initial solids fraction for each waste group (kg/kg)

G_{sj} Specific gravity of the j^{th} group of the waste solids

ρ_w Density of water (kg/m^3)

ρ_c Waste compaction density (kg/m^3)

ρ_s Density of the final cover (kg/m^3)

ρ_g Density of gas (kg/m^3)

θ Volumetric moisture content (m^3/m^3)

G Rate of generation of gas (kg/m^3/day)

L_0 Gas generation potential (m^3/kg)

v_g Velocity of gas (m/day)

D Diffusion coefficient of landfill gas (m^2/day)

K Landfill permeability (m^2)

k_g Gas conductivity (m/day)

k_w Hydraulic conductivity (m/day)

P_a Atmospheric pressure (N/m^2)

p Relative pressure, i.e. pressure beyond atmospheric pressure (N/m^2)

z	Distance measured from the bottom of the landfill (m)
t	Time since placement of waste (day)
m	Molar mass of landfill gas (kg)
R	Universal gas constant (J/mol/K)
T	Landfill temperature (K)
h	Matric potential (m)
S	Rate extraction of leachate per unit volume ($m^3/day/m^3$)
θ_r	Residual moisture content (m^3/m^3)
θ_s	Saturated moisture content (m^3/m^3)
S_e	Effective saturation
Pe	Peclet number
Cr	Courant number

CHAPTER 1

INTRODUCTION

1.1 Background

Recent advances in sanitary landfill research have indicated that the operation of landfills as bioreactors could be viable. Waste entombment in a conventional landfill slows down the process of biodegradation by minimizing moisture entry, whereas, bioreactors speed up the biodegradation process by controlled input of moisture (i.e. by leachate recirculation) and increased cycling of nutrients and bacterial populations (Reinhart and Townsend, 1998). The operation of traditional "entombed" landfills for the sole purpose of controlling groundwater contamination is not sustainable and could be counterproductive because of the slow production and atmospheric release of methane-rich landfill gas, and the loss of resources (e.g. material and space).

Being a relatively new technological innovation, full-scale operation of bioreactor landfills could be fraught with uncertainties. Therefore, the need for more fundamental and applied research has been recognized.

A novel concept formulated by University of Calgary researchers is "sustainable landfill biocell." The biocell landfill concept involves the operation of a landfill cell as an anaerobic bioreactor with leachate recirculation to recover the full energy potential of biomass waste. In a second stage, it is operated in the aerobic mode to produce compost. The input of air and operation of the cell as an aerobic bioreactor enhances waste decomposition to a level where it could be mined in a third stage for resource and space recovery, thus making the landfill operation sustainable. The biocell landfill is a novel and holistic approach to waste disposal on land; with energy recovery, landfill gas

emission control, groundwater contamination control, and compost and space recovery as direct benefits. The biocell landfill technology approach has the potential to revolutionize management of waste in both developed and developing countries.

Although the biocell landfill is an attractive alternative to conventional landfilling, a number of technical obstacles could prevent its adoption. The satisfactory resolution of one such issue is the focus of this research. This research is undertaken to address the issues associated with waste settlement in a biocell landfill when it is operated in its first phase as an anaerobic bioreactor landfill. This research investigates how the generation and dissipation of landfill gas pressure and the distribution of moisture affect waste settlement in a biocell landfill.

Enhancement of microbiological activities in a bioreactor landfill is achieved by recirculating the leachate collected. Recirculation of leachate helps the landfill to maintain a wet environment in addition to the supply of nutrients needed for the biodegradation.

In a biocell landfill, gas production is accelerated because of rapid waste decomposition making them different from conventional 'dry-tomb' landfills. Waste begins to show a high compressibility. This causes significant changes in waste properties that can be manifested as modified stability and settlement behavior.

1.2 Problem Definition

Settlement prediction is important for proper design and operation of a biocell landfill. Accurate prediction of settlement is of special importance in estimating air space, planning construction sequence, designing both intermediate and final covers as well as

planning for expansions. Accurate prediction is also essential for design of piping systems used for the delivery of recirculated leachate and collection of landfill gas. Though majority of settlement is caused by the decomposition of municipal solid waste over period of years considerable amount of settlement also takes place during the initial construction stage, which is usually unnoticeable as it happens through the stages of construction. A comprehensive model for settlement analysis of a bioreactor landfill should be able to demonstrate not only the settlements due to biodegradation but also the settlements that occur due to mechanical compression in the initial construction stage.

To calculate landfill settlement many landfill settlement models employ methods that take into consideration the entire landfill thickness. They typically consider settlement after closure; therefore, no allowance could be made for settlement during construction, or the rate of construction. The use of entire landfill depth to calculate settlement, does not allow for the calculation of strains at different depths, and requires that values of the model's parameters be a function of the thickness of the landfill (Bleiker et al. 1995).

In general, any landfill, and especially a biocell landfill, consists of interacting multiphase media (gas, liquid, and solid), with each phase exhibiting spatial and temporal variations. But the existing waste settlement models focus mainly on the compressibility of the solid phase of waste (El-Fadel and Khoury, 2000). In reality settlement of the solids phase depends on contribution from all three phases. Many mathematical models are available to evaluate the processes of biodegradation, generation and transport of gaseous products and distribution of moisture within a landfill. But none of them consider the contribution from settlement on those processes. On the other hand, the

models that are being used today for predicting settlement behavior often do not capture the importance of liquid and gas phases.

1.3 Research Objectives

The primary objectives of the current research are:

- To identify the primary mechanisms governing the process of waste settlement and to propose a basic framework to use these mechanisms to predict the settlement behavior of a biocell landfill
- To derive a general governing equation to describe the process of landfill gas pressure generation and dissipation incorporated with the settlement process
- To couple the process of distribution of moisture in a biocell landfill with the processes of settlements and generation and dissipation of landfill gas
- To determine the compressibility of fresh waste and its variation with waste degradation, for the accurate prediction of mechanical compression
- To establish a procedure to numerically solve the governing equations of the coupled system, and
- To predict the spatial and temporal variation of total settlements, gas pressure and moisture distribution of a biocell landfill.

CHAPTER 2

LITERATURE REVIEW

2.1 Introduction

This chapter provides a review of literature in the field of landfill settlement modeling. First few sections provide a detailed general discussion of landfill waste settlement mechanisms and widely used computational methods. Latter part of this chapter is devoted to literature pertaining to biocell landfills. Literature on important aspects of generation and dissipation of landfill gas and distribution of moisture within a landfill is also briefly discussed.

2.2 Settlement Behavior of Landfills

Accurate prediction of landfill settlement is a challenge because of the large number of variables involved in the settlement process. Type of waste, organic content, moisture content, compaction density, compressibility, level of nutrients available for biological activities, pH, temperature, and time since placement are some of them. The rate of settlement varies not only with time but also with depth. This variation is due to a number of factors, which include the increased strain in the waste layers due to the weight of the overlying layers (Bleiker et al. 1995). The waste at the bottom of a landfill compacts both immediately upon placement and over time as landfilling operation progresses. This results in a much greater waste density at the bottom compared to the waste at the top of the landfill.

2.2.1 Mechanisms of Waste Settlement

The mechanisms of waste settlement are many and complex due to extreme heterogeneity and large voids present in the landfill. The main mechanisms involved in waste settlement, as identified by Sowers (1973) and Edil et al. (1990) are listed below:

- Mechanical (distortion, bending, crushing, and re-orientation; similar to consolidation of organic soils)
- Ravelling (movement of fines into larger voids)
- Physico-chemical change (corrosion, oxidation, and combustion)
- Bio-chemical decomposition (fermentation and decay; both aerobic and anaerobic processes)

The majority of immediate settlement is caused by mechanical processes (Bleiker et al. 1995). Sowers (1973) estimated that these processes are completed within one month from the date of placement of waste. The last two mechanisms cause the majority of the long-term settlements. Decay of mass also causes a reduction in waste mass, leading to a decrease in the overburden stress. El-Fadel and Khoury (2000) reported that the interactions between these mechanisms may cause further subsidence. Combustion supported by generation of methane and heat released from decay and raveling triggered by decomposition are some examples. Edil et al. (1990) further identified the following factors affecting the magnitude of landfill settlement.

- Initial waste density or void ratio
- Fraction of the degradable waste
- Fill height
- Stress history

- Leachate level and fluctuations
- Environmental factors such as moisture content, temperature, and gas production

Settlement of waste is characteristically irregular (Edil et al. 1990); initially, there is a large settlement within one or two months after construction, followed by a substantial amount of secondary compression over an extended period of time. The magnitude of settlement rate decreases with time and with increasing depth below the surface of the fill.

Not only stress history but also the load increment ratio influences settlement. This was studied during the construction of an interstate highway (Oweis and Khera, 1998), where part of an old landfill was excavated prior to surcharging. About 5-7% settlement occurred due to the stress increase from the surcharge load, which was less than the stress before the excavation. Whereas, when the surcharge stress was over 40% above the pre-excavation stress, the settlement ranged from 11.4-16.8% (Sheurs and Khera, 1980).

2.2.2 Stages of Landfill Settlement

El-Fadel and Khoury (2000) identified three stages of settlement: initial compression; primary compression; secondary compression. They defined initial compression and primary compression similar to how they are defined in consolidation settlement in clay: initial compression as the settlement that occurs instantaneously when an external load is applied, which is generally associated with the immediate compression of the void space and particles due to superimposed loads and primary compression as the process of dissipation of pore water and gas from the void spaces. According to Sowers (1973) and

Edil et al. (1990), this dissipation occurs within 30 days after the placement of the load. The field measured data at several locations show that about 70-80% of the settlement took place within the first three months (Sheurs and Khera, 1980). However, applicability of these definitions in waste settlement is debatable. In reality initial compression is hard to distinguish from primary compression and landfills are seldom saturated and high porosity of waste may inhibit pore pressure buildups.

The settlement of a landfill continues after the primary compression. Sowers (1973) attributed the long-term settlement of waste to secondary compression caused by decaying mass within the landfill, as a result of the physico-chemical and bio-chemical decomposition, which continues until the waste is fully stabilized.

2.3 Modeling Landfill Settlements

Sowers (1973) documented the similarity of waste settlement to that of peat, with large initial consolidation followed by substantial secondary compression. Edil et al. (1990) confirmed that solid waste compressibility properties were rather close to those of organic soils. Therefore, concepts borrowed from soil mechanics is often used to model settlements in solid waste landfills. However, landfill waste is heterogeneous and anisotropic and hence more difficult to characterize than soils.

Current practice of landfill settlement modeling is rather empirical and usually based on measured laboratory and field parameters. El-Fadel and Khoury (2000) classified the existing models into four broad categories: soil-mechanics based models; rheological models; empirical models; and models accounting for the effect of decay on settlement.

2.3.1 Soil Mechanics Approaches

The time dependent stress-stain relationship in waste is first documented by Sowers (1973). The pattern of rapid settlement followed by a slower and declining settlement rate has driven researchers to develop several mathematical models based on theory of consolidation to simulate settlement behavior in waste. Sowers (1973), Rao et al. (1977), Oweis and Khera (1986), Morris and Woods (1990), and Edil et al. (1990) used primary and secondary compression models to describe the stress-strain-time relationship in waste. The general form of the equation is given below.

$$S = HC_c^* \log\left(\frac{P_0 + \delta P}{P_0}\right) + HC_{\alpha 1} \log\left(\frac{t_2}{t_1}\right) \qquad (2.1a)$$

Where, S (m) is the settlement due to primary and secondary compression occurring in the layer under consideration, H (m) is the initial thickness of the waste layer, C_c^* is the primary compression ratio, $C_{\alpha 1}$ is the secondary compression index, P_0 (N/m^2) is the existing overburden pressure acting at the mid level of the layer, and δP (N/m^2) is the increment of overburden pressure at the mid level of the layer under consideration from the construction of an additional layer (100% of pressure increase at the top new layer is assumed to be transferred to the layer under consideration), t_1 (day) and t_2 (day) are the starting and ending time periods for which long-term settlement of the layer is desired.

Bjarngard and Edgers (1990) compiled landfill data and proposed an extension to Equation 2.1(a) as:

$$S = HC_c^* \log\left(\frac{P_0 + \delta P}{P_0}\right) + HC_{\alpha 1} \log\left(\frac{t_2}{t_1}\right) + HC_{\alpha 2} \log\left(\frac{t_3}{t_2}\right) \quad (2.1b)$$

Where, $C_{\alpha 1}$ and $C_{\alpha 2}$ are defined as intermediate and long-term secondary compression ratios, respectively, t_1 (day) and t_2 (day) are the time for completion of initial, primary compressions, respectively, and t_3 (day) is the total period of time considered in modeling.

Bleiker et al. (1995) compared soil mechanics based waste settlement models. Most of the soil mechanics approaches used the models to calculate landfill settlement of the entire waste thickness after closure. By starting after closure, no allowance was made for settlement during construction, or the rate of construction. The use of the entire depth to calculate settlement does not allow for the calculation of strains at different depths, and requires that values of the model's parameters be a function of the thickness of the landfill. Morris and Woods (1990) proposed a mathematical model to calculate the settlement of different layers within the waste.

2.3.2 Rheological Models

Rheological models consist of elements such as springs, dashpots, and sliders. Composite models are constructed from these basic elements to describe creep behavior. A simple rheological model that has been widely reported in the literature is Gibson and Lo model. Previous research has shown that this model was useful in predicting the settlement of peat, which in turn is assumed to have compressibility characteristics similar to those of solid waste (Edil et al. 1990). Rao et al. (1977), Edil et al. (1990), and

Bleiker et al. (1995) used Gibson and Lo type of rheological models to describe the waste stress-strain-time relationship.

Figure 2.1 shows the physical rheological model, which is often used for settlement computations. The waste will settle immediately due to an applied load with strain in Hookean element 'a' and eventually, the waste skeleton supporting the load will creep, rearrange, and settle at a rate 'k' with additional strain in Hookean element 'b'. This physical model is represented by Equation 2.2, where, $\varepsilon(t)$ is the strain as a function of time and σ' (N/m^2) is the effective vertical stress.

$$\varepsilon(t) = \sigma'\{a + b(1 - \exp(-kt))\} \tag{2.2}$$

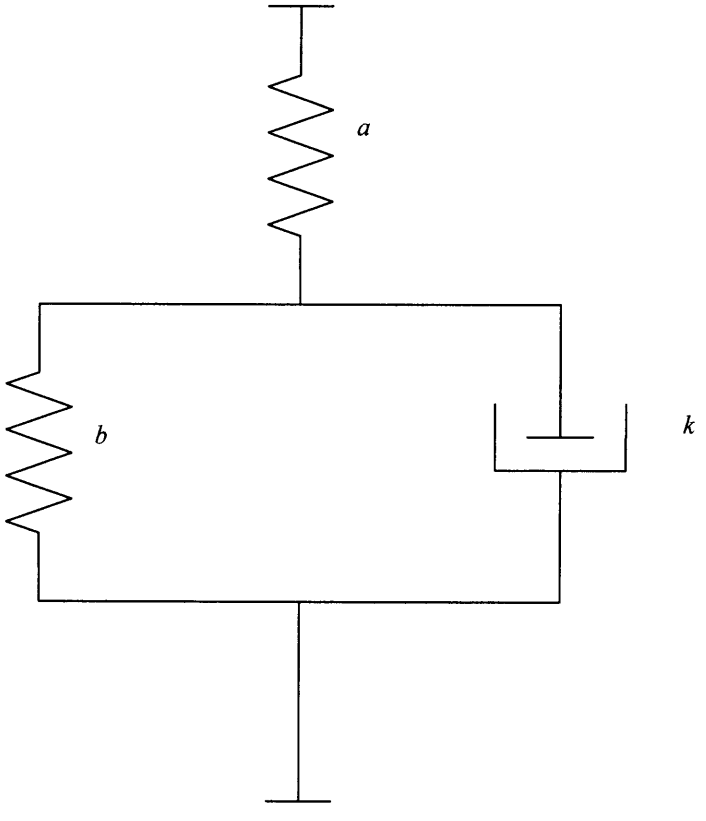

Figure 2.1 Schematic diagram of the Gibson and Lo rheological model.

Bleiker et al. (1995) used a graphical method and data published by Rao et al. (1977) to find *a* and *b* parameters. Although Rao et al. (1977) used simulated waste under laboratory conditions, their data adequately illustrated the trend and the work of Edil et al. (1990). Because of the non-linear relationship of *a* and *b* with effective stress, and the variation of effective stress, in soils with depth, the model is only accurate over a given stress ranges and waste thicknesses from which the parameters were determined.

2.3.3 Empirical Models

Practicing engineers prefer empirical relationships because of the complexity and difficulty of applying other types of models. The attempts to simulate general waste behavior by adjusting the empirical parameters, which are site specific, seldom have a physical significance (El-Fadel and Khoury, 2000). Commonly employed mathematical functions in such attempts are the logarithmic function, the power function, and the hyperbolic function. They are briefly discussed below.

Yen and Scanlon (1975) analyzed the settlement data from three waste landfills, 30 m high, with the data recorded over 9 years. They calculated the settlement rates as the ratio of change in elevation of settlement platforms to elapsed time between surveys. The strain rate (was determined and approximated using the following logarithmic relationship.

$$\varepsilon' = \frac{1}{H_0}\frac{dS}{dt} = c - d\log t \tag{2.3}$$

Where, S (m) is settlement, H_0 (m) is the initial height of the municipal solid waste (MSW) landfill, ε' (1/day) is the strain rate, t (day) time duration of interest, and c and d are strain rate parameters (1/day), respectively.

Power Creep Law has been used (Edil et al. 1990; Kumar, 2000) to relate settlement rate with time. This relationship can be written as:

$$S' = \frac{dS}{dt} = \frac{P}{t^q} \tag{2.4}$$

Where, t (day) is the difference between the time of interest and the starting time of measurements, p and q are empirical constants. Ling et al. (1998) presented Equation 2.5 as the solution for Equation 2.4.

$$S = \frac{p}{1-q} t^{1-q} = p' t^{q'} \tag{2.5}$$

In order to predict the long-term settlement of landfills, Ling et al. (1998) applied a hyperbolic function (Equation 2.6) to analyze settlement data obtained from three landfill sites.

$$S = \frac{t}{(1/S_0') + (t/S_{ult})} \tag{2.6}$$

Where, S_0' (m/day) is the initial rate of settlement, t (day) is the time duration of interest, and S_{ult} (m) is the ultimate settlement. The parameters S_0' and S_{ult} may be determined by transforming the above equation through t/S versus t relationship and conducting a linear regression analysis.

It is likely that the final settlement will be between 80-95% of this ultimate value. The time taken to reach 95% of this ultimate value is calculated as $t_f = 19(S_{ult} / \rho_0)$. Hyperbolic function offers the flexibility for it to start at any time. It is particularly useful if there is a change in loading conditions such as waste surcharging, so that the analysis may be restarted.

2.3.4 Biodegradation-induced Settlement Models

A large portion of total settlement may be caused by biodegradation, which occurs over a long period of time. Recent efforts reported mathematical expressions incorporating the effect of biological decay on settlement (Edgers et al. 1992; Park and Lee, 1997; Kang et al. 1997; Oweis and Khera, 1998). The basic assumption underlying these expressions is that the settlement is directly proportional to the biodegradation. The settlement due to biodegradation is usually expressed in terms of first order kinetics. A generalized form of the equation that has been proposed to convert decay to settlement is given in Equation 2.7 where, $S(t)$ is the settlement (m) at time t, H_0 is the initial height of waste (m), ε_{total} is the total expected strain, λ (1/day) is the first order kinetic constant, and t (day) is the time since the start of decay.

$$S(t) = H_0 \varepsilon_{total} (1 - \exp(-\lambda t)) \tag{2.7}$$

These biodegradation-induced models require determination of bacterial degradation expressions with their respective kinetic coefficients. More reliable expressions incorporating hydrolysis reactions for different types of bacteria and different types of waste components have also been proposed (El-Fadel and Khoury, 2000).

2.4 Comparison of Settlement Models

Edil et al. (1990) presented a comparison between Gibson and Lo rheological model and power creep model. Data from four sites were used in the study. The data obtained during the first year was used to predict the amount of settlement that could be expected at the end of the data collection period, which was about two years. Table 2.1 shows a comparison of the results obtained using both methods for one site.

Table 2.1 Comparison of Predicted Settlements from Gibson and Lo Model and Power Creep Law

Platform	Settlement (m)			Percentage deviation (%)	
Number	Actual	Gibson & Lo	Power Creep	Gibson & Lo	Power Creep
Minimal Filling					
1	0.52	0.43	0.53	-17	2
2	0.59	0.59	0.59	0	0
3	1.11	1.09	1.06	-2	-4
4	1.19	1.23	1.24	4	5
7	1.88	1.54	2.00	-18	6
Active Filling					
8	3.34	3.19	3.38	-4	1
10	2.99	2.93	3.18	-2	6
12	1.94	1.91	1.94	-1	0
13	2.03	2.00	1.97	-2	-3
14	2.95	2.32	2.53	-21	-14

Source: Edil et al. (1990)

This landfill site is located in southeastern Wisconsin. The settlement data was collected using settlement platforms surveyed periodically from 1984 to 1986. The data collection at this site was continued for approximately 1.8 years. Two types of loading conditions were considered in the study. First category, "minimal filling," represents a condition of settlement under essentially self-weight. The second category, "active filling," represents a condition of settlement under both self-weight and the placement of additional fills above the platforms.

The Gibson and Lo rheological model predicted the amount of settlement at the end of two years within 2-18% of actual settlement that occurred for minimal filling and 4-21% for active filling. The power creep law predictions for the same conditions were 0-6% and 0-14%, respectively. It seems that power creep law preformed better than Gibson and Lo model, which has a physical meaning and can reflect the effects of waste placement conditions.

While introducing the parabolic model, Ling et al. (1998) also compared their results with the results obtained from the power creep law and logarithmic function. The conventional settlement rate-time relationships ($\log t$ and power functions) did not lead to satisfactory agreement when the settlement was integrated using the best fit parameters. The hyperbolic function gave improved prediction of long-term settlement over $\log t$ and power functions.

In an effort to examine the decomposition effect on prediction of long-term settlement of landfills, Park et al. (2002) performed settlement calculations for seven sites in which the age of waste was young. Four of the sites (A-D) showed the characteristics of accelerated logarithmic compression rates during the measurement period; the other

three sites (E-G) did not include these characteristics. In their study, the long-term settlement was defined as the calculated settlement from the time of first measurements to 30 years is shown in Table 2.2. In the cases of sites A-D, the upper values were calculated from the overall measurements, which included the stage of accelerated compression. The values in parentheses were calculated using the settlement data measured before the accelerated compression occurred. For sites A-D, the estimated long-term settlements predicted by the rheological model (Gibson and Lo), the hyperbolic function, and the logarithmic function are much larger when the accelerated compression rate occurs due to decomposition. The power creep law seemed overestimating considerably.

In the case of sites E, F and G, the predicted long-term settlements by most of the models, excluding the power creep law, were 2-9% of the initial height of the landfill. The values are very similar to those calculated on the basis of the settlement data measured for sites A-D before the accelerated compression due to decomposition occurred. The settlement values seem smaller with respect to long-term settlements that are likely to occur in fresh landfills.

Table 2.2 Comparison of 30 Year Strains Predicted by Gibson and Lo, Hyperbolic, Logarithmic, and Power Creep Settlement Models

Site	Gibson & Lo (%)	Hyperbolic (%)	Logarithmic (%)	Power Creep (%)
A L – 1	31.5	49.3	37.2	82.3
	(6.0)	(8.8)	(5.2)	(27.8)
L - 3	33.1	49.8	36.7	85.9
	(4.9)	(8.4)	(4.2)	(30.2)
B Apartment	17.9	25.5	17.6	72.3
	(9.2)	(9.7)	(7.1)	(46.7)
Domestic	15.7	24.9	16.7	48.0
	(3.3)	(5.7)	(3.2)	(33.5)
C	16.7	14.9	10.8	47.7
	(2.8)	(3.5)	(2.3)	(46.5)
D	16.8	19.5	12.4	41.3
	(7.3)	(12.3)	(6.2)	(35.2)
E No. 26	2.8	3.9	8.9	18.6
No. 27	2.1	3.4	7.4	12.3
No. 28	3.0	3.0	5.5	11.1
F Cell 1	3.6	5.2	3.2	10.3
Cell 2	3.2	5.5	2.8	7.9
Cell 3	4.5	5.7	3.0	7.7
Cell 4	2.8	4.8	2.5	5.8
Cell 5	5.6	5.8	3.6	8.8
G	3.3	3.6	6.6	17.5

Source: Park et al. (2002)
Note: The values in parentheses were calculated using the settlement data measured before the accelerated compression occurred.

2.5 Modeling Biocell Landfill Settlements

Only a few studies of modeling settlement behavior of landfills similar to biocell landfills are found in the literature. These attempts are also limited to either laboratory or small pilot scale landfills. Some of these models used in these studies are actually adjusted versions of the traditional models that have been originally proposed for the dry landfills. They are briefly discussed in the following sections.

2.5.1 Wall and Zeiss (1995)

To predict the settlement of waste with leachate recirculation, Wall and Zeiss (1995) applied the secondary compression model, which was originally proposed by Sowers (1973) for long-term waste settlement predictions in sanitary landfills. They assumed a linear time dependent settlement behavior with respect to a logarithmic time where the variation of strain with time is given by Equation 2.8.

$$\varepsilon = C_1 \log\left(\frac{t}{t_p}\right) \quad ; t \geq t_p \tag{2.8}$$

Where, ε is the strain, C_1 is the slope of the strain versus log-time curve and t_p (day) is the time taken for the primary compression to end. Following many other previous researches (Sowers, 1973; Morris and Woods, 1990; and Edil et al. 1990) they used 30 days for t_p.

Wall and Zeiss (1995) studied the reduction in time taken to reach biological stabilization of waste and determination of effects of biodegradation on settlement. The study included a test cell (1.7 m in height and 0.57 m diameter), that was monitored for 250 days (8 months). They observed that during the first period of secondary settlement,

biodegradation had insignificant contribution on the secondary settlement rates. To determine whether an effect of solids removal on settlement is probable, the percentage of carbon decomposed during the test period (250 days) and estimated five-year predictions were compared to each other. The total mass of solids decomposed during the test period was 1% whereas the secondary settlement at the same period accounted for deformation of 4%. Wall and Zeiss (1995) concluded that decomposition did not significantly affect the rate of secondary settlement during the test period.

2.5.2 El-Fadel and Al-Rashed (1998b)

El Fadel and Al-Rashed (1998b) used power creep model and one-dimensional consolidation model to analyze data from the Mountain View bioreactor test cells in California in which leachate recirculation was one of the test parameters. El-Fadel and Al-Rashed (1998b) attributed settlement that occurs after initial settlement to secondary settlements. The two slopes observed when strain values were plotted against logarithmic time, were defined as intermediate secondary compression and long-term secondary compression. Based on this observation El-Fadel and Al-Rashed (1998b) suggested the following two equations to represent the time dependent settlement behavior in waste.

$$\varepsilon = C_1 \log\left(\frac{t}{t_i}\right) \quad ; t_i \geq t \geq t_2 \tag{2.9}$$

$$\varepsilon = C_2 \log\left(\frac{t}{t_2}\right) \quad ; t > t_2 \tag{2.10}$$

Where, C_1 is the coefficient of intermediate secondary compression, C_2 is the coefficient of long-term secondary compression, and t_i (day) is the time at the end of initial settlement period, and t_2 (day) is the time at which the slope of the strain versus logarithm time curve changes to a steeper slope and it has to be determined graphically from the field data.

The secondary settlement model proposed by El-Fadel and Al-Rashed (1998b) defines a better settlement curve when compared with that of Wall and Zeiss (1995) due to the adoption of two slopes. When time reaches t_2, the first mechanism of waste settlement given by Equation 2.9 suddenly stops and then starts a new mechanism (Equation 2.10). But this sudden change in mechanism is not justified and hence the model gives an impression of mere fitting of data to two lines. The selection of the time at which the slope of the curve changes (t_2) is also highly subjective.

El-Fadel and Al-Rashed (1998b) also used the power creep model to analyze the same set of data but they were unable to obtain satisfactory results.

2.5.3 Conceptual Model Proposed by Gabr et al. (2000)

Gabr et al. (2000) identified two stages of decomposition and proposed a conceptual two-stage model to model the settlement behavior of a biocell landfill. This approach is briefly explained below.

During early stage of biological decomposition, compressibility of the waste does not conform to the traditional Terzaghi's model. The compressibility of waste during this period is governed by changes in the void ratio due to solids loss, and the material physical size and stiffness with no consideration to hydrodynamic lag effect.

Concurrent to the change in void ratio due to decomposition, a physical change in the particle size and distribution also takes place. Therefore, assuming the amount of compression due to the increase in void ratio as well as the compressibility of solids is governed by the matrix stiffness changes under its own weight and external loads, they suggested the Equation 2.11 to calculate the change in volume.

$$\Delta V(t) = \Delta V_s(t) + \Delta V_v(t) = V_i \{C_m(t)(\Delta\sigma_{oct} - \Delta u(t)) + D_m(t)\Delta\tau_{oct}\} \quad (2.11)$$

Where, V_i is the initial volume (m^3), $\Delta V_s(t)$ is the inter-particle volumetric change with time (m^3), $\Delta V_v(t)$ is the intra-particle volumetric change with time (m^3), $C_m(t)$ is the time-dependent bulk coefficient of compressibility, $\Delta\sigma_{oct}$ (N/m^2) is the increase in the octagonal normal stress, $\Delta\tau_{oct}$ (N/m^2) is the increase in the octagonal shear stress, and $D_m(t)$ is the time dependent coefficient of the increase in the octagonal shear stress.

As decomposition takes place, the material breakdown may lead to increase in the surface area of the solid matrix. During these stages, the reduction in hydraulic conductivity to 10^{-7} m/s or less. Considering this fact they suggested implementation of such Terzaghi's model with primary and secondary settlement, for the later stage of decomposition.

Gabr et al. (2000) suggested subdividing the fill into several layers to avoid the complications and to address the changes of the waste properties with depth. Settlement due to the bottom layer can be calculated considering them to be in the second stage of

decomposition, while the settlements from the upper layers are found using the Equation 2.11.

2.5.4 Hettiarachchi et al. (2003)

As the reduction in waste mass should be reflected by increased settlement, in an attempt to estimate long-term settlement of waste, Hettiarachchi et al. (2003) used first order reaction kinetics to relate the rate of waste decay to the rate of strain. They used the Equation 2.21 to predict the settlement behavior in a biocell landfill.

$$\varepsilon(t) = \varepsilon_o + \beta C_i (1 - \exp(-\lambda t)) \tag{2.12}$$

Where, t (day) is the time since placement, $\varepsilon(t)$ is the strain at time t , ε_o is the initial strain, β is the correlation coefficient of compression due to biodegradation (kg^{-1}), C_i is the initial mass of the biodegradable waste (kg), and λ (1/day) is the first order decay constant.

Hettiarachchi et al. (2003) compared the performance of their model with those proposed by Wall and Zeiss (1995) and El-Fadel and Al-Rashed (1998b). Data from four different test biocell landfills were analyzed using all three models to predict the time dependent settlements. These settlement profiles are given in Figure 2.2.

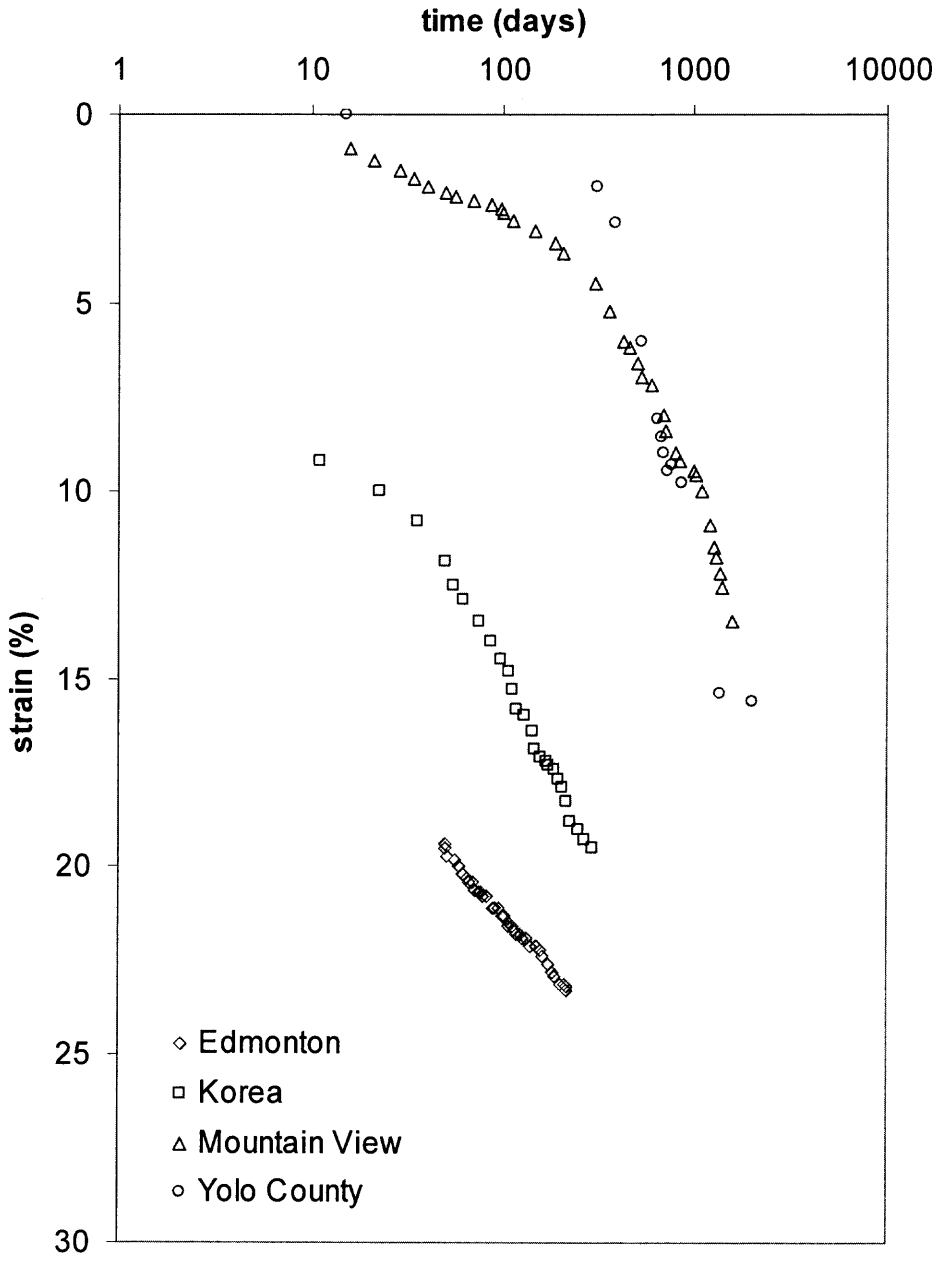

Figure 2.2 Settlement data.
Source of data: Edmonton (Wall and Zeiss, 1995), Korea (Kang et al. 1997), Mountain View bioreactor landfill (El-Fadel and Al-Rashed, 1998a), and Yolo County bioreactor landfill (Yazdani, 2003).

It was found that the Equation 2.12 used by Hetiarachchi et al. (2003) could provide a better prediction than both Wall and Zeiss (1995) and El-Fadel and Al-Rashed (1998b) models. Comparison of Hetiarachchi et al. (2003) and El-Fadel and Al-Rashed (1998b) models is provided by Figures 2.3 through 2.6. Features such as its direct relationship to biodegradation, prediction of settlement by a single equation made this attempt more attractive.

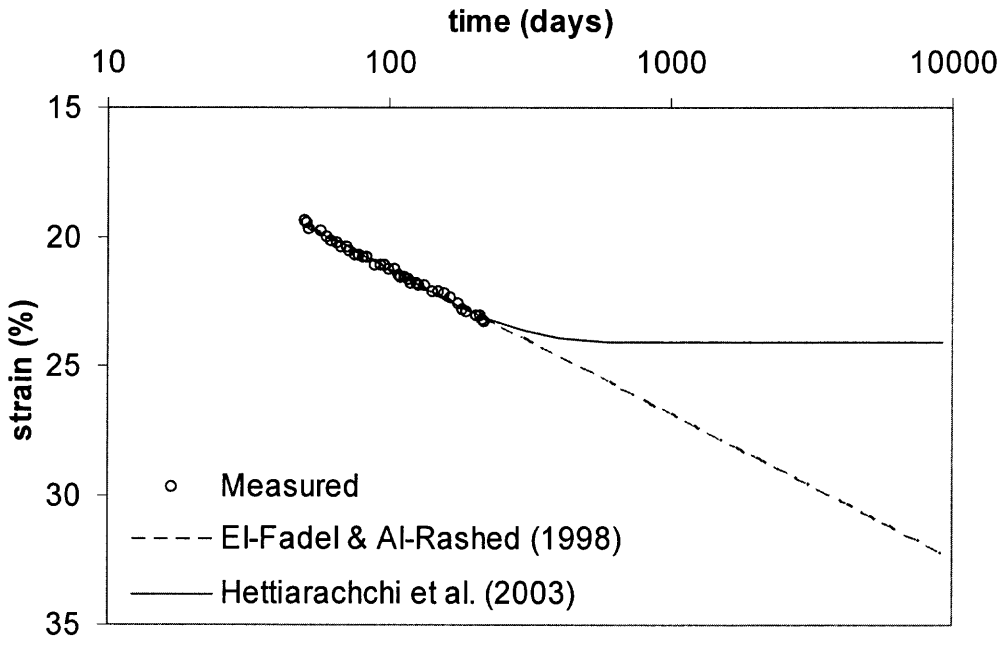

Figure 2.3 Model comparisons for data from Edmonton (Wall and Zeiss, 1995).

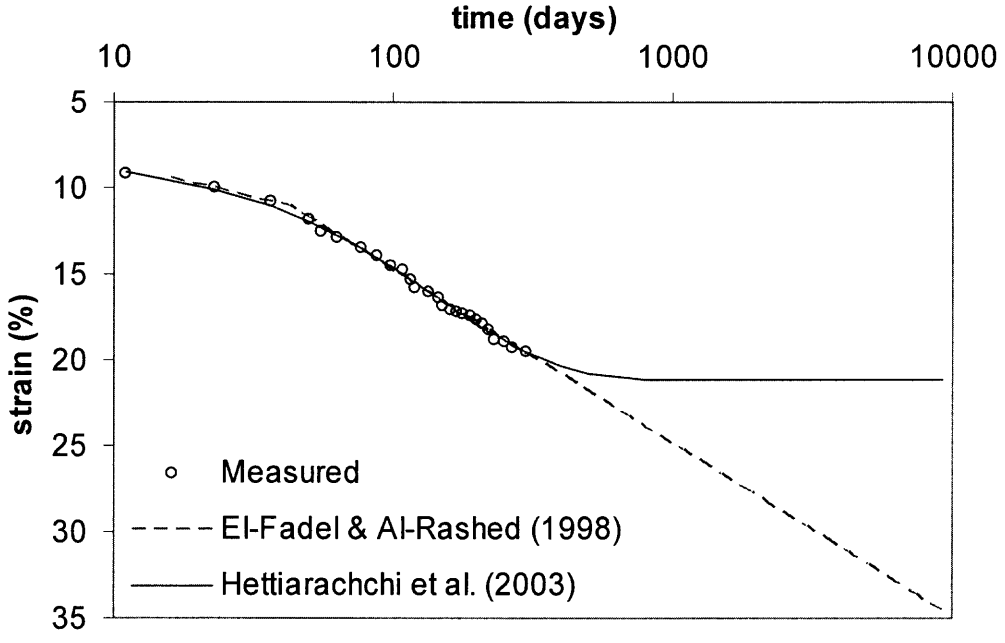

Figure 2.4 Model comparisons for data from Korea (Kang et al. 1997).

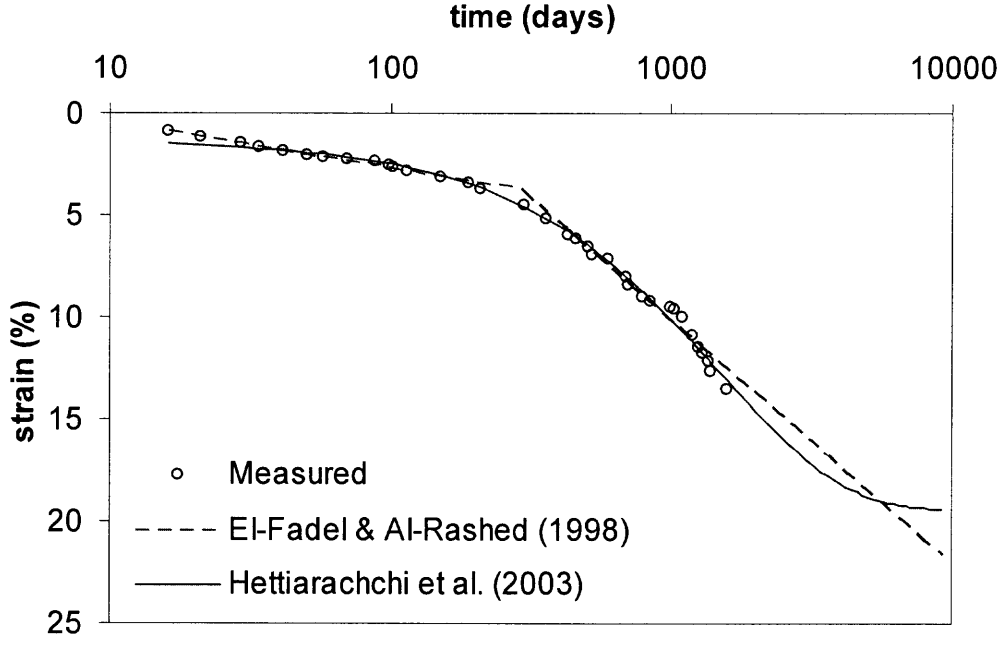

Figure 2.5 Model comparisons for data from Mountain View bioreactor landfill (El-Fadel and Al-Rashed, 1998b).

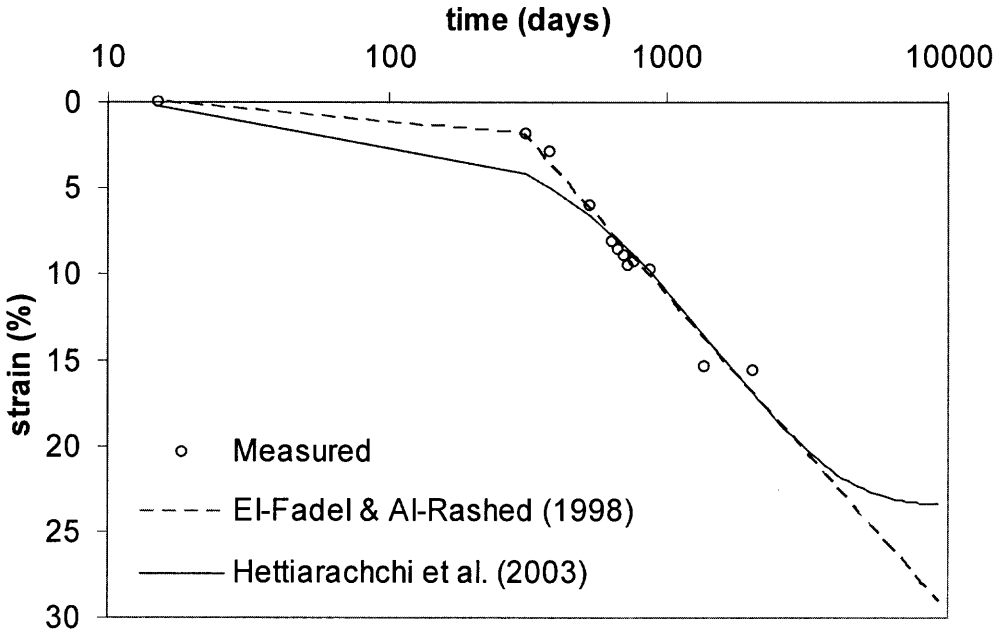

Figure 2.6 Model comparisons for data from Yolo County (Yazdani, 2003).

2.5.5 Conceptual Model Proposed by Hettiarachchi et al. (2005)

A conceptual model was proposed by Hettiarachchi et al. (2005) to predict settlement behavior of biocell landfills. They identified mechanical compression and biodegradation-induced strain as major mechanisms of waste settlement. In the absence of a proper theoretical explanation, they suggested mechanical compression to be modeled with the help of laboratory simulations. To model the settlements due to biodegradation, waste was assumed to obey the first order reaction kinetics. Therefore, this procedure allowed settlements due to mechanical reasons to be separated from that of biodegradation. The basic equations to calculate mechanical compression (ε_m) and biodegradation induced settlements (ε_b) were defined as:

$$\varepsilon_m = C^* \log\left(\frac{\sigma' + \delta\sigma'}{\sigma'}\right) \tag{2.13a}$$

$$\varepsilon_b = (1-n_i)\sum_{j=1}^{4} f_{sj}\left(\frac{G_{si}}{G_{sj}}\right)(1+w_j(t)G_{sj})[1-\exp(-\lambda_j t)] \quad (2.13b)$$

Where, C^* is the compressibility parameter, σ' (N/m^2) is the effective stress and $\delta\sigma'$ (N/m^2) is the difference in effective stress, n_i, w_j, and ρ_w are the initial landfill porosity, gravimetric water content, and the density of water, respectively, G_{si} and G_{sj} are the initial overall specific gravity of waste solids and specific gravity of the j^{th} group of the waste solids, respectively, λ_j (1/day) is the first order kinetic constant for the j^{th} group, and f_{sj} is the initial solids fraction for each waste group.

A computational framework was also proposed to numerically predict the settlements using time dependent waste properties and landfill geometry. Even though this model demonstrated a few promising features over other available settlement models, lack of verification by field data prohibits a detailed discussion.

2.5.6 Hossain and Gabr (2005)

Hossain et al. (2005) proposed a settlement prediction model for biocell landfills. The model accounts for the changes in the waste characteristics as a function of the waste degradation rate. Their approach was based on evaluating the variation of waste stiffness as a function of time and the variation of waste decomposition with depth. The model consists of four components: initial strain; initial creep; biodegradation strain; final creep. The Equation 2.14 was suggested for the total strain computations.

$$\varepsilon(t) = \varepsilon_p + C_{\alpha i}\log\left(\frac{t_2}{t_1}\right) + C_{\beta}\log\left(\frac{t_3}{t_2}\right) + C_{\alpha f}\log\left(\frac{t_4}{t_3}\right) \quad (2.14)$$

Where, ε_p is the initial strain due to applied stress. $C_{\alpha i}$ was defined as a creep index for the initial stage and it is a function of stress and degree of decomposition. C_β was defined as biodegradation index, which is a function of the extent of the solids decomposition as well as the degree of saturation. $C_{\alpha f}$ was considered as a creep index for the final stage. t_1 (day) is the time for completion of initial compression, t_2 (day) is the time duration for which creep compression is to be evaluated, and t_3 (day) is the time for completion of biological compression. Time factor t_4 was defined as the time for creep at the end of the completion of biodegradation.

This settlement model was verified using the model parameters obtained from laboratory experiments. They conducted 24 oedometer tests on shredded waste to measure compression indices. The time factors for the compressibility were determined from the gas production curve and field settlement data. They found that the initial creep index is independent of waste decomposition. Primary compression and finial creep strain components were not considered in the analysis. Therefore, the tested version of the model is deduced to the equations used by El-Fadel and Al-Rashed (1998b). However, the relationship of the model parameters to the waste properties and the gas production makes this model superior to the equations used by El-Fadel and Al-Rashed (1998b).

2.6 Generation and Transport of Landfill Gas and Distribution of Moisture within a Landfill

Existing waste settlement models mainly focus on the compressibility of solids phase of waste. But in reality, a landfill is an interacting multiphase (gas, liquid, and solid) medium, with each phase exhibiting spatial and temporal variations (El-Fadel and Khoury, 2000). Therefore, settlement of the solid phase depends on the variation of all three phases. A number of mathematical models is available to evaluate biodegradation of solid waste, gas and leachate generation and transport.

2.6.1 Rate of Gas Generation

No simple equations can adequately describe the rate of biodegradation and the gas generation in a landfill because of the heterogeneity of waste. Based on experimental observations, Farquhar et al. (1973) proposed a qualitative model to describe stages of gas generation. Quantitatively, the rate of gas generation can be predicted by considering the landfill as a batch reactor. The Monod model, or a modified version of it, remains the most widely used microbial growth model. Such a model relates variation of microbial population to substrate concentration (El-Fadel and Khoury, 2000).

The rate of gas production depends on many factors, including waste composition, age of waste, moisture content, pH, microbial population present, temperature, and quantity and quality of nutrients (McBean et al. 1995). The wide range of degradability of waste present in a landfill makes considerable difficulty in describing the rate of landfill gas generation. Theoretical approaches to characterize the rate of landfill gas generation involve models developed based on first order reaction kinetics.

USEPA Landgem model is one such model developed based on first order reaction kinetics and a model which is widely used to predict the rate of gas production in landfills (USEPA, 1998). The model is described in Equation 2.13 where, G (m^3/day) is the rate of methane generation, W (kg) is the rate of waste deposition, L_0 (m^3/kg) is the methane generation potential, and k (1/day) is the first order kinetic decay constant.

$$G = WkL_0 \exp(-\lambda t) \tag{2.13}$$

Values reported for first order kinetic decay constant in the literature are scattered in a wide range. Findikakis and Leckie (1979) and Arigala et al. (1995) used 0.0003, 0.00006, and 0.00004 $days^{-1}$ for rapidly biodegradable, moderately biodegradable, and slowly biodegradable waste groups, respectively. On the other hand McBean et al. (1995) suggested 0.001-0.004 day^{-1} for rapidly degradable wastes and 0.00003-0.0004 day^{-1} for moderately degradable waste. A considerable difference was not observed between the literate values used for dry landfills and biocell type of landfills. Hossain et al. (2003) used 0.0004 day^{-1} to model decomposition in a bioreactor. Based on limited laboratory and pilot scale studies, Sullivan (2003) suggested a range from 0.0003 to 0.0007 day^{-1} for bioreactor landfills.

2.6.2 Gas Generation Potential

The total quantity of landfill gas to be generated from a unit mass of refuse depends on both the organic content of waste and the environmental factors. Ham and Barlaz (1987) presented the Equation 2.14 to characterize methonogenic decomposition.

$$C_aH_bO_cN_d + \left(\frac{4a-b-2c+3d}{4}\right)H_2O \rightarrow \left(\frac{4a-b-2c-3d}{8}\right)CH_4 + \left(\frac{4a-b-2c+3d}{8}\right)CO_2 + dNH_3 \quad (2.14)$$

Equation 2.14 can be used to estimate an upper bound on the amount of gas produced relative to the quantity of substrate utilized. Using Equation 2.14, Ham and Barlaz (1987) also performed a theoretical estimation of total gas (methane and carbon dioxide) production from landfill solid waste. Total gas generation potential from typical US municipal waste was estimated as 0.52 m^3/kg using Equation 2.14. Theoretical estimations for organic components by degradability resulted a range of total gas generation potential of 0.1-0.3 m^3/kg. The range of total gas generation potential for anaerobic digestion of waste with sewage sludge was found as 0.21-0.26 m^3/kg. The total gas generation potential of full-size landfills, projected from existing short-term data was 0.05-0.4 m^3/kg.

McBean et al. (1995) compared a number of estimated total landfill gas generation potentials from literature sources. The values were scattered in a wide range from 0.005 to 0.5 m^3/kg. Most of the laboratory scale experiments resulted low total gas generation potential values while theoretical estimations were consistently high.

2.6.3 Transport of Landfill Gas

Most landfill gas transport models are based on the assumption that the landfill can be treated as a porous medium, and the gas velocity is given by Darcy's law (Findikakis and Leckie, 1979; El-Fadel et al. 1989; Young, 1989; Arigala et al. 1995). Gas extraction models rely on pressure change between the landfill gas pressure and atmospheric

pressure under static or dynamic vacuum applications. Young (1989) developed a model that describes transport of gas in a rectangular cross section of a landfill. Arigala et al. (1995) improved Young (1989) model by incorporating a more realistic description of waste biodegradation. In this model the waste is represented by three classes having different degree of biodegradability, as originally suggested by Findikakis and Leckie (1979).

2.6.4 Distribution of Moisture in Landfills

Usually it is assumed that the movement of moisture through a landfill occurs as a vertical wetting front. This assumption suggest that the leachate exits from the landfill when the moisture content is at its field capacity (Reinhart and Townsend, 1998). Field capacity of a porous media is often defined as the amount of water held in after the excess gravitational water has drained away (Zornberg et al. 1999). The time of arrival of this moisture front at a certain depth may be estimated based on the rate of moisture infiltration. However, impermeable items and low permeable daily and intermediate covers prevent even distribution and rate of moisture movement. This situation sometimes leads to lateral migration of moisture. In addition, gas production could also block moisture paths during the early stages of the landfill operation.

Movement of moisture in a landfill is predominantly characterized by unsaturated flow. Darcy's law may be used to describe unsaturated flow behavior (Reinhart and Townsend, 1998). However, pressure stays below atmospheric under unsaturated conditions and hence it is known as suction head (or matric potential), which is negative by definition. This negative potential is caused by the capillary forces that hold water against gravity. Moisture will flow from one area that has a negative potential to another

area at a more negative potential as long as the moisture content is above field capacity. With the introduction of more moisture, suction head declines and reaches zero at saturation. The Hydraulic conductivity in an unsaturated landfill is a function of the suction head, and therefore, the moisture content.

CHAPTER 3

MODEL FORMULATION

3.1 Introduction

The fundamental philosophy underlying this research is viewing settlements as an integral part of all the basic processes associated with settlements in a biocell landfill. Therefore, this research proposes a model that couples settlement of a biocell landfill with the generation and transport of landfill gases and distribution of moisture.

Similar to soils, waste also comprises of three phases: solids; water; and air. Each phase contributes to the total volume as:

$$V = V_s + V_w + V_g \tag{3.1}$$

Where, V (m^3) stands for volume and the subscripts s, w, and g represent solid, water, and air phases, respectively. The methodology proposed in this research is based on observing the changes of volume in each phase. The change in volume is then converted to settlement to find the time dependent heights, which are finally used in the mass balance equations to compute the landfill gas pressure and distribution of moisture.

3.2 Problem Idealization

In this research, it is assumed that the waste mass is comprised of layers of waste that are infinitely extended in horizontal direction (Figure 3.1). Therefore, based on a per unit area (say, 1 m^2) calculation, volume of any layer can be replaced by the corresponding heights as given in the Equation 3.2, where, Z stands for height (m).

$$Z = Z_s + Z_w + Z_g \tag{3.2}$$

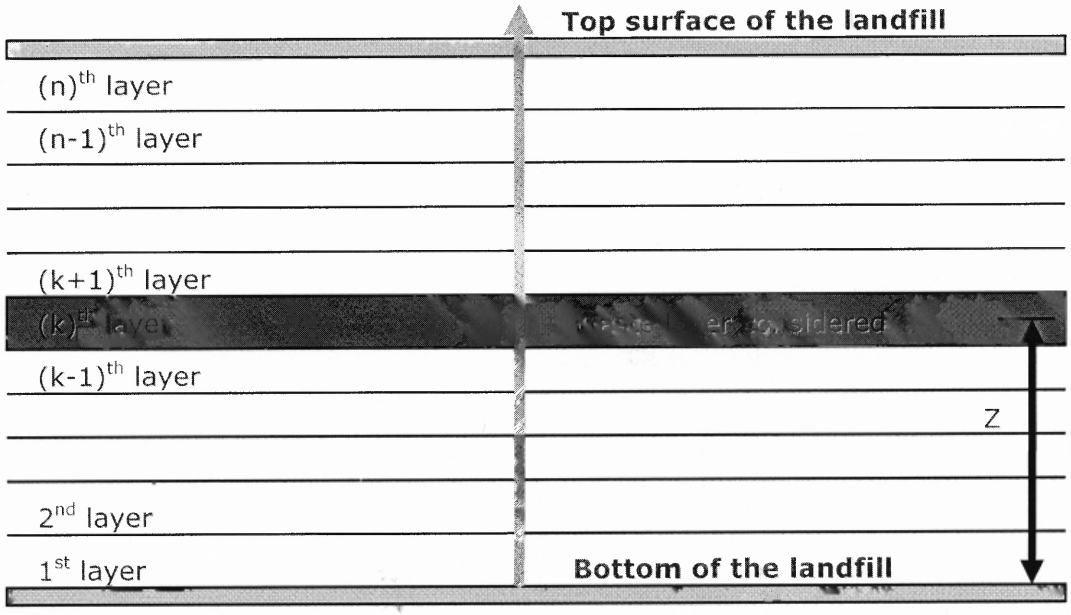

Figure 3.1 Cross-sectional view of the idealized landfill.

To avoid the complexities associated with multi-component gas transport, it is assumed that only one gas type is present (i.e. a mixture of 50% methane and 50% carbon dioxide). Movement of gas and moisture is assumed to occur in the vertical direction. It is also assumed that when time is zero, the unsaturated voids of the waste are filled with this gas, which is at atmospheric pressure. Variation in temperature in the landfill waste is not considered. It is assumed that the waste mass remains at a constant temperature of 42°C, which is favorable for biodegradation (Chynoweth and Pullammanappallil, 1996). Increase in moisture content due to precipitation during construction is assumed to be insignificant. Effects from intermediate covers on movement of fluids and density are also not considered.

3.3 Settlement

Waste changes its volume mainly due to the load (or stress) acting on it and the mass loss due to decay, hence two waste settlement mechanisms are considered in this research: mechanical compression; biodegradation-induced settlements. Even though biodegradation creates voids in the waste mass, the subsequent settlement is assumed to take place as a result of rearrangement of waste due to stress acting on it. Thus, the total settlement has to be modeled as a combined process of mechanical compression and biodegradation-induced settlements.

3.3.1 Mechanical Compression

Mechanical compression occurs due to the weight of the overlying waste. Since the strain is essentially a function of stress, mechanical compression at a given depth also remains a function of stress. While addition of new waste layers increases stress, loss of mass due to biodegradation can cause swelling or rebound. This behavior makes the stress at a given depth a function of time (Figure 3.2).

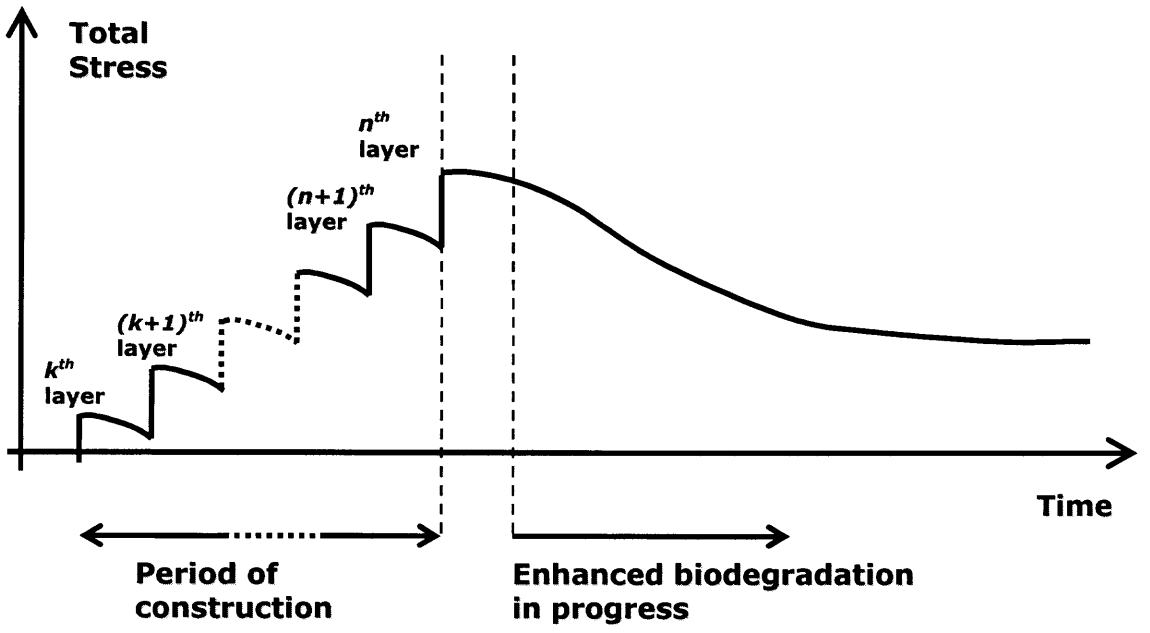

Figure 3.2 Stress at k^{th} layer as a function of time.

In this research, the relationship between mechanical compression and stress was established through a series of laboratory compression tests (details are given in Chapter 5). A given level of stress always ensures a certain level of strain if the compressibility of waste remains a constant. Unloading tends to follow a curve with a shallower slope showing that the loading produces both elastic and plastic deformations. Figure 3.3 demonstrates the basic stress-strain relationship of fresh waste, which was generated using the results of the a series of laboratory compression tests. Both curves fit well into straight lines in the logarithmic time scale. Hence the change in strain corresponding to a change in stress can be expressed as:

$$\delta\varepsilon = C^* \log\left(\frac{\sigma' + \delta\sigma'}{\sigma'}\right) \quad \text{where, } C^* = \begin{cases} C_c^* & ;\delta\sigma' > 0 \\ C_s^* & ;\delta\sigma' < 0 \end{cases} \tag{3.3}$$

Where, C_c^* is the compression ratio (slope of strain versus log of loading stress graph), and C_s^* is the swelling ratio (slope of strain versus log of unloading stress graph), σ' (N/m^2) denotes the average effective stress at the center of waste layer considered(and the initial effective stress can be calculated using the geometry of the landfill and density of the waste during the placement), and $\delta\sigma'$ (N/m^2) is the change in stress (can be either a negative or a positive quantity), which resulted the change in strain, $\delta\varepsilon$.

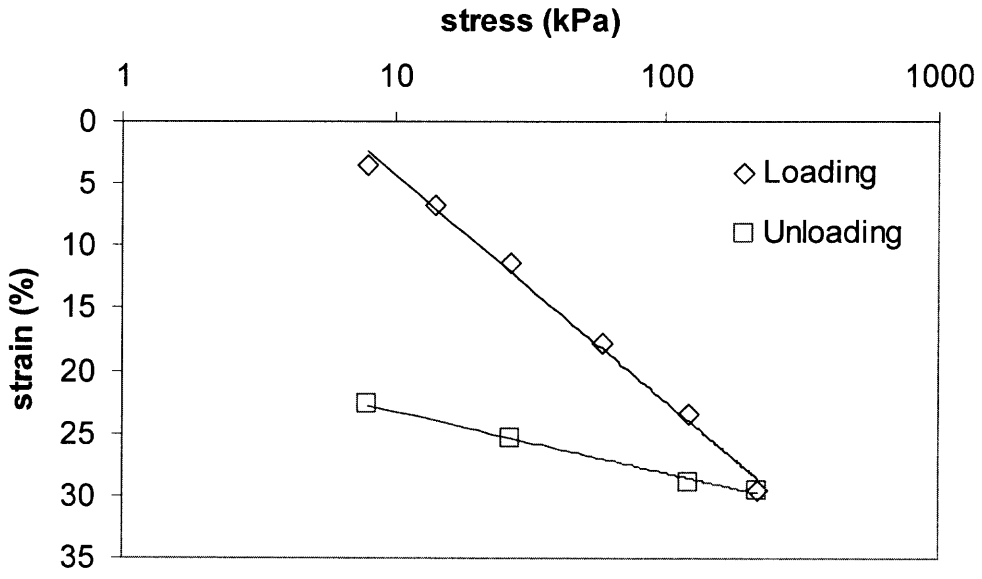

Figure 3.3 Stress-stain behavior of fresh waste under loading and unloading.

Equation 3.3 is useful in determining the initial mechanical compression due to the placement of the waste as well as in computing the release of strain (or swell) due to decomposition. It should be noted that due to the varying physical nature and the biodegradation over time, both compression ratio and swelling ratio may not remain the same. This fact needs to be addressed carefully when the calculations are performed.

The change in strain given by Equation 3.3 can be converted to the corresponding change in height (δZ) given in Equation 3.4, where Z_i (m) is the initial height.

$$\delta Z = Z_i C^* \log\left(\frac{\sigma' + \delta\sigma'}{\sigma'}\right) \tag{3.4}$$

3.3.2 Biodegradation-induced Settlement

Biodegradation of waste makes it different from soils where solid mass always remains unchanged. Since waste solids are highly heterogeneous, use of average properties could produce misleading estimations. Therefore, in this research, solid fraction of waste is divided into four groups depending on its degradability (Figure 3.4). They are: non-degradable (e.g. metals); slowly degradable (e.g. wood, rubber); moderately degradable (e.g. natural textile); and rapidly degradable (e.g. food) waste. Throughout this dissertation, V and M denote volume (m^3) and mass (kg). The subscript j denotes the number of the solids group.

It is believed that the decomposition rate of a biodegradable matter can be estimated by first order kinetics. In order to use first order kinetics to estimate decomposition, an unlimited supply of nutrients and optimum levels of moisture, temperature, and pH are assumed. It is also assumed that no toxic material, which inhibits biodegradation, is present in the landfill. The first order decay equation applied to the j^{th} group of waste solids and its solution, are presented by Equations 3.5 and 3.6, respectively, where λ_j (1/day) is the first order kinetic constant for the j^{th} group (note: $\lambda_1 = 0$).

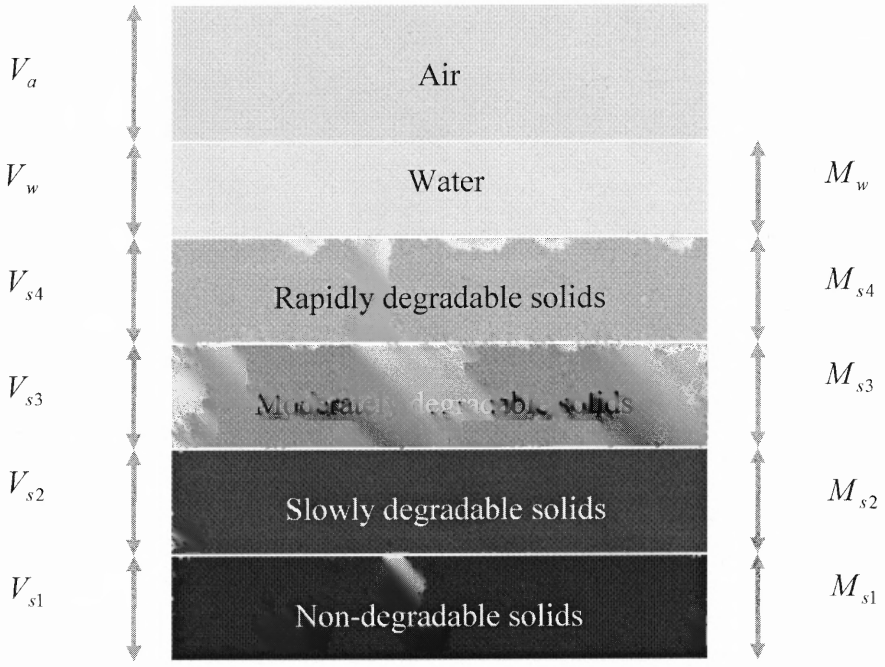

Figure 3.4 Phase diagram for waste.

$$\frac{dM_{sj}}{dt} = -\lambda_j M_{sj} \tag{3.5}$$

$$M_{sj} = M_{sj,i} \exp(-\lambda_j t) \tag{3.6}$$

If the initial solids fraction for each waste group is $f_{sj} = \left(M_{sj,i} / M_{si}\right)$, then the total solid waste mass can be expressed as;

$$M_s(t) = M_{si} \sum_{j=1}^{4} f_{sj} \exp(-\lambda_j t) \tag{3.7}$$

Volume of the waste solids can be computed as shown in Equation 3.8, where G_{sj} is the specific gravity of the j^{th} group of the waste solids and ρ_w (kg/m^3) is the density of water.

$$Z_s(t) = \frac{M_{si}}{\rho_w} \sum_{j=1}^{4} \frac{f_{sj}}{G_{sj}} \exp(-\lambda_j t) \tag{3.8}$$

Equation 3.8 is used to find the change in volume due to decay of waste solids (δV_s) as described in the following sections.

3.3.3 Total Volume and Settlement

The total volume of a waste element is controlled by the waste skeleton comprised of the solid phase. Mechanical compression and biodegradation produce changes in the volume of the solid phase resulting in settlements. The height (total volume) at a given time can be found by subtracting these changes in volume due to each mechanism from the initial volume as:

$$Z(t) = Z_i - \delta Z_s - Z_i C^* \log\left(\frac{\sigma' + \delta\sigma'}{\sigma'}\right) \tag{3.9}$$

3.3.4 Volume of Liquids and Gases

Voids in the solids skeleton is shared by both liquids and gases. The concept of volumetric water content can be used to determine the change in the volume of liquid phase. Volumetric water content (θ) is defined as the ratio of volume of water to total volume. Therefore, volume of water present in waste can be defined as:

$$Z_w(t) = \theta(t) Z(t) \tag{3.10}$$

Since the volume of the solids and liquids can be found independently, if the total volume is known, volume occupied by gas can be found by subtracting solids and water volumes from total volume (Equation 3.11).

$$Z_g(t) = Z(t) - Z_s(t) - \theta(t)Z(t) \tag{3.11}$$

3.4 Generation and Dissipation of Landfill Gas Pressure

The gas pressure is expected to build in the waste element due to generation of landfill gas as a result of biodegradation. Equations for rate of generation of gas and a general governing equation that couples gas pressure with settlement process are developed in the following sections.

3.4.1 Rate of Landfill Gas Generation

Since the only source of gas generation is degradable mass, the rate of biodegradation should be proportional to negative rate of gas production. The rate of generation of gas per unit volume $G(t)$ can be expressed as follows, where C_0 is the proportionality constant.

$$G(t) = -C_0 \frac{1}{Z} \frac{\partial M_s}{\partial t} \tag{3.12}$$

$$G(t) = C_0 \frac{M_{si}}{Z} \sum_{j=1}^{4} f_{sj} \lambda_j \exp(-\lambda_j t) \tag{3.13}$$

Because of the negative exponential in Equation 3.13, mathematically, the maximum rate of degradation occurs when the time is zero. However, this is unlikely in reality and the peak rate of generation has usually been observed some time after the placement of waste (Findikakis et al. 1988). Therefore, a linear increase is assumed until it reaches the peak rate, which is quantitatively equivalent to $G(0)$ from Equation 3.13. Considering these facts, the rate of gas generation is modified as:

$$G(t) = C_0 \frac{M_{si}}{Z} \begin{cases} \left(\sum_{j=1}^{4} f_{sj}\lambda_j\right)\left(\frac{t}{t_0}\right) & ;t \le t_0 \\ \sum_{j=1}^{4} f_{sj}\lambda_j \exp\left(-\lambda_j\left(t-t_0\right)\right) & ;t > t_0 \end{cases} \tag{3.14}$$

The value of C_0 can be approximated by taking the concept of gas generation potential into account. Gas generation potential is usually defined as the volume of gas a unit mass of waste could produce and it is denoted by L_0 (m^3/kg). Since Equation 3.14 is based on mass generated per unit volume of waste, L_0 has to be converted to its corresponding mass. Using ideal gas law (assuming an average molar mass of 30 g) and it can be showed that a 1 m^3 of landfill gas mixture weighs approximately 0.86 kg at atmospheric pressure and 42^{0}C (selected landfill temperature). To establish a relationship between L_0 and C_0, Equation 3.14 is integrated for its entire time span considering the waste volume at the time of placement. It should be noted that a unit volume of waste at the time of placement weighs, ρ_c (kg) and the decay constant of solid group one is zero.

$$\int_0^{\infty} G(t)dt = C_0 \frac{M_{si}}{Z_i}\left(\sum_{j=1}^{4} f_{sj}\lambda_j\right)\int_0^{t_0}\left(\frac{t}{t_0}\right)dt + C_0 \frac{M_{si}}{Z_i}\int_{t_0}^{\infty}\sum_{j=1}^{4} f_{sj}\lambda_j \exp\left(-\lambda_j\left(t-t_0\right)\right)dt$$

$$0.86L_0\rho_c = C_0\rho_c\left(\sum_{j=1}^{4} f_{sj}\lambda_j\right)\int_0^{t_0}\left(\frac{t}{t_0}\right)dt + C_0\rho_c\int_{t_0}^{\infty}\sum_{j=1}^{4} f_{sj}\lambda_j \exp\left(-\lambda_j(t-t_0)\right)dt$$

$$0.86L_0 = C_0\left(\sum_{j=2}^{4} f_{sj}\lambda_j\right)\left(\frac{t_0}{2}\right) + C_0\left(\sum_{j=2}^{4} f_{sj}\right) \approx C_0\left(\sum_{j=2}^{4} f_{sj}\right)$$

$$C_0 = \frac{0.86L_0}{\left(\sum_{j=2}^{4} f_{sj}\right)} \tag{3.15}$$

3.4.2 Mass Balance for Gases

Considering the amount of gas present in a unit volume of landfill the overall mass balance can be established in the following manner.

$$\begin{pmatrix}\text{Rate of change of mass of gas}\\ \text{in the waste element}\end{pmatrix} = \begin{pmatrix}\text{Gass flux rate through}\\ \text{the waste element}\end{pmatrix} + \begin{pmatrix}\text{Rate of gas generation}\\ \text{within the waste element}\end{pmatrix}$$

$$\left(\frac{1}{Z}\frac{\partial M_g}{\partial t}\right) = -\frac{\partial}{\partial z}\left(\rho_g v_g - D\frac{\partial C_g}{\partial z}\right) + G(t) \tag{3.16}$$

Where, ρ_g (kg/m^3) is the density of the landfill gas in the element, v_g (m/day) is the gas velocity, D (m^2/day) is the diffusion coefficient, C_g (kg/m^3) is the concentration of landfill gas, and $G(t)$ is the rate of generation of gas per unit volume of waste (kg/m^3/day).

Velocity of landfill gas is calculated using Darcy's equation as given in Equation 3.17, where k_g (m/s) is the gas conductivity of waste, P_a (N/m^2) is the atmospheric

pressure, and p (N/m^2) is the pressure beyond atmospheric pressure (or relative pressure).

$$v_g = -k_g \frac{\partial}{\partial z}\left(\frac{1}{\rho_g g}(P_a + p) + z\right) \tag{3.17}$$

Mass of gas present in the waste element (Equation 3.18) and its density or concentration (Equation 3.19) can be estimated using the ideal gas law.

$$M_g = \frac{m}{RT}(P_a + p)Z_g \tag{3.18}$$

$$\rho_g = C_g = \frac{m}{RT}(P_a + p) \tag{3.19}$$

Where, R (J/mol/K) is the universal gas constant, m (kg) is the molar mass of the landfill gas, and T is the average landfill temperature in Kelvin. A general governing equation, which links landfill gas pressure to settlement can be obtained by combining Equations 3.16 through 3.19 as:

$$\frac{\partial p}{\partial t} + (P_a + p)\frac{\partial}{\partial t}(\ln Z_g) = \left(\frac{Z}{Z_g}\right)\left(k_g \frac{\partial p}{\partial z} + D\frac{\partial^2 p}{\partial z^2} + \frac{RT}{m}G\right) \tag{3.20}$$

3.5 Distribution of Moisture

The amount of moisture present in the waste plays a significant role in the settlement process. The efficiency of dissipation of gases depends on the percentage of voids space available for the transport of gaseous products. Therefore, moisture distribution has to be

coupled with the settlement process. However, moisture profile of a bioreactor landfill is highly site specific due to the arrangement and frequency of leachate recirculation.

3.5.1 Leachate Flow in Unsaturated Waste

Richards equation can be used to estimate the spatial and temporal variation of volumetric moisture content (θ) with respect to matric potential (h) in an unsaturated medium. Combination of Darcy's law and the principle of conservation of mass results in the Richards equation, which in the vertical dimension (sign convention for z here is upward positive) can be written as:

$$\frac{\partial \theta}{\partial t} = \frac{\partial}{\partial z}\left(k_w \frac{\partial h}{\partial z}\right) + \frac{\partial k_w}{\partial z} - S_w(t) \tag{3.21}$$

Where, S_w represents a sink used to extract water from the system, which is analogous to a leachate removal system in a biocell landfill.

3.5.2 Matric Potential and Hydraulic Conductivity of Waste

Van Genutchen Model (van Genutchen, 1980), which presented both matric potential (h) and unsaturated hydraulic conductivity (k_w) as functions of volumetric water content (θ) has been widely used in solving Richards equation. These relationships are used to solve the Richards equation in this research and hence they are briefly introduced herein. Van Genutchen equations to determine h and k_w can be written as:

$$h(\theta) = -\frac{1}{\alpha}\left((S_e)^{(-1/m)} - 1\right)^{1/n} \tag{3.22}$$

$$k_w(\theta) = k_{ws}(S_e)^p\left(1-\left(1-(S_e)^{1/m}\right)^m\right)^2 \tag{3.23}$$

Where, $\alpha\left(m^{-1}\right)$, n, $m(=1-1/n)$, and p are model parameters, which can be considered as constants for a given porous media. k_{ws} (m/day) is the saturated hydraulic conductivity of the porous medium. Effective saturation, S_e is defined as in the Equation 3.24, where θ_s and θ_r are saturated moisture content and residual moisture content of the porous media, respectively.

$$S_e = \left(\frac{\theta-\theta_r}{\theta_s-\theta_r}\right) \tag{3.24}$$

3.6 Coupling Gas Pressure and Moisture with Settlement

When settlement process is coupled with gas generation and dissipation and moisture distribution, there are some important points where they interact with each other. These issues are briefly addressed in the next few sections.

3.6.1 Variable Height of the Waste

Changing heights of the waste layers caused by waste settlement has to be taken in to consideration when the equations are solved for gas pressure and moisture distribution. Although the Richards and Van Genuchten's equations are not intended to be used for changing heights, it is assumed that they could provide reasonably accurate results in this case.

3.6.2 Pressure Correction in Effective Stress

When gas pressure values are available, the effective stress term in the settlement calculations should be corrected as in Equation 3.25, where σ (N/m^2) is the total stress.

$$\sigma' = \sigma - p \tag{3.25}$$

3.6.3 Variable Gas Conductivity

Because of the presence of liquids in the waste voids, only a fraction of the void space is available for gas movement. Therefore, the unsaturated gas conductivity varies with the amount of water present in the waste element. Scanlon et al. (2002) derived an equation similar to Equation 3.23 for gas conductivity by replacing the effective saturation in the Van Genuchten's equation by $(1 - S_e)$.

$$k_g(\theta) = k_{gs}(1 - S_e)^p \left(1 - \left(1 - (1 - S_e)^{1/m}\right)^m\right)^2 \tag{3.26}$$

Where, k_{gs} (m/day) is the saturated gas conductivity of the porous medium.

3.6.4 Saturated Moisture Content

Due to the varying nature of the porous media, saturated moisture content does not remain as a constant. Variable saturated volumetric moisture content can be calculated from Equation 3.27.

$$\theta_s(t) = 1 - \frac{Z_s(t)}{Z(t)} \tag{3.27}$$

CHAPTER 4

NUMERICAL SOLUTION

4.1 Introduction

This chapter describes the solution technique used in this research. In the absence of a closed-form analytical solution, numerical techniques were used to solve the governing equations, which provide the settlement of a biocell landfill coupled with generation and dissipation of gas pressures and moisture distribution. Explicitly computed settlement and moisture values were then used to find an implicit solution for the governing equation for gas pressure. A computer program was developed using MATLAB to implement this procedure of numerical solution and the code is included in the Appendix.

Detailed explanations of numerical solution for each governing equation are given in the following sections. The subscript 'k' and the superscript 'l' denote space (grid point) and time (time steps), respectively.

4.2 Settlement Computations

The idealized landfill cross-section considered in the numerical computations is given in Figure 4.1. It is assumed that each waste layer (or lift) comprise a constant initial height and placement density. It is also assumed that each layer has undergone an immediate mechanical compression governed by the stress-strain relationship presented in Equation 3.4.

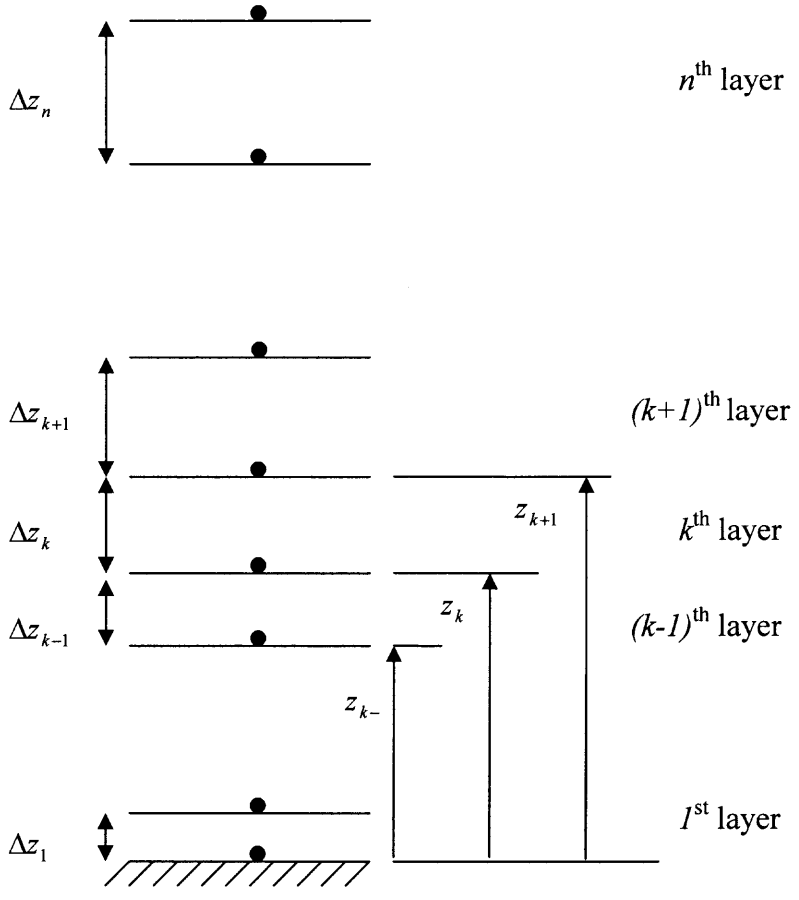

Figure 4.1 Idealized landfill cross-section considered in the numerical analysis.

Initial height of the k^{th} waste layer is calculated as given in Equation 4.1, where Δz_i (m) is the initial layer thickness, C_{c1} is the compression ratio for fresh waste, ρ_c (kg/m^3) is the dry density of waste at the time of placement (or compaction density), ρ_s (kg/m^3) and Δz_s (m) are the density and thickness of the final top cover, respectively.

$$(\Delta z)_k^1 = \Delta z_i - \Delta z_i (C_{c1}^*) \log\left(n - (k-1) + \frac{\rho_s \Delta z_s}{\rho_c \Delta z_i} \right) \tag{4.1}$$

Total mass of k^{th} waste layer and the effective stress at the k^{th} node for the $(l+1)^{th}$ time step are calculated as shown below, where g (m/s^2) is acceleration due to gravity and $(g/1000)$ is used to convert the units from Pa to kPa.

$$M_k^{l+1} = (\rho_c \Delta z_i)\sum_{j=1}^{4} f_{sj} \exp(-\lambda_j (l\Delta t)) + \rho_w \left(\frac{\theta_k^l + \theta_{k+1}^l}{2}\right)(\Delta z)_k^l \tag{4.2}$$

$$(\sigma')_k^{l+1} = \left(\frac{g}{1000}\right)\left(\sum_{j=k}^{n} M_k^{l+1} + \rho_s \Delta z_s\right) - p_k^{l+1} \tag{4.3}$$

Thickness of the k^{th} waste layer for the $(l+1)^{th}$ time step and the selection of the compressibility parameters are presented as:

$$(\Delta z)_k^{l+1} = (\Delta z)_k^l - \left((\Delta z_s)_k^l - (\Delta z_s)_k^{l+1}\right) - \Delta z_i C^* \log\left(\frac{(\sigma')_k^{l+1}}{(\sigma')_k^l}\right) \tag{4.4}$$

C^* is the compressibility parameter introduced in Chapter 3 (Equation 3.3).

$$C^* = \begin{cases} C_c^* \ ; (\sigma')_k^{l+1} > (\sigma')_k^{l+1} \\ C_s^* \ ; (\sigma')_k^{l+1} < (\sigma')_k^{l+1} \end{cases} \tag{4.5}$$

In this research, time dependency of compressibility is taken into consideration and hence, a suitable value should be selected depending on the age of the waste (or state of biodegradation). The selection procedure is explained in Equations 4.6 and 4.7.

$$C_c^* = \begin{cases} C_{c1}^* \ ; (l\Delta t) < 200 \text{ days} \\ C_{c2}^* \ ; 200 \text{ days} < (l\Delta t) < 2{,}000 \text{ days} \\ C_{c3}^* \ ; 2{,}000 \text{ days} < (l\Delta t) < 20{,}000 \text{ days} \\ C_{c4}^* \ ; (l\Delta t) > 20{,}000 \text{ days} \end{cases} \tag{4.6}$$

$$C_s^* = \begin{cases} C_{s1}^* & ; (l\Delta t) < 200 \text{ days} \\ C_{s2}^* & ; 200 \text{ days} < (l\Delta t) < 2{,}000 \text{ days} \\ C_{s3}^* & ; 2{,}000 \text{ days} < (l\Delta t) < 20{,}000 \text{ days} \\ C_{s4}^* & ; (l\Delta t) > 20{,}000 \text{ days} \end{cases} \tag{4.7}$$

Heights of each phase in the k^{th} waste layer for the $(l+1)^{th}$ time step can be calculated using the following equations, where ρ_w (kg/m^3) is the density of liquids in the landfill and it is assumed to be equal to density of water.

$$(\Delta z_s)_k^{l+1} = \left(\frac{\rho_c \Delta z_i}{\rho_w}\right) \sum_{j=1}^{4} \left(\frac{f_{sj}}{G_{sj}}\right) \exp\left(-\lambda_j (l\Delta t)\right) \tag{4.8}$$

$$(\Delta z_w)_k^{l+1} = \left(\frac{\theta_k^l + \theta_{k+1}^l}{2}\right) (\Delta z)_k^{l+1} \tag{4.9}$$

$$(\Delta z_g)_k^{l+1} = (\Delta z)_k^l - (\Delta z_s)_k^{l+1} - (\Delta z_w)_k^{l+1} \tag{4.10}$$

4.3 Gas Pressure Computations

The governing equation for mass balance of gases (Equation 3.20) is solved implicitly using finite difference approximations and finite grid with variable non-uniform grid spacing (Figure 4.2). The central difference scheme is used in determining space derivatives and hence a second order accuracy is expected with respect to space (Hoffman, 2001). The stencil used for developing implicit numerical solution is shown in Figure 4.3.

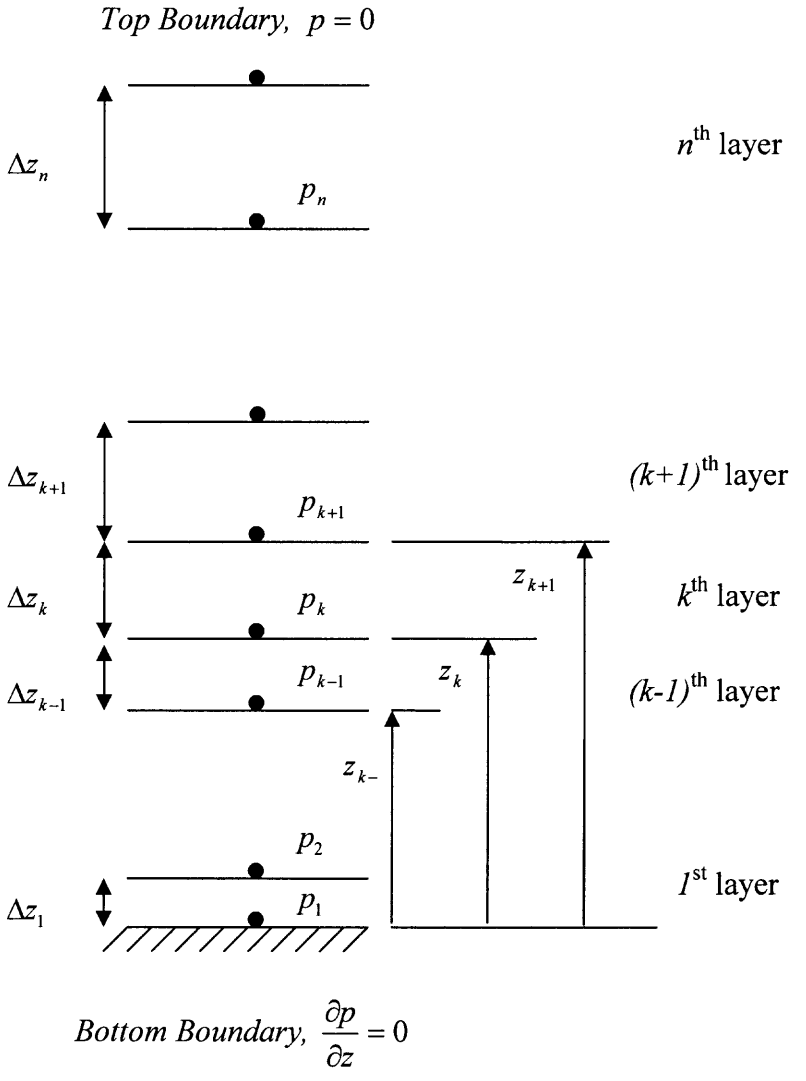

Figure 4.2 Computation grid and the boundary conditions for pressure equation.

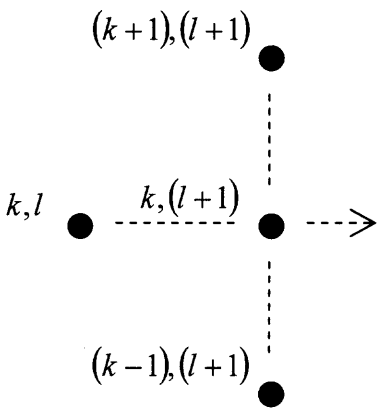

Figure 4.3 The stencil used for implicit numerical pressure calculations.

4.3.1 Finite Difference Approximations for the Pressure Equation

The time derivative of pressure (p) and $\ln Z_g$ are approximated using forward time (FT) scheme as shown in following equations (Hoffman, 2001).

$$\left(\frac{\partial p}{\partial t}\right)_k^{l+1} = \frac{p_k^{l+1} - p_k^l}{\Delta t} \tag{4.11}$$

$$\left(\frac{\partial}{\partial t}\ln Z_g\right)_k^{l+1} = \frac{1}{\Delta t}\ln\frac{(\Delta z_g)_k^l}{(\Delta z_g)_k^{l-1}} \tag{4.12}$$

The space derivatives are approximated using center space (CS) scheme. Since the space in not uniform and layer thicknesses vary with time, explicitly computed 'Δz' are used in the denominator.

$$\left(\frac{\partial p}{\partial z}\right)_k^{l+1} = \frac{p_{k+1}^{l+1} - p_{k-1}^{l+1}}{\Delta z_{k-1}^l + \Delta z_k^l} \tag{4.13}$$

$$\left(\frac{\partial^2 p}{\partial z^2}\right)_k^{l+1} = \frac{\left(\frac{p_{k+1}^{l+1} - p_k^{l+1}}{\Delta z_k^l}\right) - \left(\frac{p_k^{l+1} - p_{k-1}^{l+1}}{\Delta z_{k-1}^l}\right)}{0.5\left(\Delta z_{k-1}^l + \Delta z_k^l\right)} \tag{4.14}$$

Following pressure equation is generated by substituting Equations 4.11 through 4.14 in Equation 3.19.

$$\left(a_k^{l+1}\right)p_{k-1}^{l+1} + \left(b_k^{l+1}\right)p_k^{l+1} + \left(c_k^{l+1}\right)p_{k+1}^{l+1} = \left(d_k^{l+1}\right) \tag{4.15}$$

The coefficients of Equation 4.15 are defined as follows.

$$a_k^{l+1} = \Delta t\left(\frac{\Delta z}{\Delta z_g}\right)_k^l \left(\frac{\left(k_g\right)_k^l}{\left(\Delta z_{k-1}^l + \Delta z_k^l\right)} - \frac{2D}{\left(\Delta z_{k-1}^l\right)\left(\Delta z_{k-1}^l + \Delta z_k^l\right)}\right) \tag{4.16}$$

$$b_k^{l+1} = 1 + \ln\frac{\left(\Delta z_g\right)_k^l}{\left(\Delta z_g\right)_k^{l-1}} + \Delta t\left(\frac{\Delta z}{\Delta z_g}\right)_k^l \frac{2D}{\left(\Delta z_{k-1}^l\right)\left(\Delta z_k^l\right)} \tag{4.17}$$

$$c_k^{l+1} = -\Delta t\left(\frac{\Delta z}{\Delta z_g}\right)_k^l \left(\frac{\left(k_g\right)_k^l}{\left(\Delta z_{k-1}^l + \Delta z_k^l\right)} + \frac{2D}{\left(\Delta z_{k-1}^l + \Delta z_k^l\right)\left(\Delta z_k^l\right)}\right) \tag{4.18}$$

$$d_k^{l+1} = p_k^l + \Delta t\left(\frac{\Delta z}{\Delta z_g}\right)_k^l RTG_k^l - P_a \ln\frac{\left(\Delta z_g\right)_k^l}{\left(\Delta z_g\right)_k^{l-1}} \tag{4.19}$$

4.3.2 Correction of Pressure due to Movement of the Nodes

Due to the continuing process of settlement, k^{th} node also settles with time and hence a correction has to be applied to the pressure from the previous time step $\left(p_k^l\right)$ used in Equation 4.19. Linear pressure variation is assumed between two consecutive nodes to

find the corrected pressure at the k^{th} node by linear interpolation. The correction procedure is illustrated in Figure 4.4 and the mathematical expression is presented in Equation 4.20, where $\bar{p}_k^l$ (N/m^2) is the corrected pressure.

$$\bar{p}_k^l = p_k^l + \left(p_{k-1}^l - p_k^l\right)\left(\frac{\sum_{j=1}^{k-1}\left(\Delta z_j^l - \Delta z_j^{l+1}\right)}{\Delta z_{k-1}^l - \sum_{j=1}^{k-1}\left(\Delta z_j^l - \Delta z_j^{l+1}\right)}\right) \tag{4.20}$$

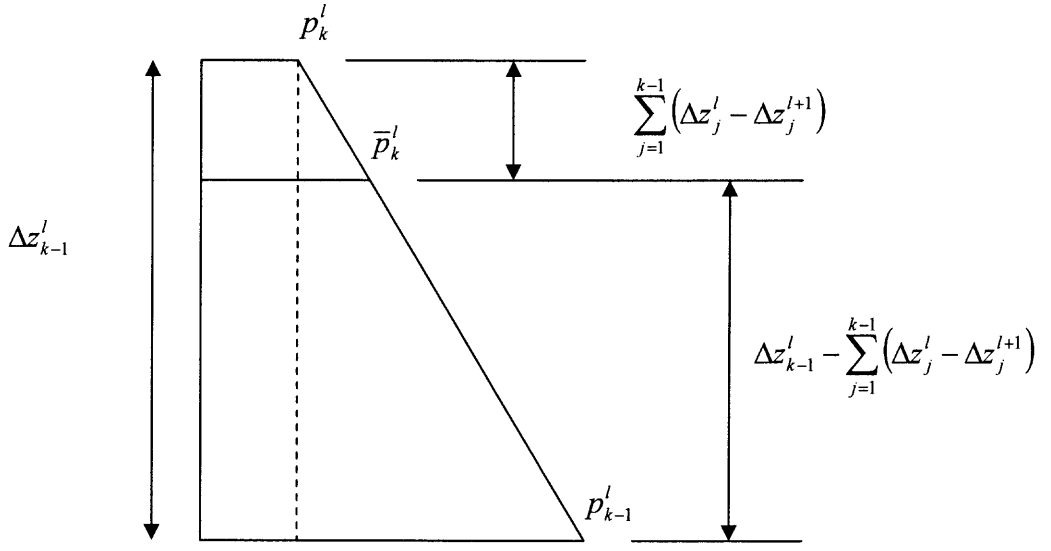

$$\frac{\bar{p}_k^l - p_k^l}{p_{k-1}^l - p_k^l} = \frac{\sum_{j=1}^{k-1}\left(\Delta z_j^l - \Delta z_j^{l+1}\right)}{\Delta z_{k-1}^l - \sum_{j=1}^{k-1}\left(\Delta z_j^l - \Delta z_j^{l+1}\right)}$$

Figure 4.4 Correction of pressure due to the movement of the nodes.

4.3.3 Numerical Approximation of the Rate of Gas Generation

The rate of gas generation $\left(G_k^l\right)$ term in Equation 4.19 is numerically approximated as follows:

$$G_k^{l+1} = C_0 \frac{M_{si}}{0.5\left(\Delta z_k^l + \Delta z_{k-1}^l\right)} \begin{cases} \left(\sum_{j=1}^{4} f_{sj}\lambda_j\right)\left(\frac{l\Delta t}{t_0}\right) & ; \ (l\Delta t) \le t_0 \\ \sum_{j=1}^{4} f_{sj}\lambda_j \exp(-\lambda_j(t_0 - l\Delta t)) & ; \ (l\Delta t) > t_0 \end{cases} \tag{4.21}$$

4.3.4 Boundary Conditions for the Pressure Equation

It is assumed that the upper boundary always remain at atmospheric pressure irrespective of the downward movement of top surface due to settlement. Therefore, the relative pressure at the top boundary is always zero.

$$p_{n+1}^{l+1} = 0 \tag{4.22}$$

Two types of boundary conditions are considered for the bottom. In general, bottom of the landfill is assumed to be comprised of an impermeable boundary. Therefore, a no gas flow condition can be imposed at the bottom node.

$$\left(\frac{\partial p}{\partial z}\right)_2^{l+1} = \frac{p_3^{l+1} - p_1^{l+1}}{\Delta z_1^l + \Delta z_2^l} = 0 \tag{4.23a}$$

In case the bottom is equipped with a gas extraction point, pressure at the bottom is expected to maintain at the atmospheric. For this, a special zero pressure condition is imposed at the bottom.

$$p_1^{l+1} = 0 \tag{4.23b}$$

4.4 Moisture Content Computations

The governing equation for the distribution of moisture (Equation 3.21) is solved explicitly using finite difference approximations and finite grid with variable non-uniform grid spacing (Figure 4.5). The central difference scheme is used in determining space derivatives, thus a second order accuracy is expected with respect to space (Hoffman, 2001). The stencil used in developing explicit numerical solution is shown in Figure 4.6.

4.4.1 Finite Difference Approximations for Richards Equation

The time derivative of moisture content (θ) is approximated using forward time (FT) scheme as shown in Equation 4.14 (Hoffman, 2001).

$$\left(\frac{\partial \theta}{\partial t}\right)_k^{l+1} \frac{\theta_k^{l+1} - \theta_k^l}{\Delta t} \tag{4.24}$$

The space derivatives are approximated using center space (CS) scheme. Since the space is not uniform and layer thicknesses vary with time, explicitly calculated 'Δz' are used in the denominator.

$$\left(\frac{\partial k_w}{\partial z}\right)_k^{l+1} = \frac{(k_w)_{k+1}^l - (k_w)_{k-1}^l}{\left(\Delta z_{k-1}^l + \Delta z_k^l\right)} \tag{4.25}$$

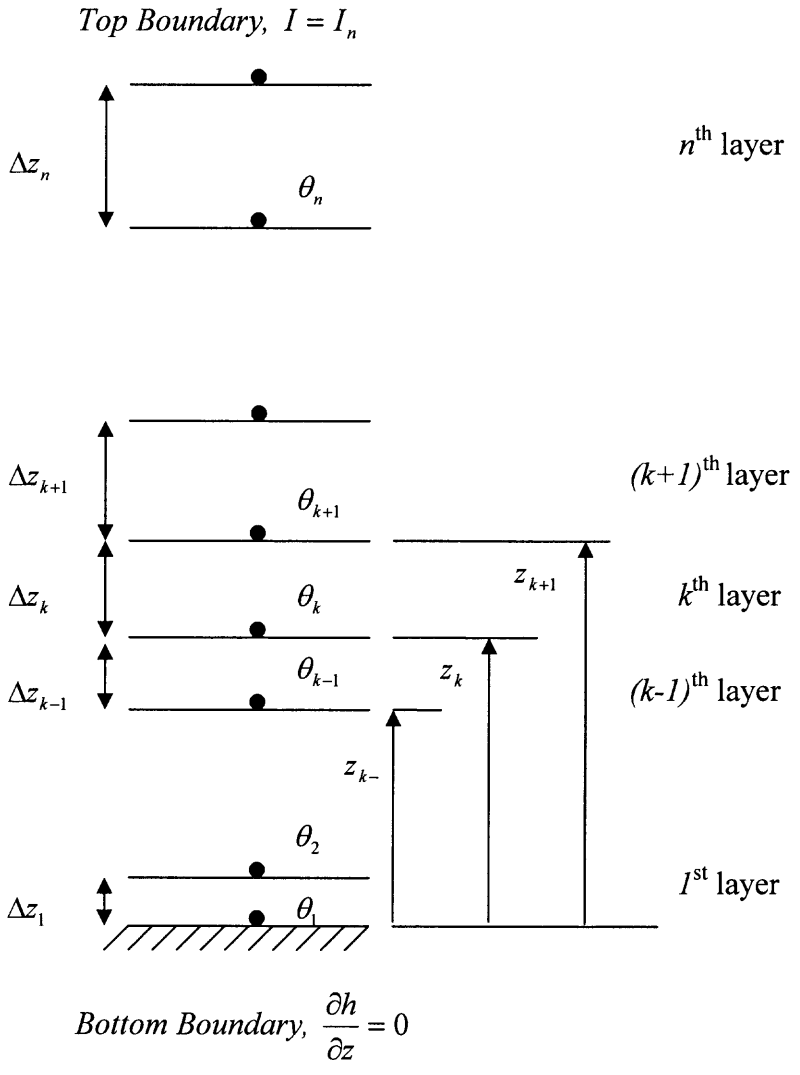

Figure 4.5 Computation grid and the boundary conditions for Richards equation.

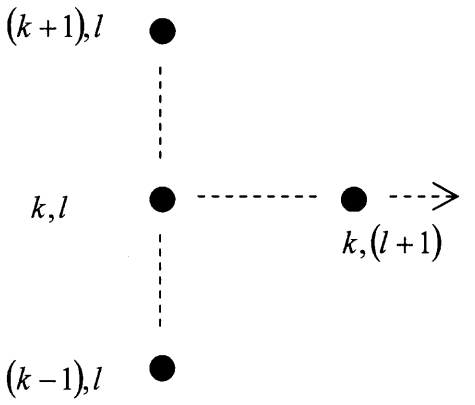

Figure 4.6 The stencil used for explicit numerical moisture calculations.

$$\left(\frac{\partial}{\partial z}\left(k_w\frac{\partial h}{\partial z}\right)\right)_k^{l+1}=\frac{\left(\frac{(k_w)_k^l+(k_w)_{k+1}^l}{2}\right)\left(\frac{h_{k+1}^l-h_k^l}{\Delta z_k^l}\right)-\left(\frac{(k_w)_{k-1}^l+(k_w)_k^l}{2}\right)\left(\frac{h_k^l-h_{k-1}^l}{\Delta z_{k-1}^l}\right)}{0.5\left(\Delta z_{k-1}^l+\Delta z_k^l\right)} \tag{4.26}$$

Following equation for moisture is generated by substituting Equations 4.24 through 4.26 in Equation 3.21.

$$\theta_k^{l+1}=\left(A_k^{l+1}\right)h_{k-1}^l+\left(B_k^{l+1}\right)h_k^l+\left(C_k^{l+1}\right)h_{k+1}^l+\left(D_k^{l+1}\right) \tag{4.27}$$

Coefficients of Equation 4.27 are defined as follows.

$$A_k^{l+1}=\frac{\Delta t\left((k_w)_{k-1}^l+(k_w)_k^l\right)}{\Delta z_{k-1}^l\left(\Delta z_{k-1}^l+\Delta z_k^l\right)} \tag{4.28}$$

$$B_k^{l+1}=-\frac{\Delta t\left((k_w)_k^l+(k_w)_{k+1}^l\right)}{\left(\Delta z_{k-1}^l+\Delta z_k^l\right)\Delta z_k^l}-\frac{\Delta t\left((k_w)_{k-1}^l+(k_w)_k^l\right)}{\Delta z_{k-1}^l\left(\Delta z_{k-1}^l+\Delta z_k^l\right)} \tag{4.29}$$

$$C_k^{l+1} = \frac{\Delta t\left((k_w)_k^l + (k_w)_{k+1}^l\right)}{\left(\Delta z_{k-1}^l + \Delta z_k^l\right)\Delta z_k^l} \tag{4.30}$$

$$D_k^{l+1} = \theta_k^l + \frac{\Delta t\left|(k_w)_{k+1}^l - (k_w)_{k-1}^l\right|}{\left(\Delta z_{k-1}^l + \Delta z_k^l\right)} - \Delta t S^l \tag{4.31}$$

In reality, the amount of moisture retained by waste is decided by its field capacity. Therefore, in the solution, the moisture content computed from Equation 4.27 was subjected to a maximum, which is equal to the filed capacity of waste. It was assumed to reach its field capacity when volumetric moisture content is 60% of the saturated moisture content.

4.4.2 Correction of Moisture Content due to the Compression of the Waste Layer

Moisture content from the previous time step $\left(\theta_k^l\right)$ used in Equation 4.31 is corrected for the compression of the waste layers below and above the calculation point (k^{th} node), between two consecutive time steps. The basis for the correction is the amount of moisture represented by θ_k^l in a volume of $0.5\left(\Delta z_k^l + \Delta z_{k-1}^l\right)$. Correction factor is obtained by redistributing the same amount of liquid in the compressed waste layers. Corrected moisture content at the k^{th} node $\left(\overline{\theta}_k^l\right)$ is given by Equation 4.32, and the correction procedure is illustrated in Figure 4.7.

$$\overline{\theta}_k^l = \left(\frac{\Delta z_k^l + \Delta z_{k-1}^l}{\Delta z_k^{l+1} + \Delta z_{k-1}^{l+1}}\right)\theta_k^l \tag{4.32}$$

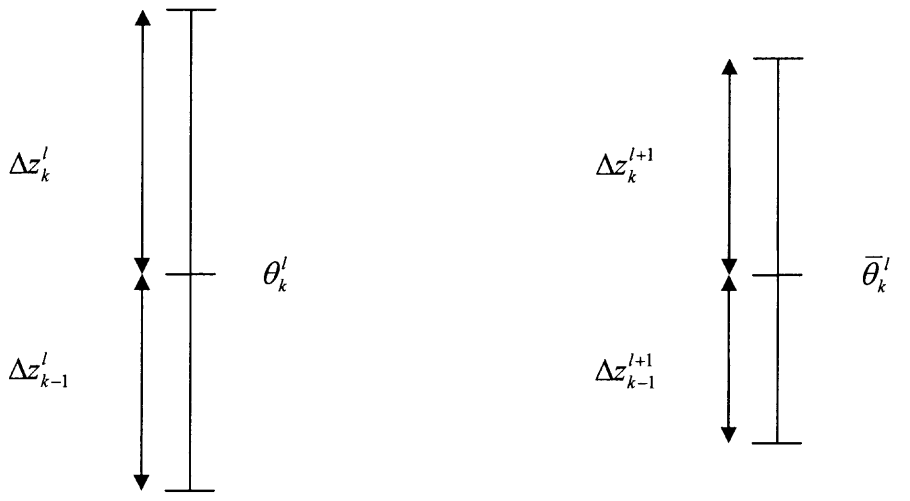

$$0.5\left(\Delta z_k^{l+1} + \Delta z_{k-1}^{l+1}\right)\bar{\theta}_k^l = 0.5\left(\Delta z_k^l + \Delta z_{k-1}^l\right)\theta_k^l$$

Figure 4.7 Correction of pressure due to the movement of the nodes.

4.4.3 Boundary Conditions for Richards Equation

Moisture (leachate) is added to the landfill at the top surface by means of leachate recirculation. This is assumed to be achieved by maintaining a constant head (h_t) at the top surface.

$$h_{n+1}^l = h_t \tag{4.33}$$

A no-flow condition is imposed at the bottom node similar to the pressure problem.

$$\left(\frac{\partial h}{\partial z}\right)_2^{l+1} = \frac{h_3^{l+1} - h_1^{l+1}}{\Delta z_1^l + \Delta z_3^l} = 0 \tag{4.34}$$

When the whole waste mass reaches its intended maximum (i.e. 60% of the saturated moisture content), the excess water was removed from the bottom waste layer using $\Delta t S_w{}^l$ term in Equation 4.31. The excess amount was determined as follows.

$$\Delta t S_w{}^l = \sum_{k=1}^{n} dZ_k^l \left(\frac{\theta_k^l + \theta_{k+1}^l}{2} \right) - \sum_{k=1}^{n} dZ_k^l (\theta_s)_k^l \; > \; 0 \qquad (4.35)$$

Field capacity is a function of compaction (Qian et al. 2002). Because an exact relationship for the field capacity was unable to find, the field capacity and total porosity values reported for individual soils were investigated. The ratio between field capacity and total porosity (≈saturated moisture content) changes from 0.50-0.77 with an average of 0.61 with a standard deviation of 25%. Due to the unavailability of a comprehensive research to predict the variation of field capacity with the change of porosity (due to decomposition and compaction), the ratio between field capacity and the total porosity of a given waste mass was selected as 0.6.

CHAPTER 5

COMPRESSIBILITY CHARACTERISTICS OF WASTE: EXPERIMENTAL INVESTIGATION

5.1 Introduction

In order to investigate the compressibility of fresh waste and the variation of compressibility with degradation, experiments were conducted using a simulated waste. This simulated waste was tested to obtain compression characteristics, compaction characteristics and the specific gravity, using standard laboratory procedures.

5.2 Preparation of the Waste Sample

The composition of municipal solid waste (MSW) has been recorded over the years and summarized by United States Environmental Protection Agency (USEPA). The MSW composition considered in this research was taken from USEPA reports (USEPA, 1997) and shown in Table 5.1. The proportions given in Table 5.1 represent dry weight of each component. Some of the components in Table 5.1 had to be replaced by carefully selected substitutes for the sake of repeatability and to avoid biodegradation that could occur during the tests. To simplify the selection of representative material, some components were grouped with others. Considering the silica content in compost, glass percentage was added to the yard waste category. Inorganic wastes and 'other' types of wastes were also grouped with yard waste. Final composition selected for the tests is given in Table 5.2. The materials selected to produce the simulated waste sample are shown in Figure 5.1.

Table 5.1 Typical MSW Composition

Component	Dry weight (%)
Paper & paperbound	39.2
Yard trimming	14.3
Wood	7.1
Plastics	9.1
Metals	7.6
Food waste	6.7
Glass	6.2
Textiles	3.6
Rubber and leather	2.9
Miscellaneous inorganic wastes	1.5
Other	1.8

Source: USEPA (1997)

Table 5.2 Components and Their Percentages of the Simulated Waste

Component	Selected material	Dry weight (%)
Paper & paperbound	A mixture of equal amounts of old newspapers, used photocopy papers and cardboard	39.2
Yard trimming, glass, inorganic waste and other types of waste	Compost which included 75% soil content	23.8
Plastics	Mixture of plastic soda bottles (#1 – Polyethylene Terephthalate or PET), milk containers (#2- High Density Polyethylene HDPE), and baked goods containers (#6- Polystyrene, PS)	9.1
Metals	Scrap steel from a lathe	7.6
Wood	Woodchips	7.1
Food waste	Cooked macaroni	6.7
Textiles	Equal amounts of cotton and polyester	3.6
Rubber and leather	Rubber	2.9

When the simulated waste was developed, every effort was made to keep the maximum particle size under 5 mm in order to minimize the size effects due to particle size. Dry material of each component was weighed according to the weight proportions given in Table 5.2 and mixed to produce the simulated waste sample. Although proper mixing of components is not anticipated in the field, the sample was thoroughly mixed manually to assure reproducibility. A sample of the final product is shown in Figure 5.2.

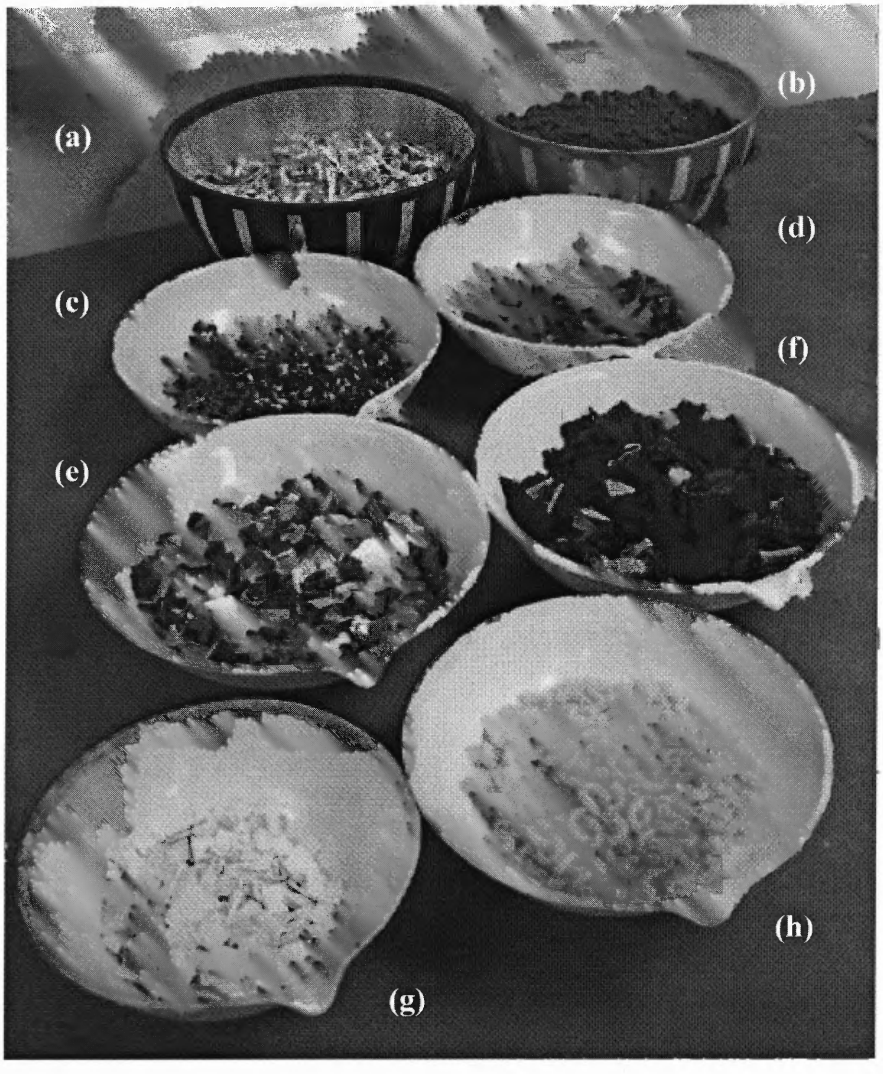

Figure 5.1 Ingredients used in preparing simulated waste; (a) paper, (b) compost, (c) metal, (d) wood chips, (e) plastics, (f) textiles, (g) rubber, (h) cooked macaroni.

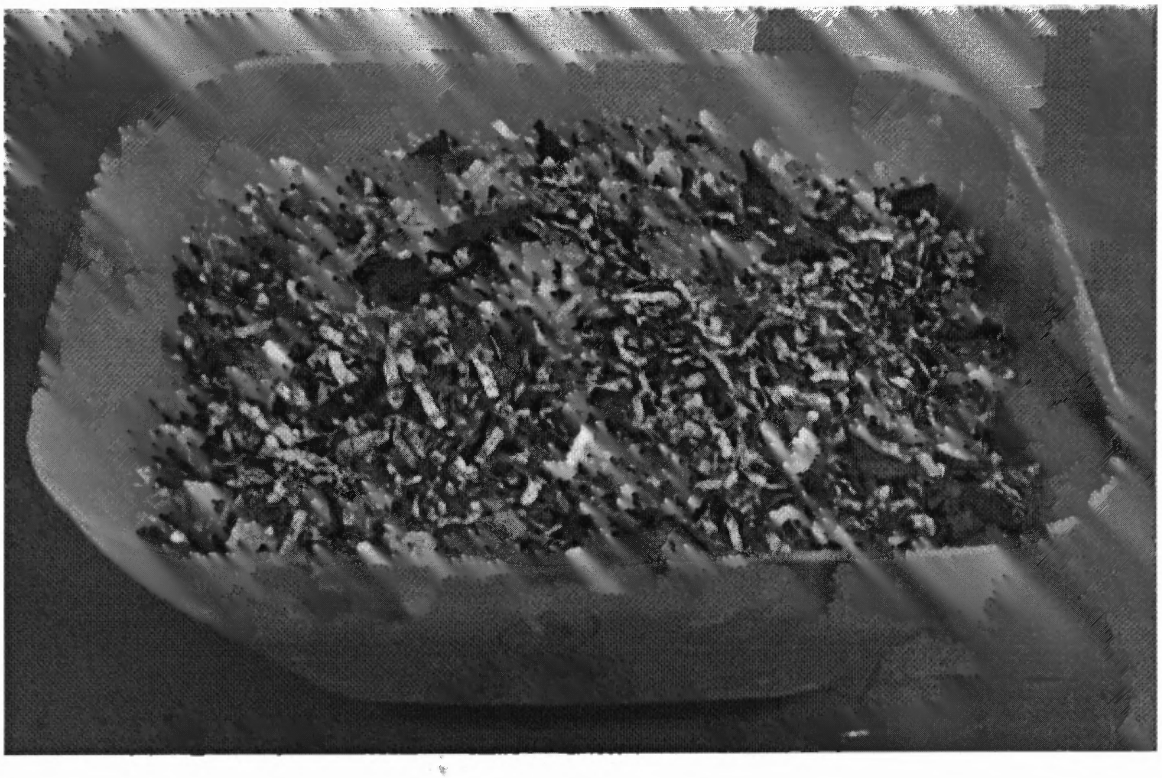

Figure 5.2 A sample of simulated waste.

5.3 Specific Gravity of Simulated Waste

Specific gravity of the simulated waste was found by using the laboratory procedure given in ASTM D-854 (ASTM, 2002). Three samples were prepared using two different mixing methods. Waste sample for Test 1 was specially prepared to ensure the intended mix proportions of different waste components (method 1). Percentages of components of the simulated waste given in Table 5.2 were measured in grams separately and then added to make a sample of 100g for test 1. Waste samples for Tests 2 and 3 were taken from well mixed simulated waste (method 2). The results are given in Table 5.3.

The objective of using two different mixing methods was to see if the mixed waste could produce a representative (fairly homogeneous) mixture of waste. It is evident from Table 5.3 that the specific gravity of the samples taken from mixed waste

(test samples 2 and 3) are close to the specific gravity of the sample made by adding measured amounts of individual waste components (test sample 1).

Table 5.3 Specific Gravity of the Simulated Waste

Test sample description	Specific gravity (G_s)
1 – Components measured individually	1.65
2 – Mixed waste	1.59
3 – Mixed waste	1.67

5.4 Compaction Characteristics of Simulated Waste

Standard Proctor test procedure (ASTM D-698) was used to evaluate the compaction characteristics of simulated waste. The equipment used in the compaction test is shown in Figure 5.3. After determining the initial water content of the waste, a predetermined amount of water was added to the sample so that the first reading can be obtained at desired water content. Sample was thoroughly mixed after adding water and it was kept covered overnight for uniform distribution of moisture.

Two series of compaction tests were conducted to study its compaction behavior. Based on the observations of these trial runs, two more series of tests were performed on the same sample. The results are shown in Figure 5.4. It should be noted that trial-3 was done on a sample, which was used 23 times before trial-3 and trial-5 was done on a sample, which was used 43 times before trial-4. Reuse of the sample caused the waste to increase the maximum dry density as well as the optimum moisture content. As a resul,t the curve shifted more towards the zero air voids line. Therefore, to simulate fresh waste, a new fresh sample was used to obtain each data point in the trial-5 (Figure 5.4). For fresh waste a maximum dry density of 525 kg/m^3 was observed corresponding to an

optimum moisture content (gravimetric) of 60%. These results are presented in Table 5.4.

Reinhart et al. (2002) reported results of compaction tests on synthetic municipal solid waste, which has been prepared according to composition published by in Florida Solid Waste Management Report (Florida Department of Environmental Protection, 1999). Their results also suggested that the maximum compaction occurs approximately at 60% moisture content (gravimetric).

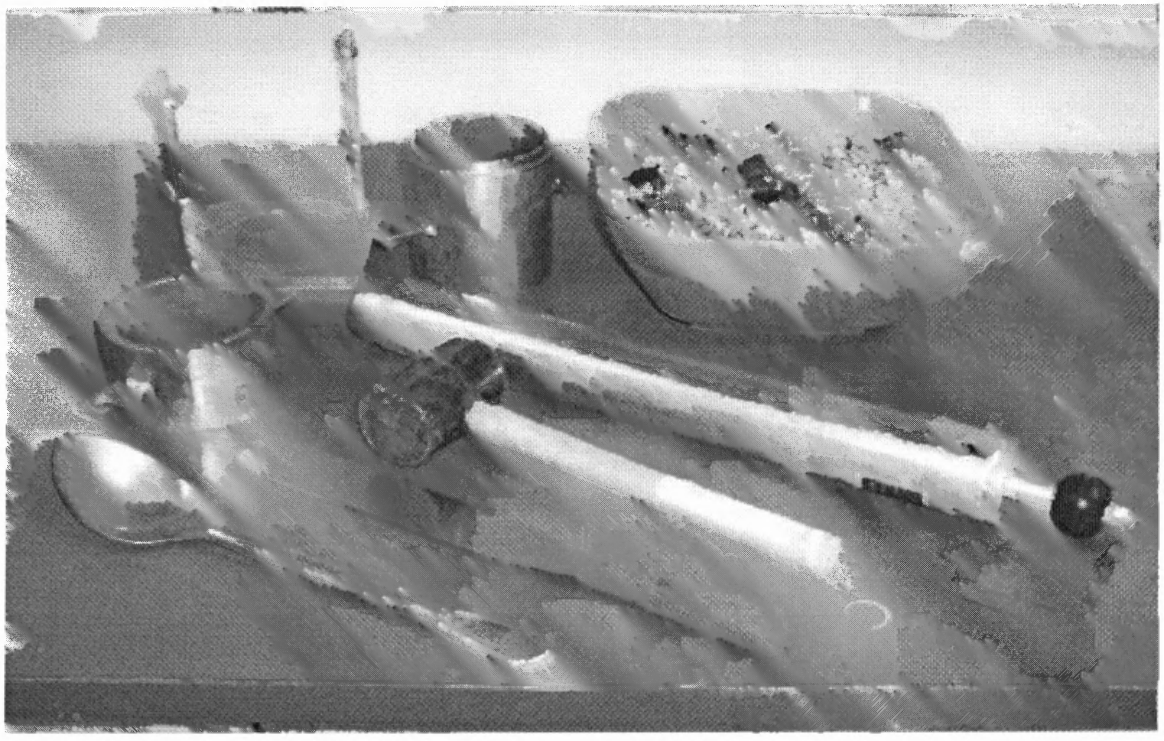

Figure 5.3 Equipment used for the compaction test.

Table 5.4 Compaction Characteristics of Simulated Waste

Test No.	Sample	Maximum dry density (kg /m^3)	Optimum water content (%)
Trial 3	23 times used	580	70
Trial 4	43 times used	610	80
Trial 5	Fresh waste	525	62

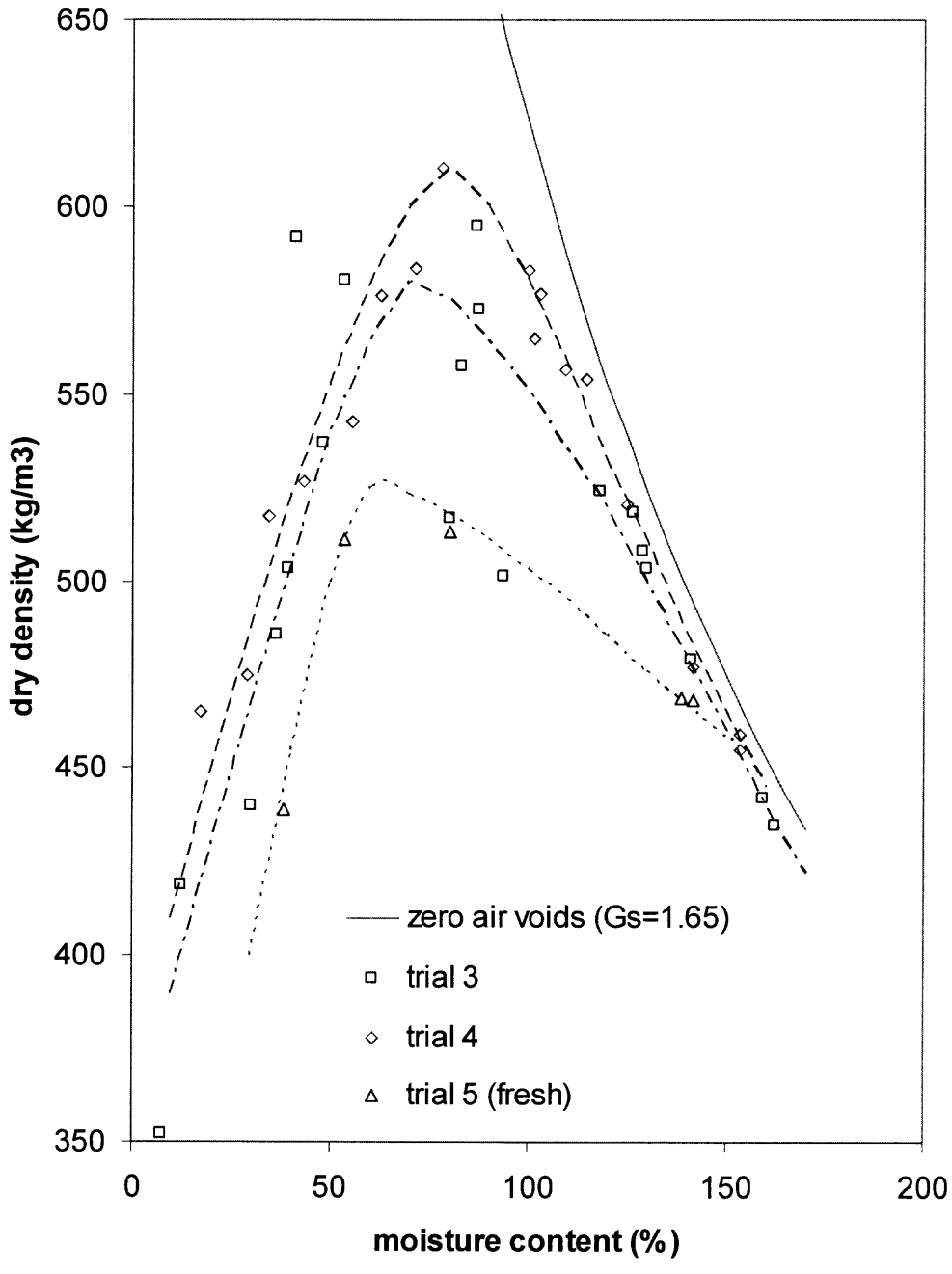

Figure 5.4 Compaction behavior of simulated waste.

5.5 Compressibility Characteristics of Simulated Waste

A compression test (similar to consolidation tests on clay) was designed to study the compressibility characteristics of simulated waste. A Teflon cylinder of 63 mm internal diameter was used as the cell. Initial heights of the samples were maintained in an approximate range of 25-30 mm. Test cell was assembled as shown in Figure 5.5 and a special setup described in Figures 5.6 and 5.7, was used to directly load the sample.

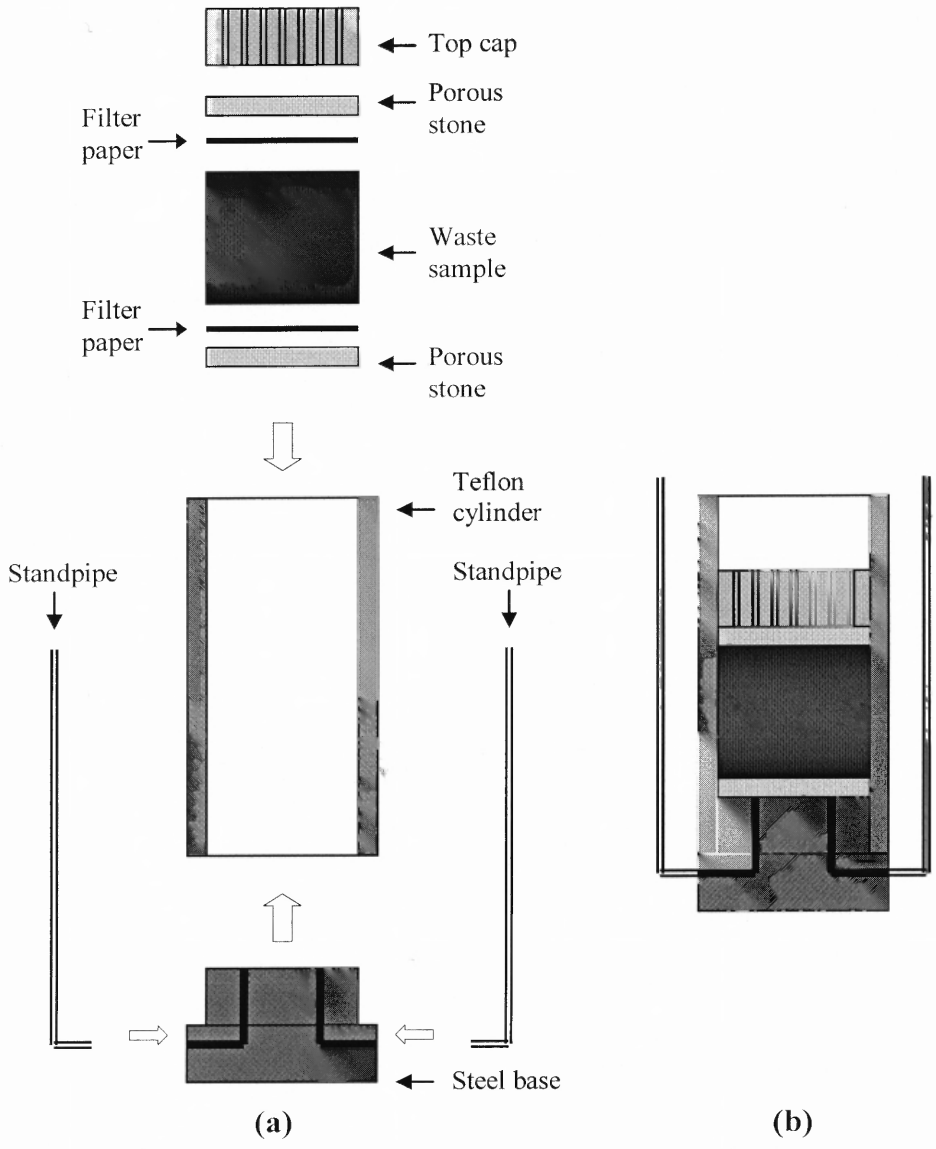

Figure 5.5 (a) Components and (b) assembled cell used for compression test.

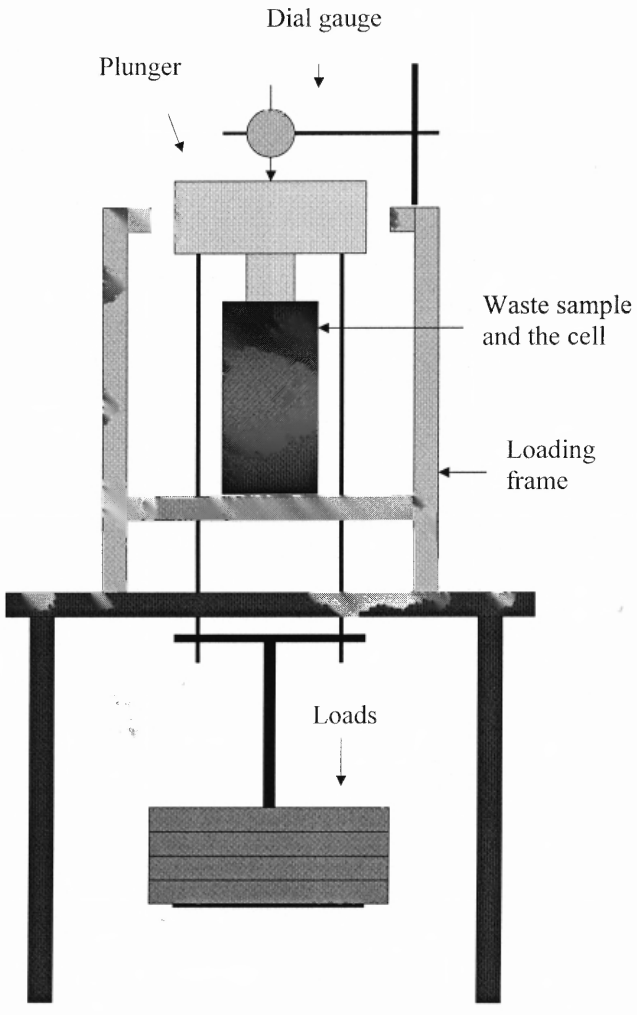

Figure 5.6 Loading setup (not to scale).

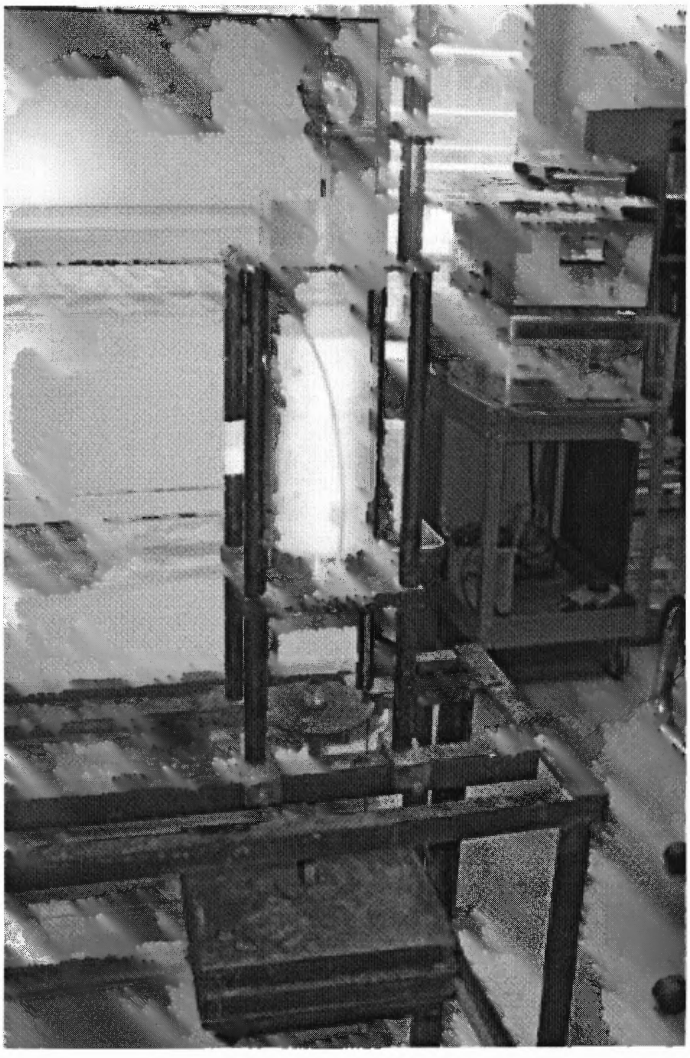

Figure 5.7 A compression test in progress.

5.5.1 Compressibility Characteristics of Simulated Fresh Waste

The test sample was first compacted approximately to the maximum dry density of fresh simulated waste (Figure 5.4) keeping the moisture content close to the optimum value. In order to see the effect of moisture on mechanical compression, two samples were tested simultaneously: 1) water content maintained approximately at its optimum value; 2) cell completely filled with water once loading was started. The initial moisture content of the first sample was maintained by placing moist cloths at the top of the sample to act as a moisture barrier.

The settlement values were recorded using dial gauges. Samples were subjected to each loading levels for 24 hours before it was doubled. A typical time-strain graph is shown in Figure 5.8. Samples were loaded to a maximum of 68.6 kg (stress = 216.1 kPa) in six stages and unloaded in three stages. Stress-strain curve for both cases are compared in Figure 5.9. Compressibility parameters computed from Figure 5.9 are given in Table 5.5.

Table 5.5 Compressibility Characteristics of Simulated Fresh Waste

Test No.	Sample description	Compression Ratio	Swell Ratio (C_s^*)
1	At optimum water content	0.181	0.049
2	Cell filled with water	0.205	0.069

It is interesting to note that although the maximum strain observed in Test 2 was 8.5% higher than the other sample, the irrecoverable strain shown by both samples were similar (21.1% and 19.2%, respectively).

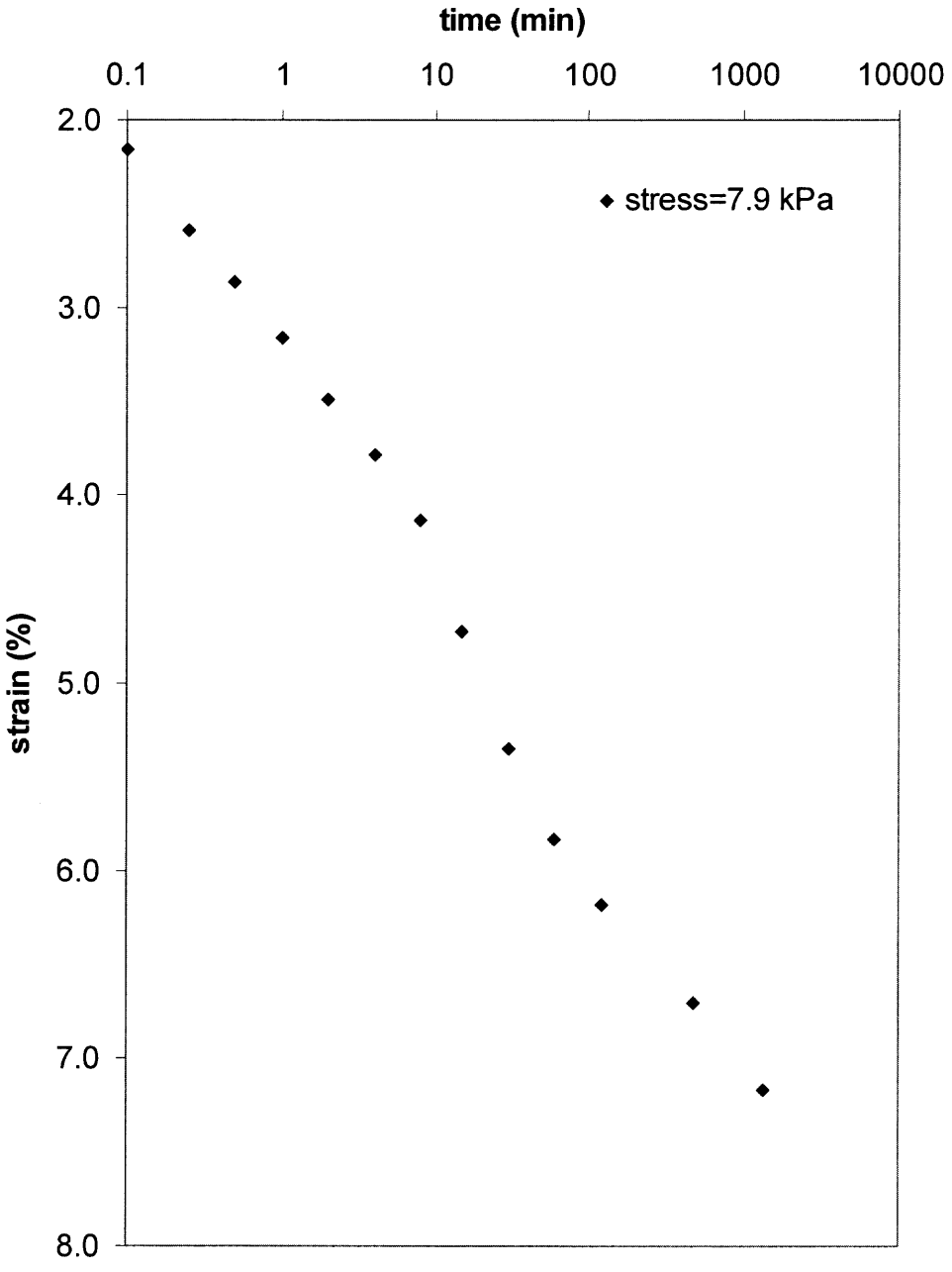

Figure 5.8 Time-strain graph for simulated waste under a load of 7.9 kPa.

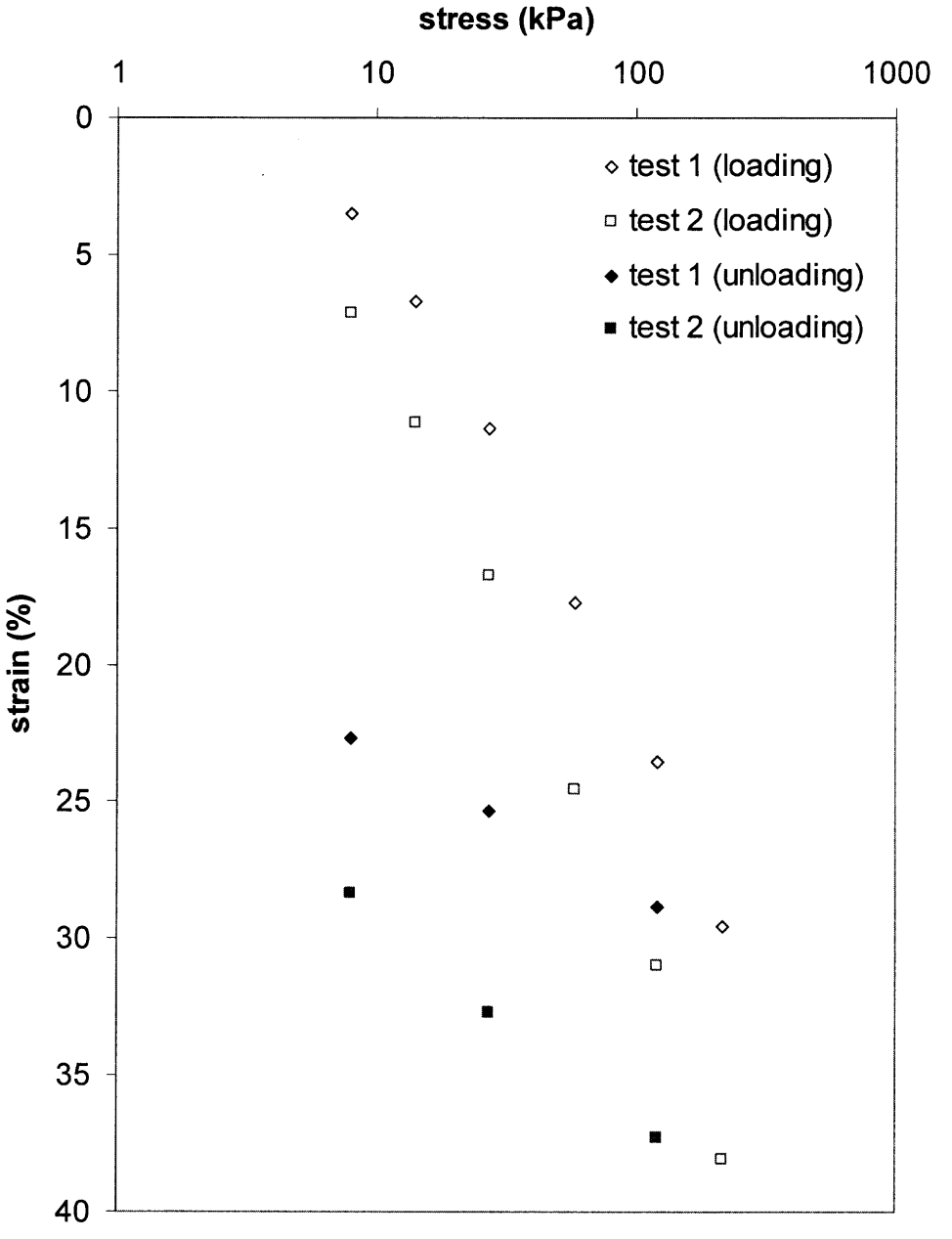

Figure 5.9 Stress-strain behavior of simulated fresh waste.

5.5.2 Variation of Compressibility with Time

Due to the difficulty of obtaining old waste samples, which had original composition similar to the composition given in Table 5.1 (or Table 5.2), 'simulated old waste' samples were developed to simulate old waste. Waste mass remaining after 1,000days, 10,000 days, and 100,000 days were estimated using first order decay equation (Equation 3.6). For this purpose, waste was classified in to four solids groups as suggested in Chapter 3. Decay constants for (1) non-degradable, (2) slowly degradable, (3) moderately degradable, and (4) rapidly degradable waste groups were assumed as 0, 5×10^{-6}, 5×10^{-5}, and 5×10^{-4} day^{-1}, respectively (Findikakis and Leckie, 1979; Arigala et al. 1995). These information together with the adjusted waste compositions used to simulate old waste, are provided in Table 5.6.

Three samples were prepared based on the calculated compositions presented in Table 5.6 to simulate 1,000 days, 10,000 days, and 100,000 days old waste. The samples were then tested for their compressibility characteristics using the procedure explained in the previous section. All cells were filled with water as soon as loading was started. The stress was varied in an approximate range of 5-240 kPa. Results are reported in Figure 5.10 and Table 5.7.

Table 5.6 Calculated Compositions of Old Waste

Description of waste components	Solids group number	Fresh waste (g)	10^3 days old		10^4 days old		10^5 days old	
			(g)	(%)	(g)	(%)	(g)	(%)
Paper and paper bound								
- Slowly biodegradable	2	19.2	18.0	19.2	10.2	14.3	0.0	0.0
- Moderately biodegradable	3	20.0	19.8	21.2	18.3	25.7	8.1	20.8
Combined, represented by compost								
- Yard (Rapidly biodegradable)	4	7.0	4.78	5.1	0.15	0.2	0.0	0.0
- Yard (Slowly biodegradable)	2	7.3	6.85	7.3	3.90	5.5	0.0	0.0
- Glass	1	6.2	6.20	6.6	6.20	8.7	6.2	16.0
- Inorganic	1	1.5	1.50	1.6	1.50	2.1	1.5	3.8
- other	3	1.8	1.78	1.9	1.65	2.4	0.7	1.8
Wood	3	7.1	7.00	7.5	6.49	9.1	2.9	7.5
Plastics	1	9.1	9.10	9.7	9.10	12.8	9.1	23.5
Metal	1	7.6	7.60	8.1	7.60	10.7	7.6	19.6
Food (Cooked macaroni)	4	6.7	4.58	4.9	0.15	0.2	0.0	0
Textile	3	3.6	3.56	3.80	3.29	4.6	1.5	3.9
Rubber	3	2.9	2.87	3.10	2.65	3.7	1.2	3.1
Total		100	93.6	100	71.2	100	38.8	100

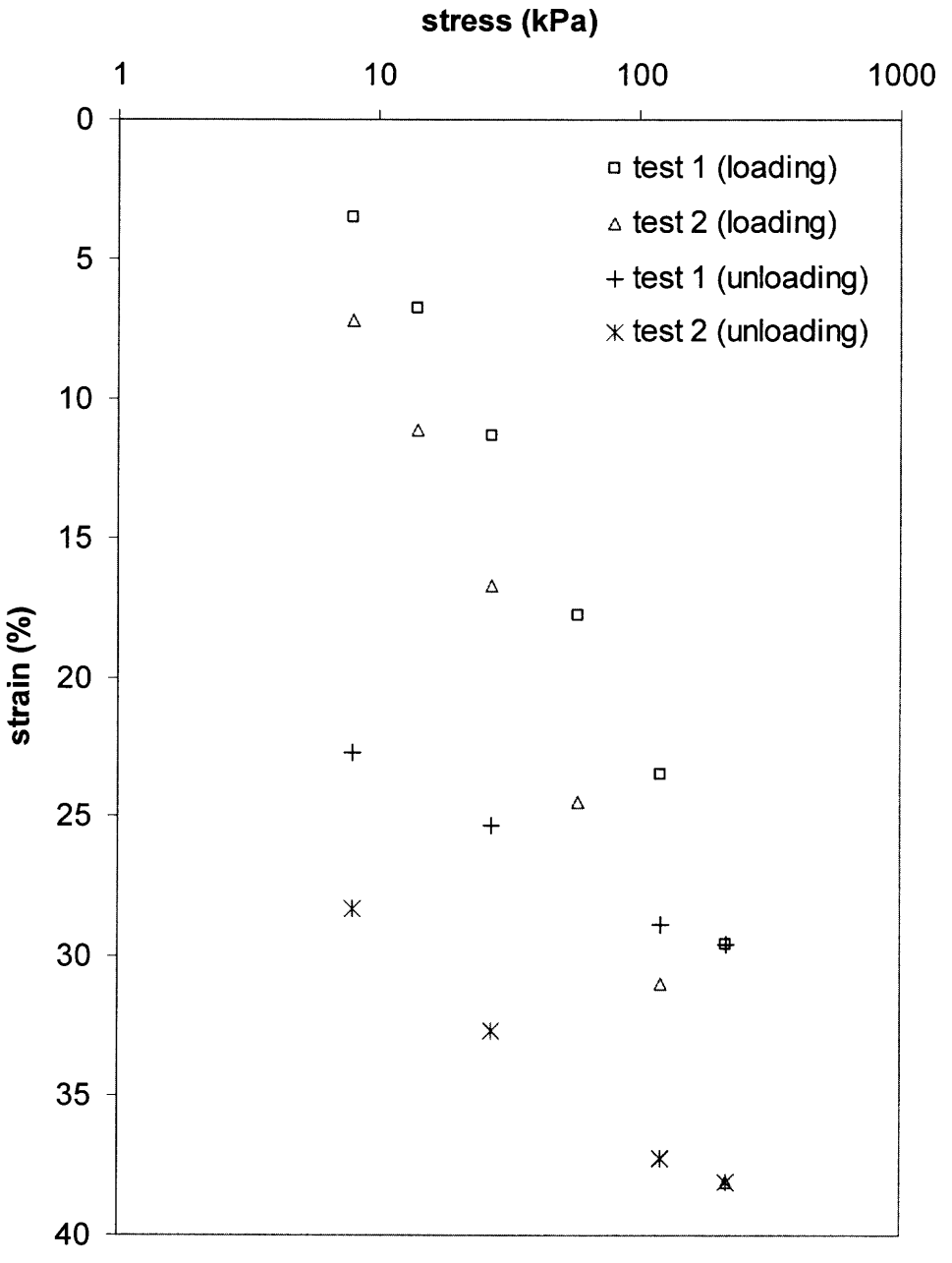

Figure 5.10 Stress-strain behavior of 1,000 days, 10,000 days and 100,000 days old laboratory simulated waste.

Table 5.7 Compressibility Characteristics of Simulated Old Waste

Test No.	Sample description	Compression Ratio	Swell Ratio (C_s^*)
1	Simulated 1,000 days old waste	0.184	0.067
2	Simulated 10,000 days old waste	0.174	0.064
3	Simulated 100, 000 days old waste	0.163	0.048

By comparing the in Tables 5.6 and 5.8, it is evident that this simulated waste has not shown a considerable variation in the compressibility with time. This could be predominantly due to the poor simulation of 'old waste' in the laboratory. With time waste changes its physical characteristics including the particle size due to degradation. Even though degradation process transforms fresh waste intermediate products, this feature was not captured in the above lab simulation. The mathematical formula used in the computations only provided remaining masses that also, was based on assumed decay constants. A noticeable difference may be observed if real old waste was used in the experiments.

Hossain et al. (2003) conducted 24 oedometer tests on residential waste to investigate the changes in waste compressibility as a function of the state of decomposition. Their values for compression ratio were in a range from 0.16 to 0.36. According to them, the compressibility was shown to increase as waste decomposed. This fact is highly debatable but lack of information on the initial composition of their waste sample prevents a further discussion. However, as far as the magnitudes are concerned what was obtained from the current research agrees with what they have observed.

CHAPTER 6

STABILITY AND MODEL VALIDATION

6.1 Introduction

The stability of the numerical solution is briefly discussed in the first half of this chapter. The second half explains the modeling effort to verify the performance of the model, in which settlement and pressure data measured at landfills are compared with the settlement and pressure profiles generated by the current model.

6.2 Stability of the Numerical Solution

The settlement model developed in this research is comprised of three main components, and different numerical techniques had to be employed to model each of them. The settlement computations include a series of calculations to track down the changes in the volume in each waste layer. This is primarily based on the stress-strain relationship to model the mechanical compression and the analytical solution of the first order decay equation to model the biodegradation-induced settlements. Since there were no numerical approximations in the settlement part (other than simple volume calculations) there was no stability issue.

Second part of the model, the generation and dissipation of landfill gases, is described by a second order partial differential equation. Finite difference method is used to approximate the time as well as space derivatives. Numerically approximated equations were solved implicitly, thus unconditional stability is expected in the pressure computations.

Final part of the model, the distribution of moisture, is described by Richards equation. Again, finite difference method was used to approximate the time and space derivatives but the equations were solved explicitly for volumetric moisture content values. Like most of the explicit finite difference schemes, the numerical method used in volumetric water content computations, is only conditionally stable. Therefore, stability of the entire model is decided by the stability of moisture content computations.

Artificial oscillations and numerical dispersion are two major obstacles encountered in the finite difference method when is applied to advection dominated transport problems. The use of a large time step could result in unstable oscillations. These oscillations grow larger as the simulation progresses, causing the simulation to fail eventually.

No numerical dispersion is associated with the spatial discritization when the central weighting scheme is used (Chunmiao and Gordon, 1995). Therefore, numerical dispersion related stability problems are not expected as all the space derivatives were approximated using central difference scheme. However, the use of central difference approximation to discritize spatial derivatives could lead to artificial oscillations (overshoot or undershoot) especially when the flow is advection dominated. The suitable time step and grid size for numerical simulations were selected based on the stability criteria introduced in the following sub-sections.

6.2.1 Peclet Number

The degree to which the fluid transport problem is dominated by advection can be determined by the grid Peclet number (Pe) in a unidirectional flow field.

$$Pe = \frac{q\Delta z}{nD} \tag{6.1}$$

Where, q (m/day) is the average linear Darcy velocity of fluid, and n is the porosity of the medium, and D (m^2/s) is the soil-water diffusivity (Warrick, 2003). If Δz is selected in such a way that Peclet number is less than two $(Pe \leq 2)$, the oscillatory behavior is eliminated when the central difference approximation is used to determine spatial derivatives.

6.2.2 Courant Number

Courant number (Cr) is a parameter that gives the fractional distance relative to grid spacing traveled due to advection in a single time step (Steefel and MacQuarie, 1996). When forward difference approximation is used to determine time derivative, transport equation stays stable as long as Courant number stays less than one.

$$Cr = \frac{q\Delta t}{n\Delta Z} \tag{6.2}$$

6.3 Validation of the Model

As it was identified in the literature review, traditional practice in the landfill studies is to handle gas and leachate issues as problems separate from the settlement issues. This situation left no chances for existence of a complete set of field data that could be used to

verify the current model. Therefore, the settlement and gas pressure components of the model had to be tested separately. As moisture component of the model is based on a widely accepted equation (Richards equation), that part was excluded from validation.

6.3.1 Landfill Settlement Data

Data published by El Fadel and Al-Rashed (1998a) was selected for the verification of settlement component of the model purposes. They reported data gathered from Mountain View landfill test cells in which experiments were conducted to measure settlement rates under different operational-management practices, including leachate recirculation. Out of six cells in operation leachate recirculation was practiced only in Cell-A, and hence settlement data from Cell-A was taken to validate this analysis.

The site was constructed within the Mountain View Landfill located approximately 25 km Northwest of San Jose, California, U.S.A. The selected cell, which is 30 m × 30 m in area and 15 m in depth, and with the practice of leachate recirculation, can be treated equivalent to a single cell biocell landfill. MSW from San Francisco was deposited in it in fifteen layers. Top surface of the waste was covered with an impermeable plastic membrane and a 150 mm thick gravel cover had been placed on it. Most of the information needed for the model to simulate settlement behavior, was found in El Fadel and Al-Rashed (1998a) and they are reproduced in Table 6.1.

Best possible assumptions were made in gathering the missing data. Density of the gravel cover was taken as 2000 kg/m^3. Waste was separated in to four groups as explained in Chapter 5. First order decay constant values reported in literature are scattered in a wide range. Values suggested for bioreactor landfills are in a range from 0.0003 to 0.0007 day^{-1}. However, considering the high amount of sludge expected to be

added in the Calgary Biocell Landfill, fist order decay constant was assumed as 0.001 day^{-1} for the rapidly degradable waste. Decay constants for moderately and slowly degradable waste were assumed one and two orders less than the value selected for the rapidly degradable waste group. The assumed waste composition was described in Chapter 5. Specific gravity for solids groups 1, 2, 3, and 4 were assumed as 3.0, 2.0, 1.2, and 1.0, respectively. Compressibility parameters were selected from the information gathered from the experiments presented in Chapter 5.

Table 6.1 Waste Related Data from Mountain View Landfill

Waste solid mass	4,888
Voids ratio	0.98
Porosity (%)	50
Sludge solids mass	151
Buffer solids mass	10
Total solids mass	5,053
Water mass	2,643
Total mass	7,696
Percent wet weight	34
Average sludge to waste solids ratio	0.032
Average buffer to water ratio	0.0036
Cell volume (m^3)	10,055
Waste density (kg/m^3)	765
Precipitation	134
Added water	1700
Overall moisture content (%)	46

Source: El Fadel and Al-Rashed (1998a)
Notes: (1) Waste moisture content was 25 %
(2) Sludge moisture content was 85 %
(3) All masses are in thousands of kilograms

6.3.2 Comparison of Measured and Predicted Settlement Profiles

Settlement profile obtained from the first attempt was compared with the measured values in Figure 6.1. It was noted that even though the prediction gives the same trend and the same difference in strain (approximately 12.6% in measured and 12.3% in prediction), there is a huge difference in the initial strain and a mismatch in the starting time of the settlement process. The reason for this discrepancy was understood to occur as a result of the difference between the settlement philosophy used to develop the model and that of El Fadel and Al-Rashed (1998a) used, in recording and plotting settlement data.

According to the description given by El Fadel and Al-Rashed (1998a), the landfill was filled in 15 layers and the first point of strain value appears in the graph after 15 days. The most probable conclusion is that, they have only started recoding settlements on the 15^{th} day after completing the fill (after the top cover was placed) and the small amount of initial settlement must be the result of compression by the weight of the top cover. On the other hand, the current model keeps track of settlement for each layer. When it was simulated again using a computer code adjusted to disregard the layer compression during filling, agreement was seen between the measured and predicted strains (Figure 6.2).

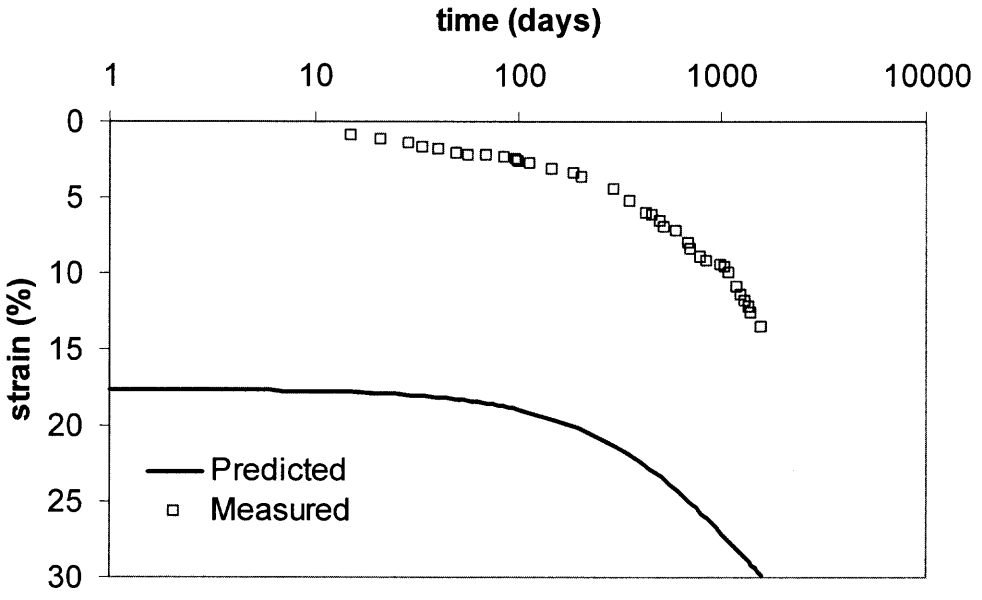

Figure 6.1 Measured strains and prediction using unadjusted model.

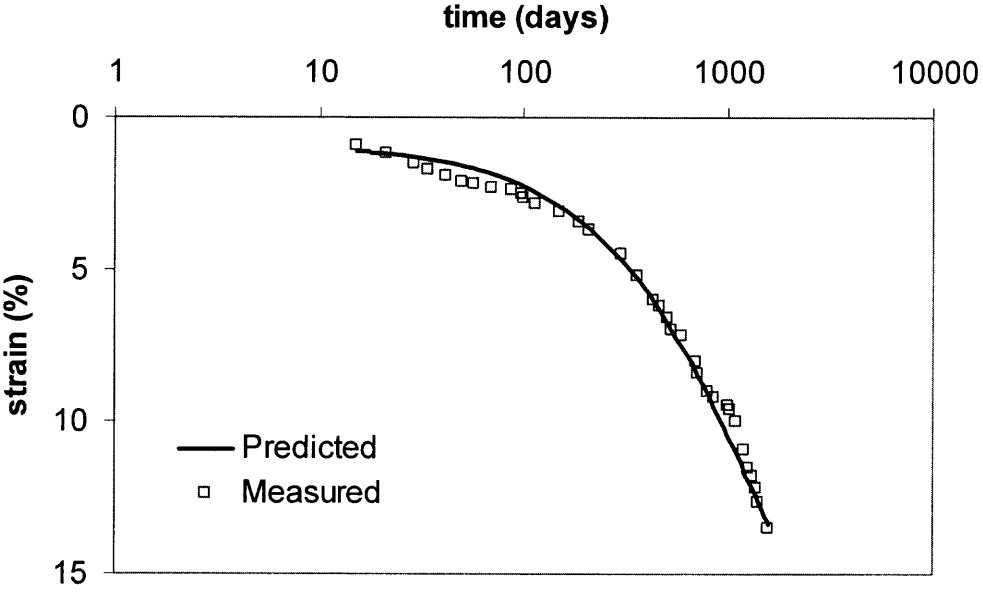

Figure 6.2 Measured strains and prediction using model adjusted for initial strains.

6.3.3 Landfill Gas Pressure Data

Findikakis and Leckie (1979) published landfill pressure data measured at Palos Verdes Sanitary Landfill, in California,USA. This includes two pressure profiles: 10 years and 15 years after closure of the landfill. These two profiles from Palos Verdes landfill was selected to verify the pressure component of the current model. Relevant waste parameters for Palos Verdes landfill as reported by Findikakis and Leckie (1979) are reproduced in Table 6.2.

Table 6.2 Waste Related Data from Palos Verdes Landfill

Landfill depth (m)	33
Cover thickness (m)	1
Waste permeability (Darcy)	1
Waste porosity	0.5
Waste density (kg/m^3)	700
Moisture content as a % of wet weight	30
Gas generation potential (m^3/kg)	0.12
Cover permeability (Darcy)	0.1
Waste composition, percentage	
- readily degradable	15
- moderately degradable	55
- slowly degradable	30
Waste composition, $t_{1/2}$ (years)	
- readily degradable	0.5
- moderately degradable	3.5
- slowly degradable	25.0

Source: Findikakis and Leckie (1979)
Note: 1 Darcy = $9.86 \times 10^{-13} m^2$

Half-life values given for the waste were also converted to their corresponding decay constant values. Initial dry density and the initial moisture contents were estimated from the given data as 490 kg/m^3 and 21%, respectively. Coefficient of diffusion of landfill gas was assumed as 0.6 m^2/d. Compressibility parameters were selected from the information gathered from the experiments presented in Chapter 5.

According to the information given by Findikakis and Leckie (1979), the landfill was not equipped with a gas recovery system and hence gas was expected to reach top surface and penetrate the top cover to mix with the air at the atmospheric pressure. Therefore, top cover was also included in the analysis as a layer of the landfill. A no-gas flow condition was employed to model the bottom boundary.

6.3.4 Comparison of Measured and Predicted Gas Pressure Profiles

Gas pressures predicted for 10 and 15 years are compared in Figure 6.3 with the measured values reported by Findikakis and Leckie (1979). The agreement between predicted and measured pressure values is poor. This mismatch may be attributed to a few reasons. Some of the data (such as waste composition and cover permeability) reported by Findikakis and Leckie (1979) are actually not real values but only estimations. They also assumed that the landfill was filled over a period of 15 years.

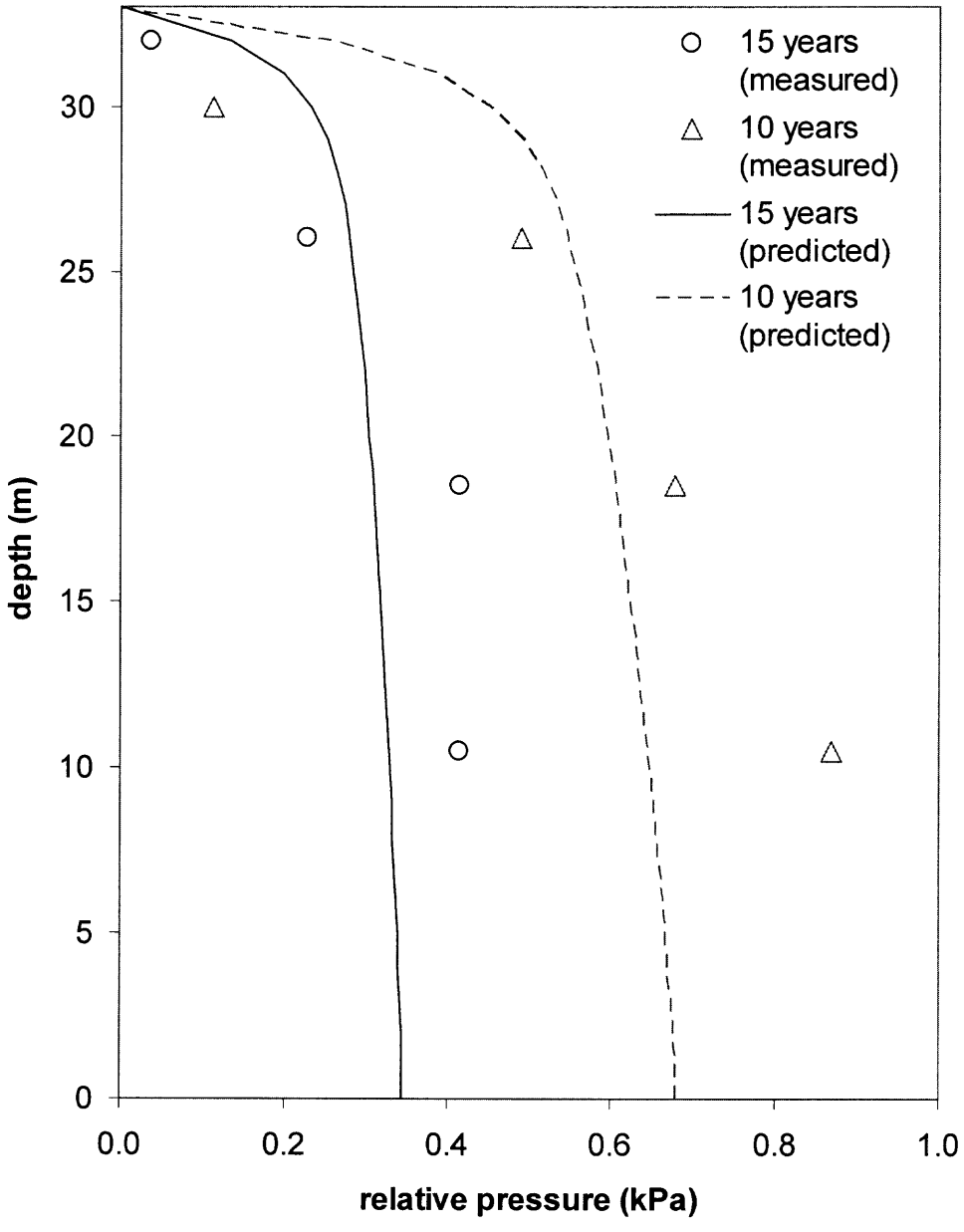

Figure 6.3 Measured pressures and prediction using model.

CHAPTER 7

PREDICTIONS AND SENSITIVITY ANALYSIS

7.1 Introduction

The settlement model described in this dissertation was developed to predict the settlements of the City of Calgary Biocell Landfill (fully instrumented, 15 m high, 3-lift biocell landfill). Due to the unavailability of data as a result of the delay in construction, assumed waste and other landfill related properties were used in this research. Every attempt was made to select the values from their typical ranges that are most suitable for conditions in Calgary, Canada. This chapter includes how the input data were selected, the cases considered in the analysis, and a discussion of results. The last section of this chapter is devoted to sensitivity analysis.

7.2 Selection of Input Data

Each lift of the Calgary Biocell Landfill was divided in to 20 layers of waste, which is 0.25 m thick at the placement. Delay in construction between two lifts was assumed as 50 days. The increase in moisture due to precipitation was assumed insignificant. Thickness of the final cover and its density were assumed as 0.5 m and 2000 kg/m^3, respectively. Properties of waste, landfill gas, moisture (leachate) and landfill permeability are presented in the following sub-sections.

7.2.1 Waste Properties

Typical composition of North American waste given in Chapter 5 (USEPA, 1997) was used for Calgary. Maximum dry density of fresh waste reported in Chapter 5 was used as the compaction density. It was assumed that only 95% of the maximum could be achieved in the field, hence 500 kg/m^3 was used as the dry density after compaction. As described in Chapter 2, measured and estimated values of total gas generation potentials for waste are in a wide range of 0.005-0.5 kg/m^3. Ham and Barlaz (1987) estimated the range of total gas generation potential value for landfills as 0.05-0.52 kg/m^3. Therefore, an average value of 0.28 m^3/kg was selected as the total gas generation potential in this analysis.

Waste composition, first order decay constant, and specific gravity of waste solids data used to verify the model (discussed in Chapter 6) were assumed for this analysis. These values are given in Table 7.1. Input data for compressibility parameters were also selected from the data obtained from the laboratory experiments, which are presented in Chapter 5. Compressibility values selected to represent time durations decided in Chapter 4, are reproduced in Table 7.2.

Table 7.1 Group Properties of Waste Solids

Group	Non -degradable waste (1)	Slow degradable waste (2)	Moderately Degradable waste (3)	Highly degradable waste (4)
Initial fraction (f_s)	0.35	0.25	0.25	0.15
Specific gravity (G_s)	3.0	2.0	1.2	1.0
Decay constant $(\lambda, 1/\text{days})$	0.0	0.00001	0.0001	0.001

Table 7.2 Compressibility Parameters

Time (days)	Compression ratio (C_c^*)	Swelling ratio (C_s^*)
$< 2 \times 10^2$	0.205	0.069
$2 \times 10^2 - 2 \times 10^3$	0.184	0.067
$2 \times 10^3 - 2 \times 10^4$	0.174	0.064
$> 2 \times 10^4$	0.163	0.043

7.2.2 Properties of Landfill Gas

Coefficient of diffusion of landfill gas mixture in waste was computed by modifying the diffusion coefficient of landfill gas in air using Millington-Quirk second model (Jin and Jury, 1996). Millington-Quirk second model is described as follows.

$$D = \frac{\theta_g^{\,2}}{n^{2/3}} D_g \tag{7.1}$$

Where, D_g and D are diffusion coefficient (m^2/day) of landfill gas in air and in waste, respectively, θ_g is the gas content, and n is the total porosity. D_g for carbon dioxide was found as 1.22 m^2/day (Hashimoto and Suzuki, 2002). D_g for methane was found as 1.82 m^2/day (Hettiarachchi, 2005). Therefore, average of these two values were used in Millington-Quirk second model to compute diffusion coefficient of waste. Average gas content and total porosity values of the landfill was found as 0.35 and 0.60, respectively, based on trial settlement simulations. Finally the diffusion coefficient of waste was computed as 0.28 m^2/day. As Millington-Quirk second model usually tend to underestimate diffusion coefficient, computed value was increased by 40% (Wilshusen et al. 2004) and hence 0.40 m^2/day was used in the settlement simulations.

As described in Chapter 3, it was also assumed that the landfill is operated under a temperature of 42^0C (315 K), which is favorable for biodegradation. Atmospheric pressure was taken as 101 kPa.

7.2.3 Parameters Associated with Landfill Moisture

Density of leachate was assumed to be equivalent to that of water. Density of water at 42^0C was taken as 990 kg/m^3 (Scanlon et al. 2002). Van Genuchten parameters for solid waste estimated by Benson and Wang (1998) using laboratory experiments on water characteristic curve of waste, performed at the University of Wisconsin – Madison, was used. Parameter p was assumed as 0.5. They are listed in Table 7.3. However, the constant value reported for the saturated volumetric moisture content (θ_s) was not realistic due to the varying volume of a settling waste mass. Hence the saturated volumetric moisture content was made a variable and it was computed for each time step.

Table 7.3 Van Genuchten Parameters for Solid Waste

α	26 m^{-1}
n	2.2
p	0.5*
θ_r	10 %

Source: * Assumed, other values from Benson and Wang (1998)

7.2.4 Permeability of the Landfill

Permeability (sometimes referred to as intrinsic permeability) of a porous medium is a function of the characteristics of the porous medium and conductivity of fluids. If porosity remains unchanged, it is considered as a constant for a given porous medium. Arigala et al. (1995) used 10^{-12} m^2 as the permeability of a landfill medium. Waste hydraulic conductivity values reported by many others (Blieker et al. 1993; Oweis and Khera, 1986; Schroeder et al. 1984; and Young, 1989, Nastav et al. 2001) when converted to permeability, are in a range from 10^{-12} to 10^{-14} m^2. Therefore, an average value of 10^{-13} m^2 was used in this simulation.

In order to compute variable unsaturated gas and hydraulic conductivities their corresponding saturated values are required. Definition of permeability can be used to build a relationship between the saturated gas and hydraulic conductivities.

$$K = k_{ws}\left(\frac{\mu_w}{\rho_w g}\right) = k_{gs}\left(\frac{\mu_g}{\rho_g g}\right) \tag{7.2}$$

Where, K (m^2) is the permeability of the solid waste and μ (Pa · day) is the viscosity of the corresponding fluid component. The following equations are developed by assuming suitable values for density and viscosity for each fluid component.

$$k_{ws} = 1.4x10^{12}(K) = 1.4x10^{-1} \ (\text{m/day}) \tag{7.3}$$

$$k_{gs} = 8.0x10^{9}(K) = 8.0x10^{-4} \ (\text{m/day}) \tag{7.4}$$

Conductivities are obtained in m/day when K is in m^2. Viscosity values corresponding to a temperature of 315 K for landfill gas mixture and water were taken as 1.16×10^{-10} and 1.62×10^{-9} Pa · day, respectively (Scanlon et al. 2002; LMNO Engineering, 2003). An average density of 1.21 kg/m^3 was assumed for landfill gas mixture.

7.3 Cases Considered for Analysis

The settlement model developed in this research is a combination of three processes: settlement calculations (due to decomposition and mechanical compression); gas generation and transport; distribution of moisture (as a result of leachate recirculation). The computer program developed to numerically solve the governing equations is capable of modeling each process separately as well as a combination of them. This feature was made use to simulate the settlement behavior of the biocell landfill in four different ways so that a comparisons can be made to identify the strengths and weaknesses of the model.

7.3.1 Case 1 - Constant Pressure and Moisture Profiles

In this case, only the time dependent variation of decomposition and mechanical compression was considered. This form of the model is the one closest to a typical biodegradation-induced model identified in Chapter 2. Gas pressure was kept at its atmospheric level in the numerical computations and hence this approach indirectly assumes smooth and quick dissipation of pressure. Presence of a steady level of 30% of (volumetric) moisture was assumed, thus the solution was not expected to be sensitive to any possible variation in loading due to changes in moisture.

7.3.2 Case 2 - Variable Pressure and Constant Moisture Profiles

Variation in gas pressure due to generation and dissipation of gas was incorporated. Atmospheric pressure was taken as the initial condition for gas. Maximum rate of generation of gas was assumed to occur after 30 days. Gas extraction points were introduced to cell boundaries in addition to top and bottom of the landfill. Atmospheric pressure was maintained at these extraction points assuming that gas was immediately mixed with outside air, which is at the atmospheric pressure. For this case also, presence of a steady level of 30% of moisture was assumed in the computations.

7.3.3 Case 3 - Constant Pressure and Variable Moisture Profiles

Variation in moisture was incorporated. Gas pressure was kept at its atmospheric level. Thus this approach assumes smooth and quick dissipation of gas pressure. Variable moisture profile was used to simulate leachate recirculation. Initial level of 20% moisture (volumetric) was assumed. A maximum head of 0.1 m was maintained at the top surface. In the beginning, head at the top surface was linearly increased to its

maximum over a period of 60 days. When the whole waste mass reached its intended field capacity, excess water was removed from the bottom of the landfill simulating the performance of a leachate removal system.

7.3.4 Case 4 - Variable Pressure and Moisture Profiles

Variation in gas pressure due to generation and dissipation of gases as well as the variation in moisture was incorporated. For variable gas pressure and variable moisture, conditions similar to those described in the previous sections were adopted.

7.4 Analysis of Results

Settlement behavior of the City of Calgary Biocell Landfill was simulated for a period of 10,000 days (approximately 25 years) for all the cases considered. Results obtained are shown in Figures 7.1 through 7.10. Following subsections present a discussion of these results.

7.4.1 Strain (or Settlement) Behavior of the Biocell Landfill

Total average strain profiles for all four cases analyzed are given in Figure 7.1. All methods produce the typical shape of a waste settlement curve. In a typical settlement curve a small or zero initial strain is usually observed because many do not consider the settlement during construction. But in this analysis the settlement behavior during construction was modeled assuming a 50 day time lag between two consecutive lifts. But no time delay was assumed between placements of two consecutive layers in one lift. Initial high strain (25%) is due to the consideration of mechanical compression occurs as a result of the self weight. Sudden increase in strain at days 50 and 100 are because of

the increase in stress due to addition of new waste layers. It should be noted that in this methodology, the total of initial heights of each layer at the placement (which is 15 m), was used as the basis for the strain computations.

It is evident from Figure 7.1 that the model predicts higher strain values, when moisture as well as gas pressure are incorporated into the simulation. It is also noted that this difference is clearly visible in the steeper portion of the curves approximately after 100days. This coincides with top wastes reaching its field capacity. Increase in stress as a result of introduction of additional moisture, is therefore, clearly reflected as an increase in strain. When gas pressure is added, it further increases strain by a considerable amount.

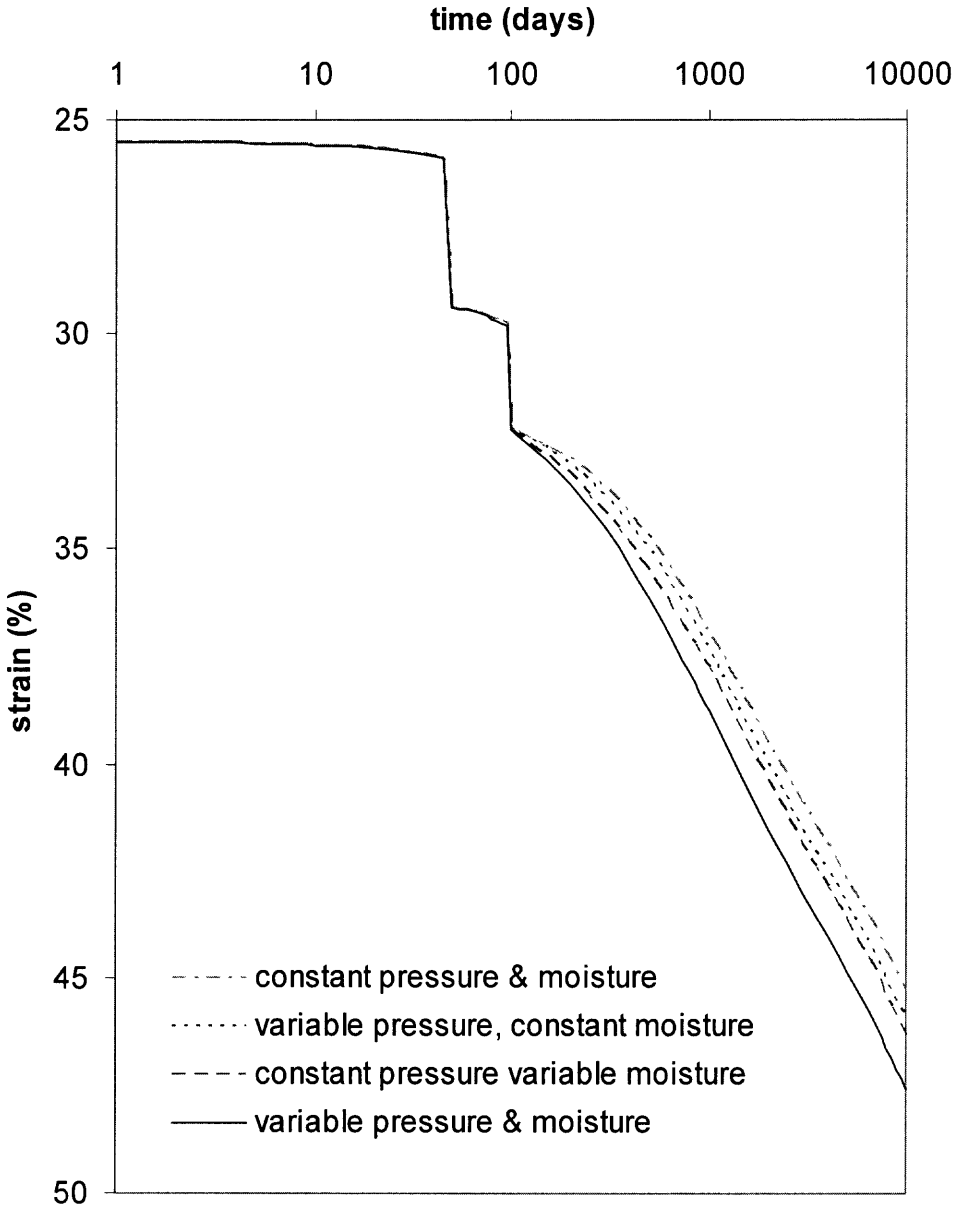

Figure 7.1 Variation of average total strain with time.

Variation of average strain of waste layer-60 predicted for all four cases is given in Figure 7.2. With the introduction of more moisture, gas pressure goes up. As layer-60 is close to the top surface, the total stress available at that level is small. Therefore, effective stress at that depth responds even to minor changes in pressure. This could be the reason for the clearly visible difference between the strains predicted for layer-60 by method employed in cases 3 and 4 (compared with the insignificant difference observed between total strains predicted for cases 3 and 4 given in Figure 7.1). On the other hand layer-30 (Figure 7.3) which is located in the middle shows a strain variation which is very similar to the general trend shown by the total average strain given in Figure 7.1. Hence, for a quick estimate of the total settlement of the total profile can be accomplished by analyzing the settlement behavior of a middle layer.

Variation of average strain of few waste layers at different depths is presented in Figure 7.4. Initial strain increases with the depth and the slightly different slopes of the curves suggest that they are settling at different rates.

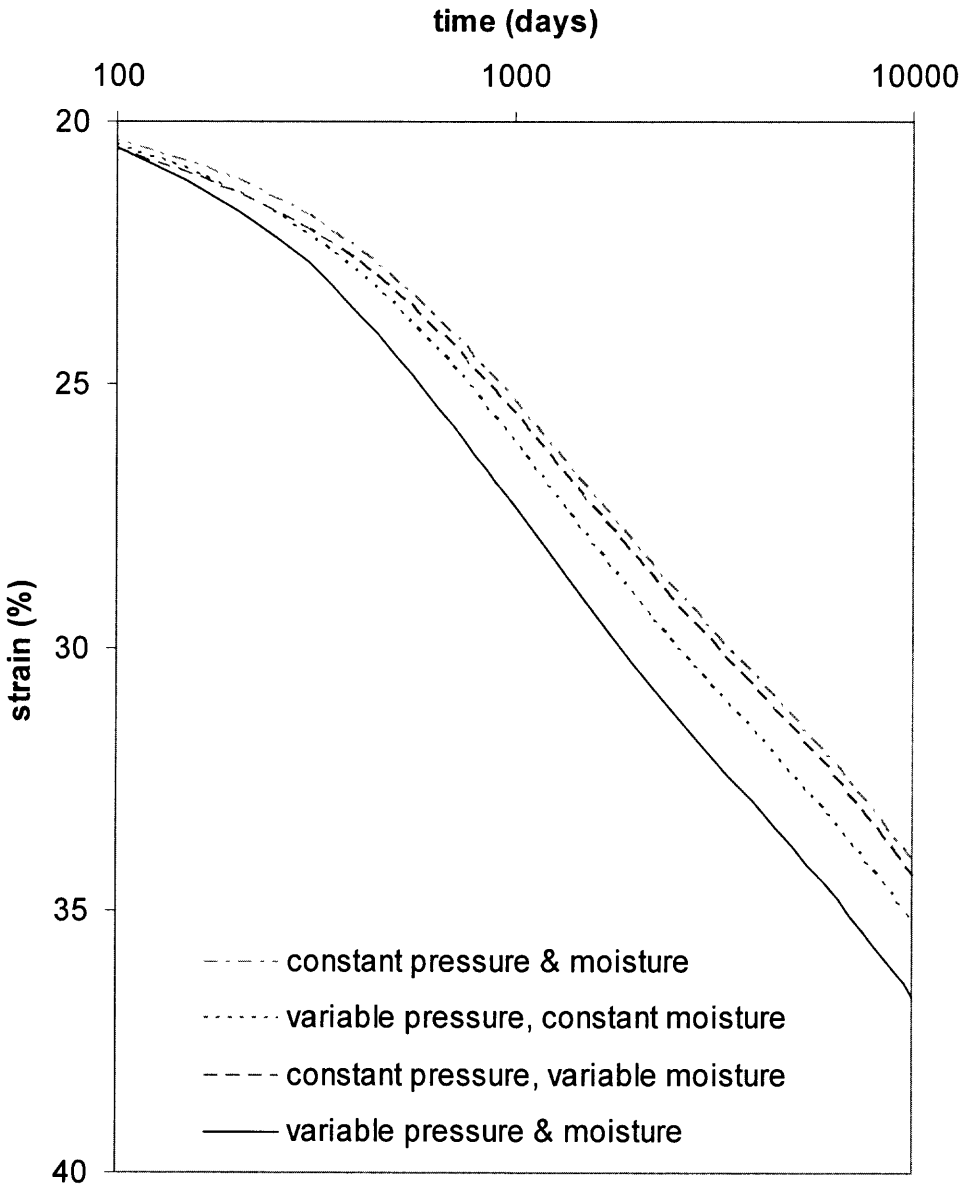

Figure 7.2 Variation of average strain of waste layer 60.

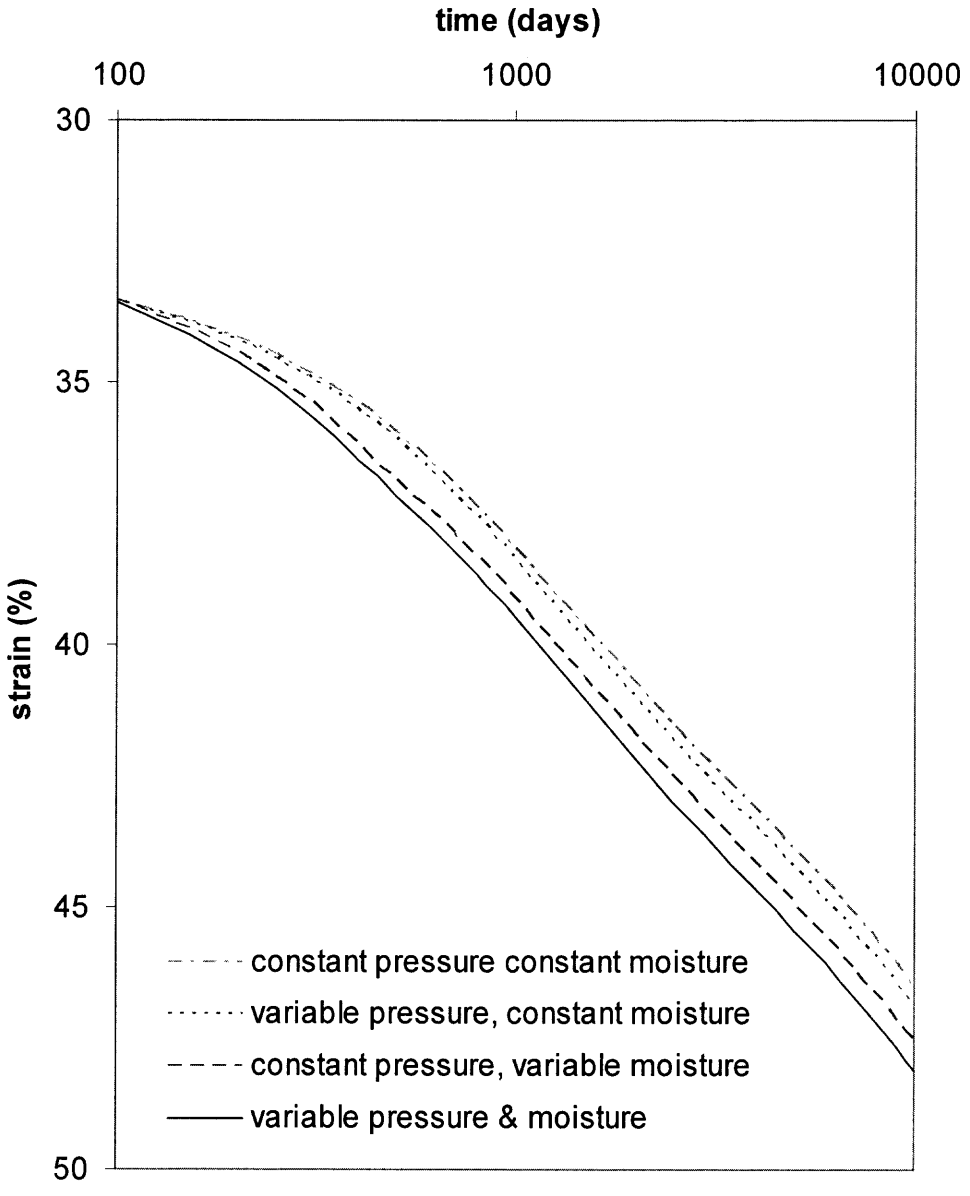

Figure 7.3 Variation of average strain of waste layer 30.

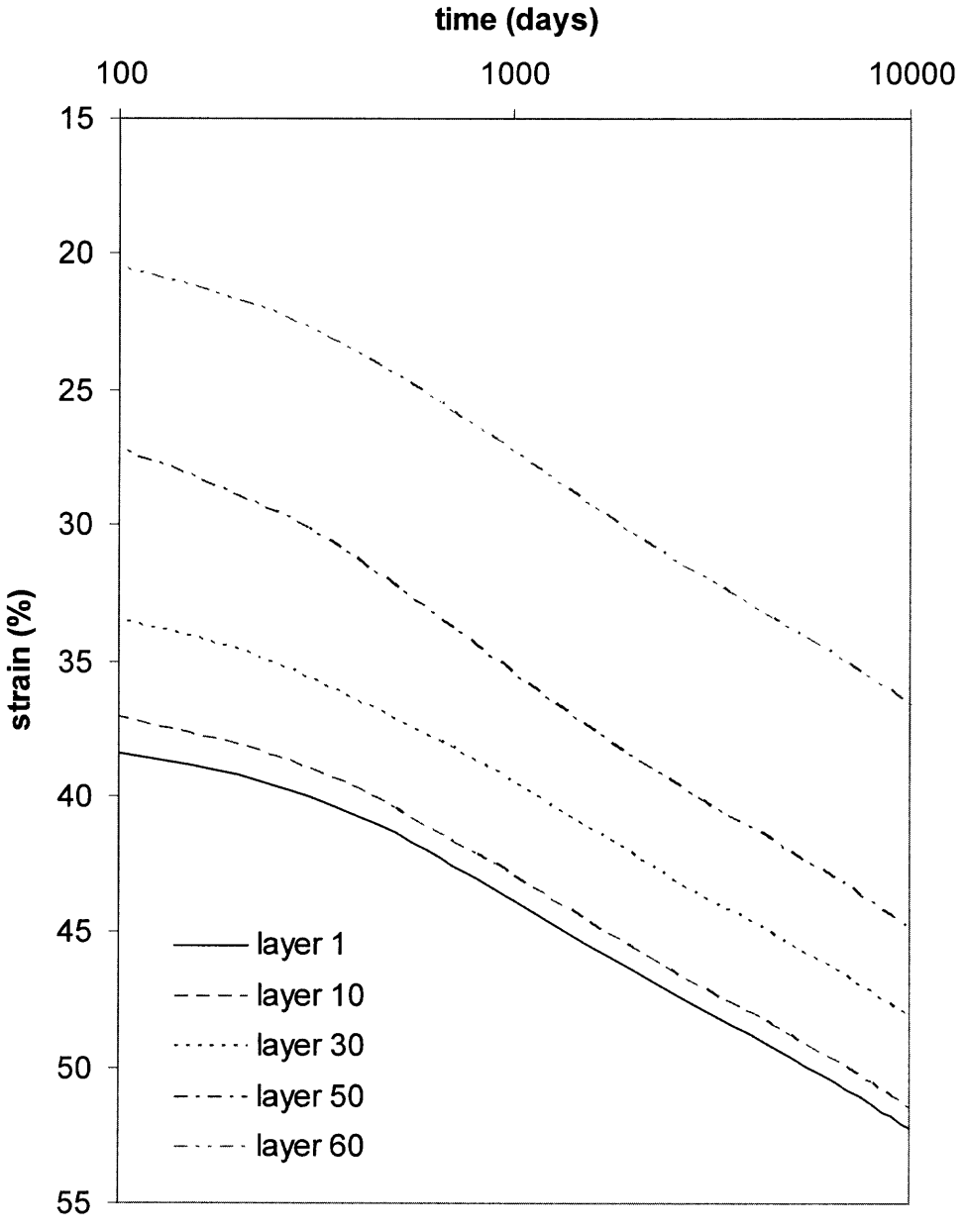

Figure 7.4 Variation of average strain at different depth.
Note: layer 1 - bottom, layer 60 – top

7.4.2 Variation of Gas Pressure

The variation of landfill gas pressure with time is shown in Figure 7.5. The magnitude of the maximum relative landfill gas pressure observed was approximately 8 kPa. However, because of the rather random selection of values for input variables, it is premature to discuss the magnitude. The sudden spike in the pressure is seen in all profiles in Figure 7.5a. Occurrence of this sudden increase in gas pressure can be explained using the timeline of movement of moisture front (Figure 7.5b).

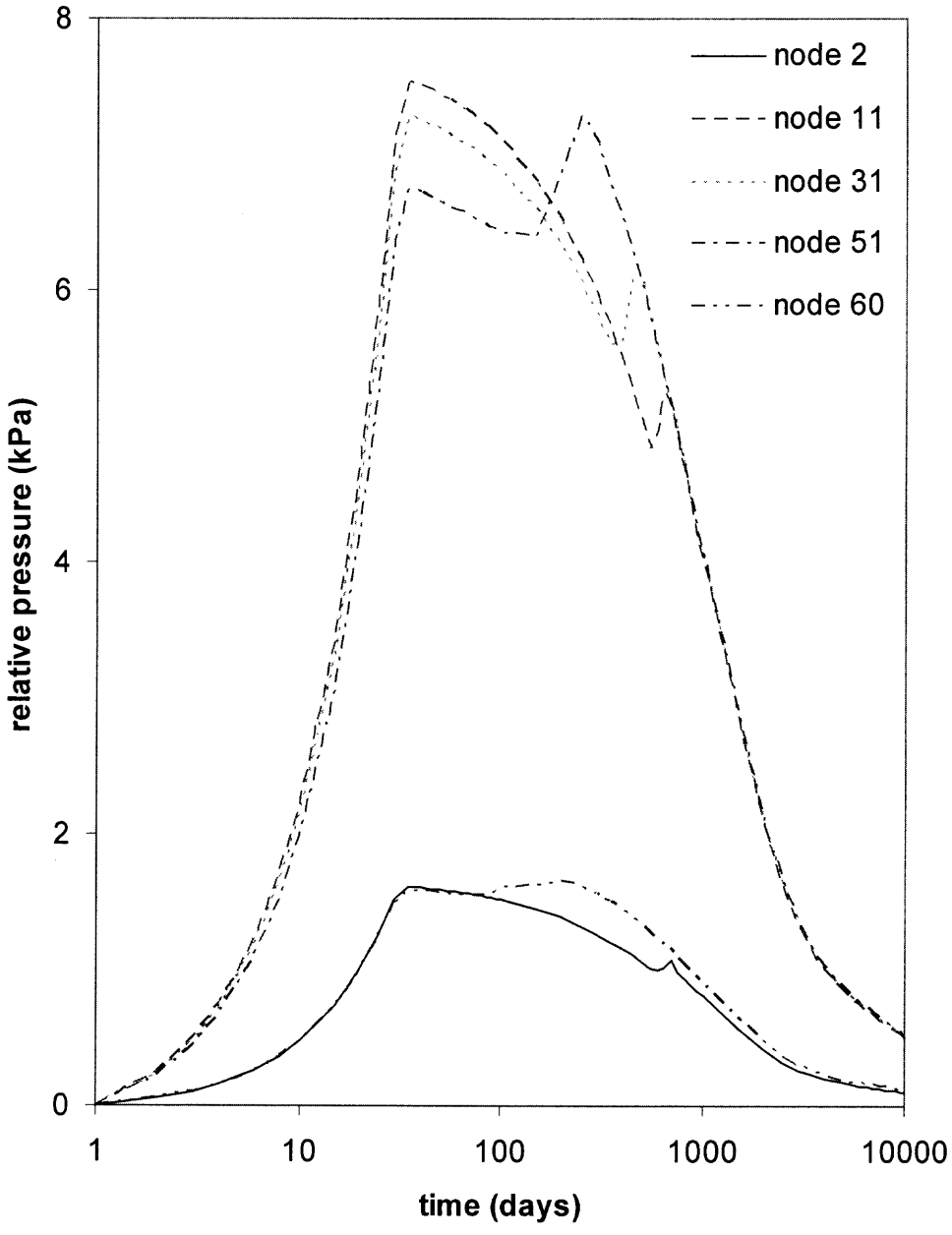

Figure 7.5(a) Variation of gas pressure with time.

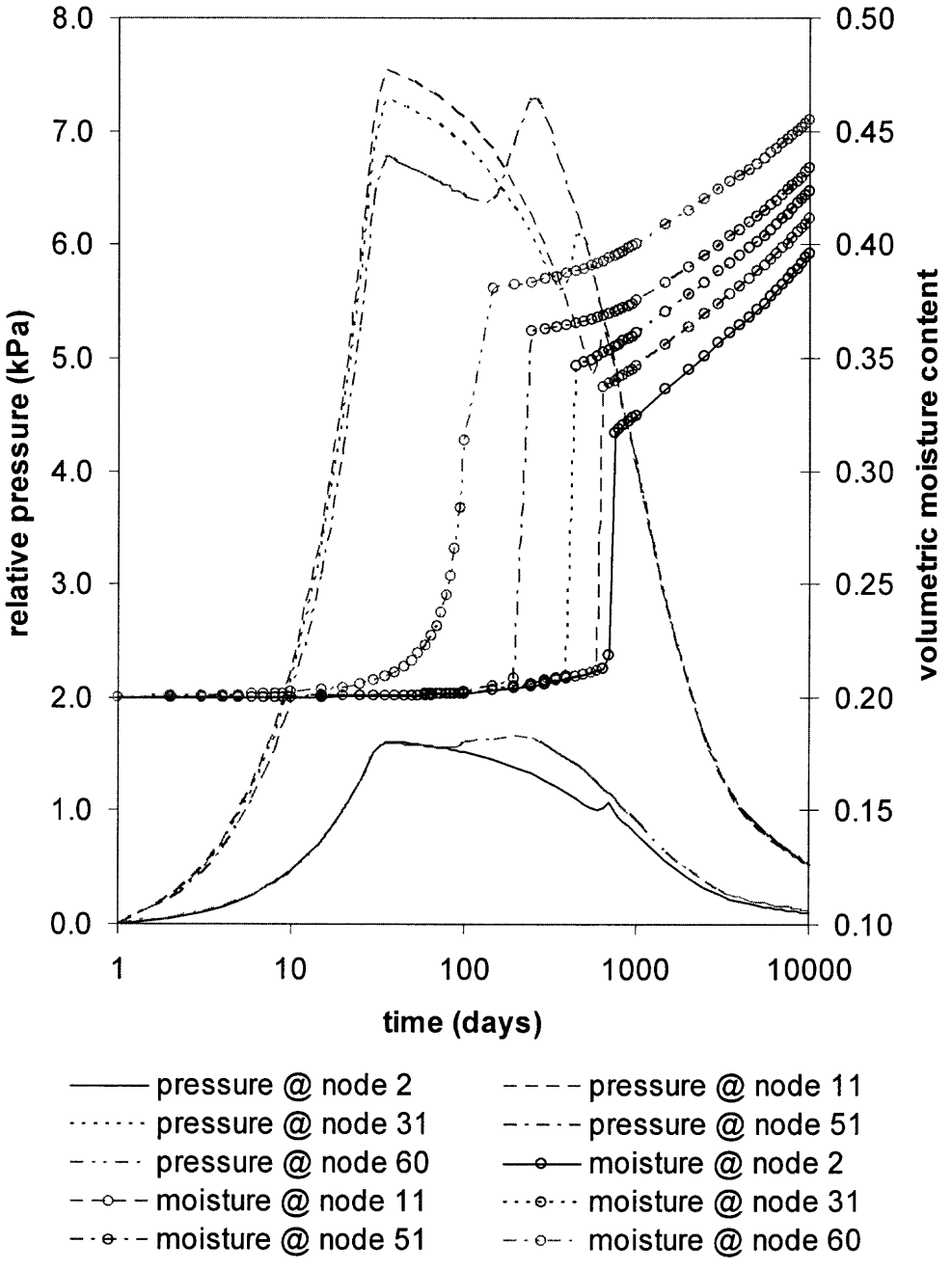

Figure 7.5(b) Variation of gas pressure compared with movement of moisture.

Figure 7.6 compares the pressure predicted by the model with constant moisture profile and variable moisture profile, at nodes 2 and 51. Constant moisture profile assumes 0.30 throughout the period of simulation, while in the other approach moisture content change from 0.20 to 0.45. High constant moisture content in the constant moisture simulation, leads to high gas pressure from the beginning. This prevents comparison. This is also reflected in the pressure profile given in Figure 7.7 (compare 1-month and 1-year pressure profiles in Figures 7.7a and 7.7b). As moisture is introduced to the system from the top, sudden pressure increase first occurs near the top surface and this is seen in the pressure profile given in Figure 7.7b.

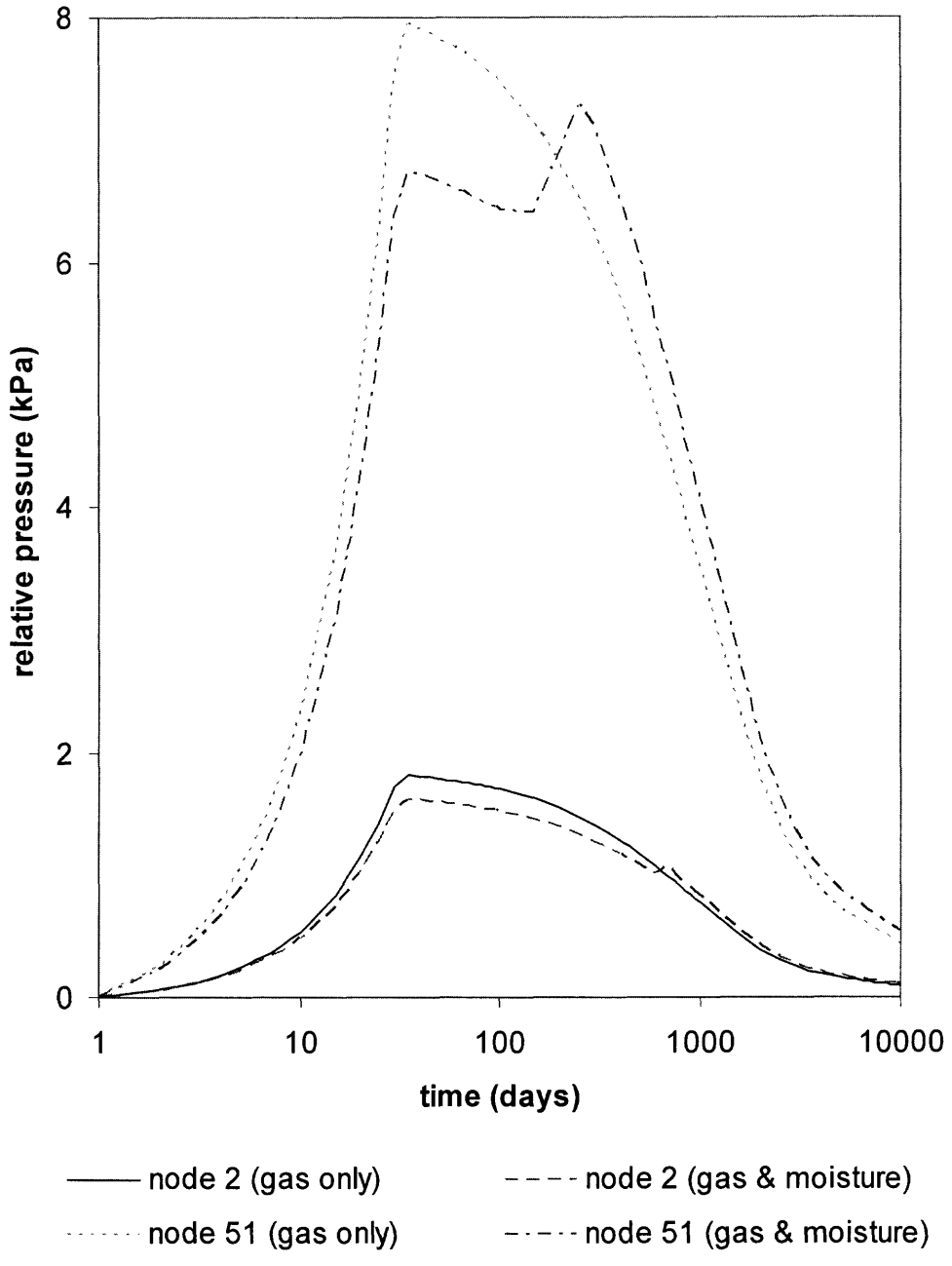

Figure 7.6 Comparison of gas pressure at nodes 2 and 51.
Note: node 1 - bottom, node 61 – top

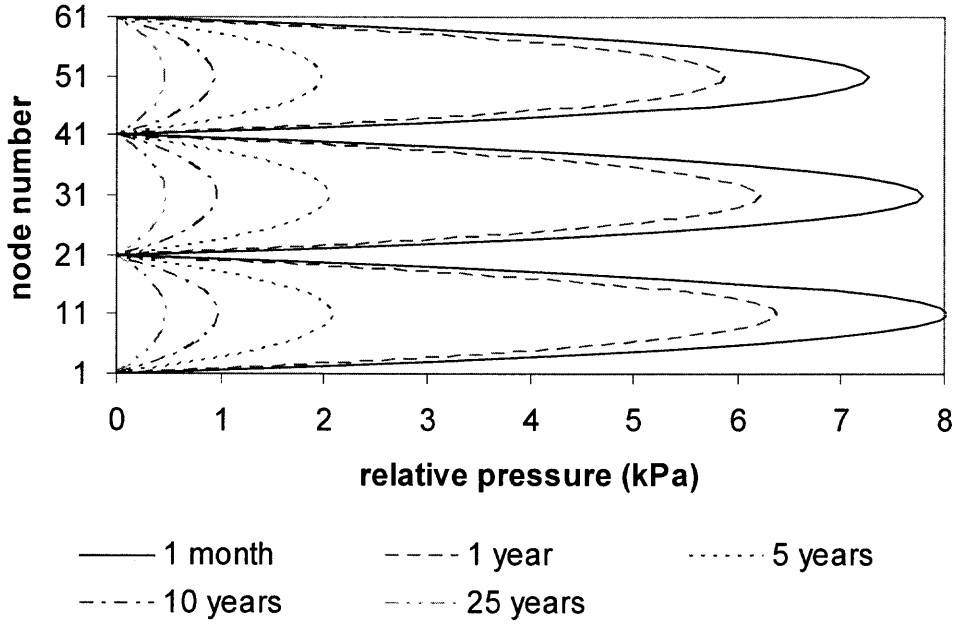

(a)

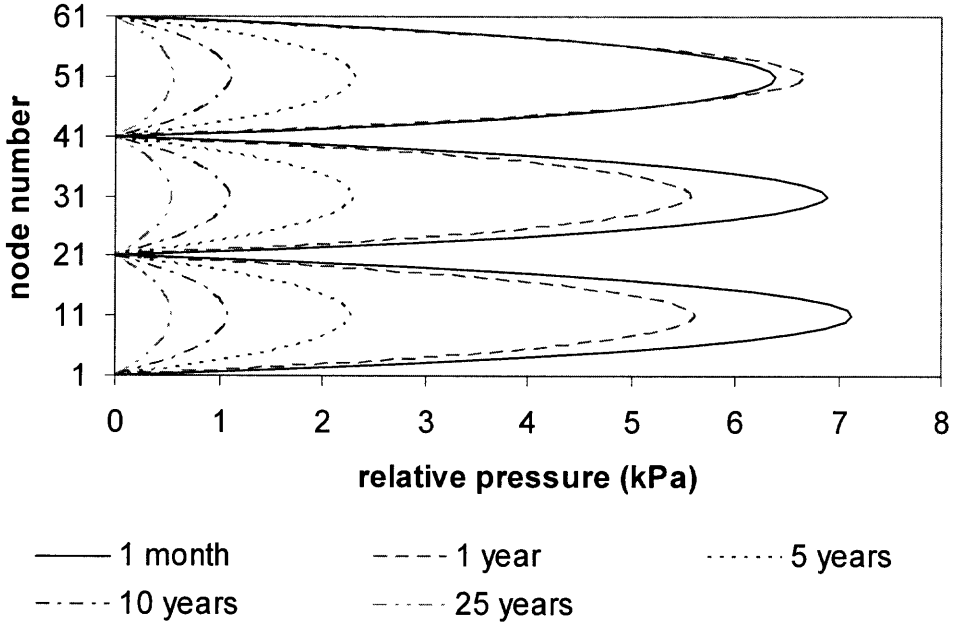

(b)

Figure 7.7 Variation of gas pressure with depth with constant moisture profile (a) and with variable moisture profile (b).

7.4.3 Distribution of Moisture

Moisture variations with time and space are shown in Figures 7.8 and 7.9, respectively. When moisture moves to a certain waste layer, it makes the waste to reach its field capacity in a relatively short time before it moves to the next layer. This is why a sudden increase of moisture is seen in each curve in Figure 7.8. In this simulation moisture takes approximately 750 days to reach the field capacity of the bottom waste layer. This duration depends not only on the waste properties but also the approach (and quantity) used in leachate recirculation. Movement of the moisture front with time is demonstrated in the moisture profile given in Figure 7.9.

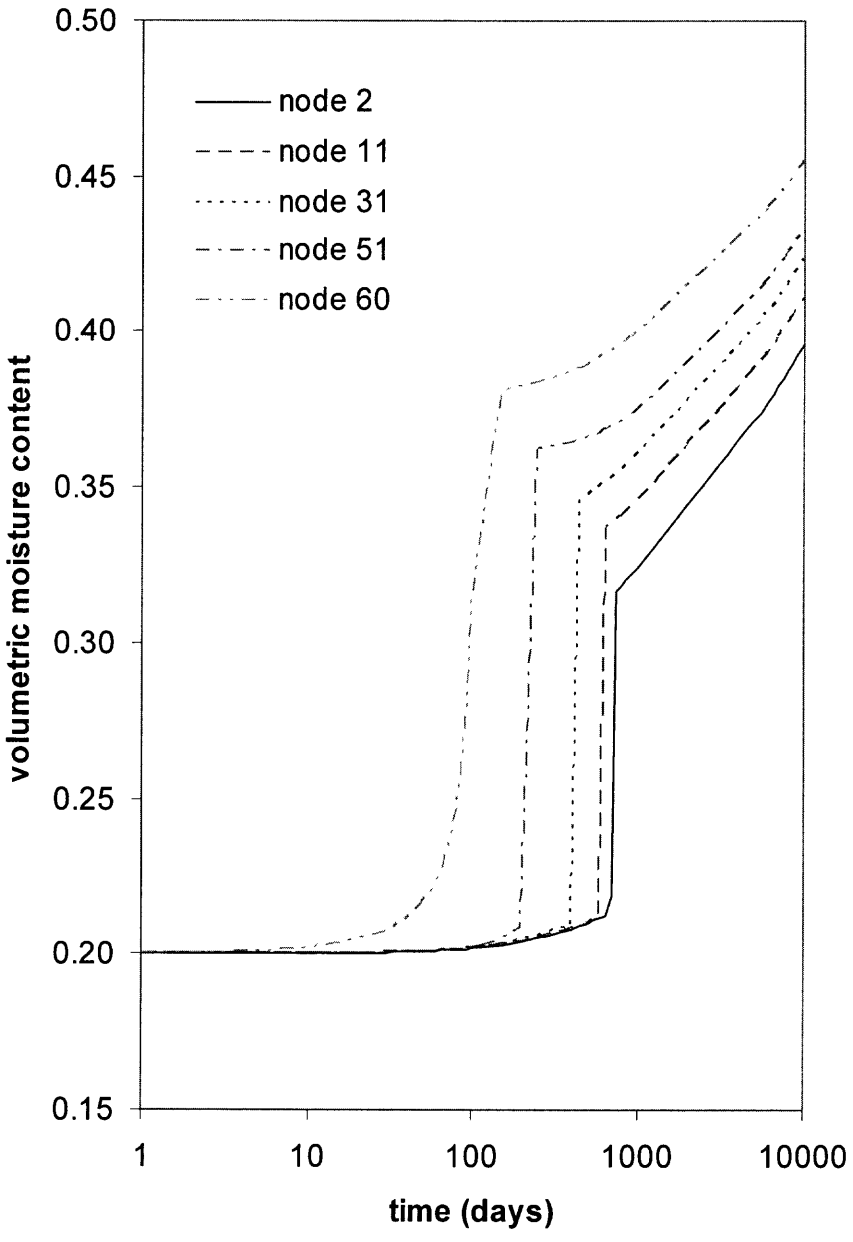

Figure 7.8 Variation of volumetric moisture content with time.

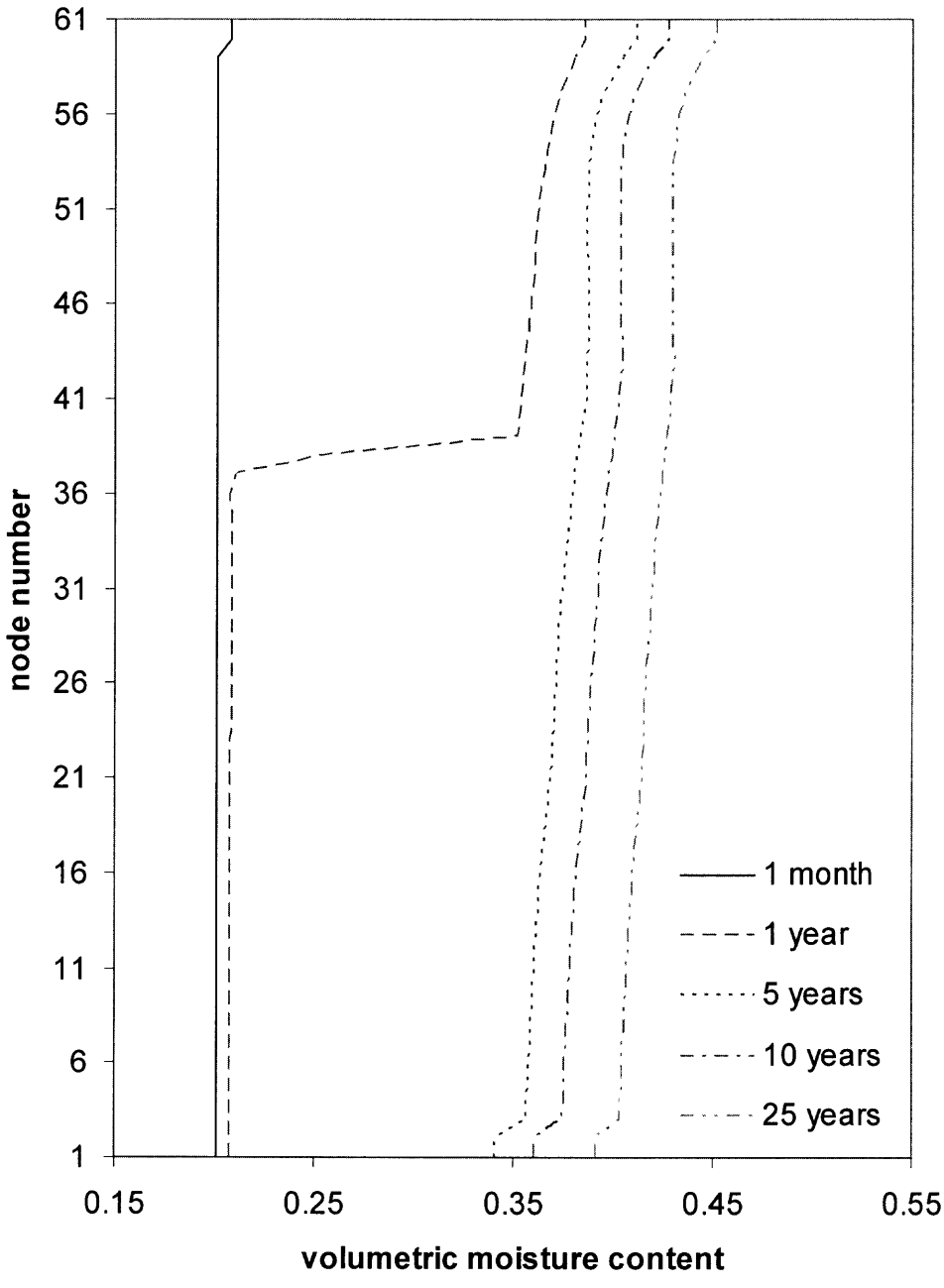

Figure 7.9 Variation of volumetric moisture content with depth.

7.4.4 Variation of Density

Since this model keeps track of mass of each waste layer, variation of wet density of waste can be easily predicted. Variation of wet densities predicted by the model (with variable gas pressure and variable moisture incorporated) is presented in Figure 7.10. Wet density of the waste (or landfill density) is in an approximate range of 825 to 1125 kg/m^3. It is interesting to note that the maximum density observed at the bottom of the landfill after 25 years is within the typical range reported in the literature (Oweis and Khera, 1986; Bleiker et al. 1993; Bleiker et al. 1995). In Figure 7.10, wet waste density of layer-1 after 25 years is smaller than the density of layer-10. This has happened due to the adoption of the leachate removal system (simulated) at the bottom layer (see the time versus moisture content plot given in Figure 7.9). Final moisture content available at layer-1 is approximately 0.39. But if the general trend of the moisture curve was followed, it should have been 0.41. When 0.41 moisture content was used in density computation the 25 year wet density for layer-1 is approximately 1135 kg/m^3, which is higher than wet 25 year wet density of layer-10.

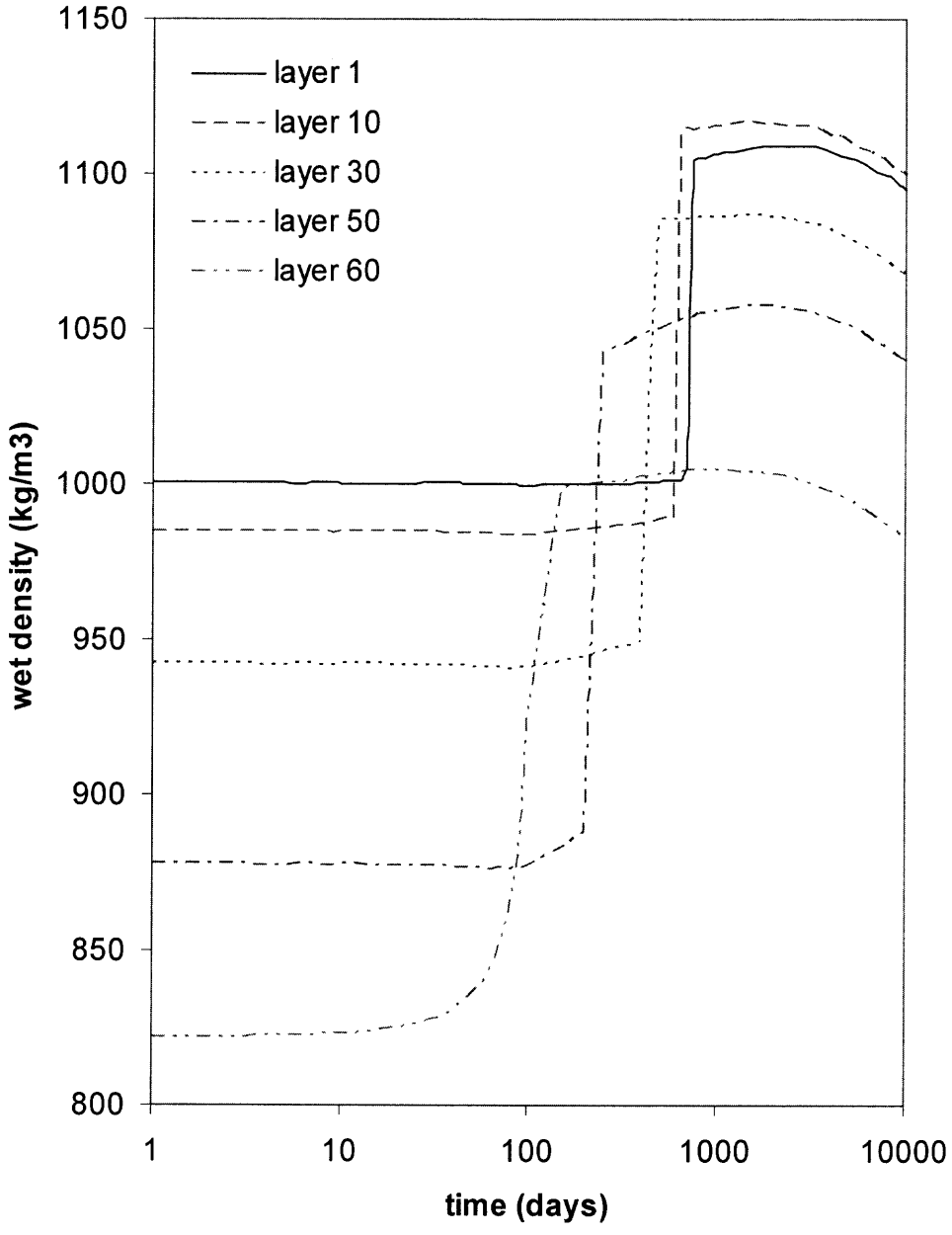

Figure 7.10 Variation of wet waste density with time.

7.4.5 A Typical Settlement Curve for Rapidly Degradable Waste

The total settlement curve should level off as the landfill stabilizes with time. Because of low decay constant values selected for the above analysis, this level off feature was not exhibited within the time period considered. A hypothetical landfill, which comprise of 65% rapidly degradable waste (assumed decay constant 0.001 $days^{-1}$) and 35% of non-degradable waste was analyzed. The total strain for this landfill is shown in Figure 7.11.

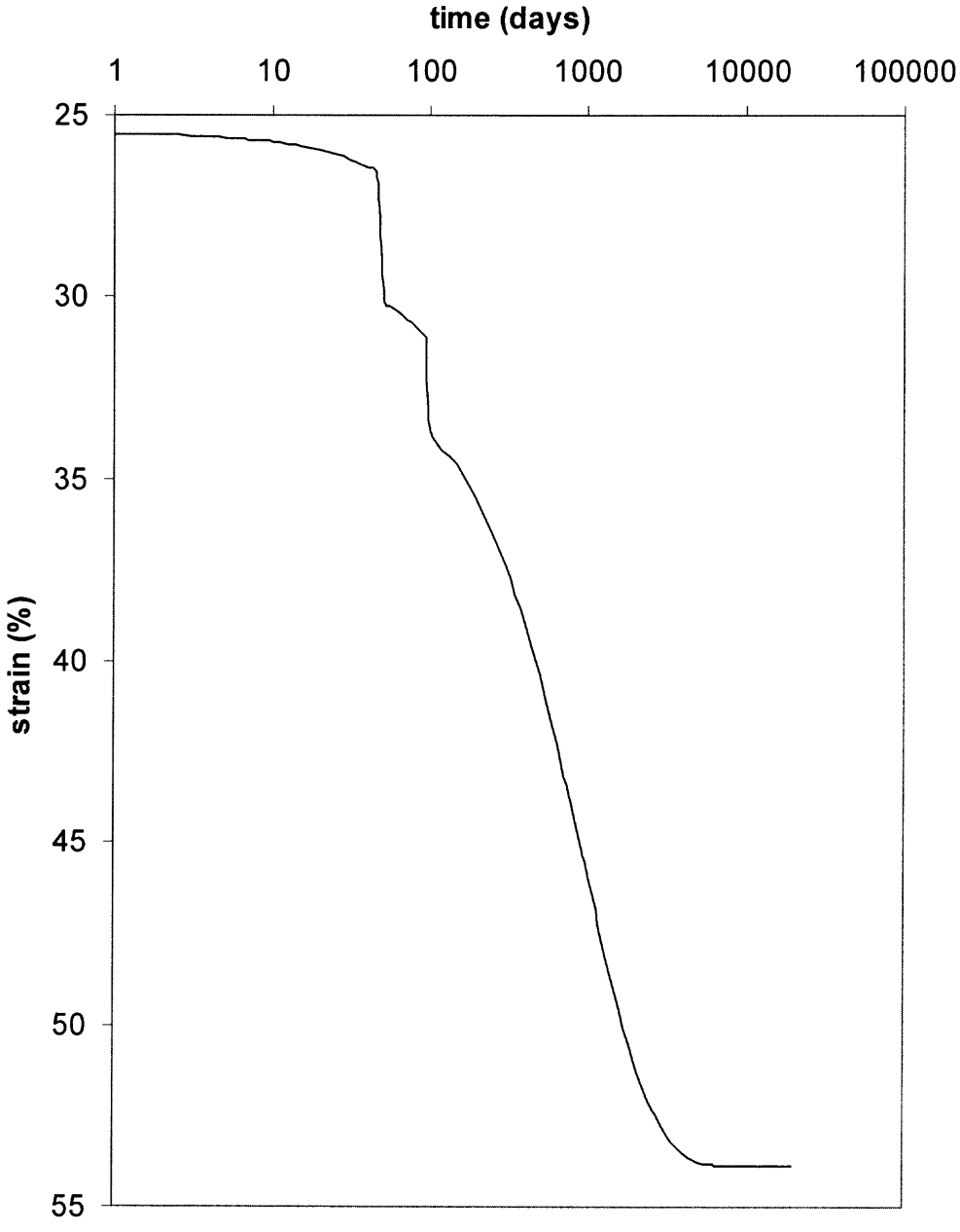

Figure 7.11 Variation of total strain of rapidly degradable waste.

7.5 Sensitivity Analysis

The purpose of this sensitivity analysis is to investigate the influence of key parameters on the overall performance of the model. This analysis may be helpful to understand and quantify the impact of uncertainty of input data used in the model.

Landfill permeability, decay constant, compressibility parameters, coefficient of diffusion, and landfill temperature are the variables selected for the sensitivity analysis. Values of these parameters were changed by a realistic amount above and below the original value. Average total strain predicted after 1000 days was compared with the corresponding strain value produced by such variations for the settlement model coupled with both gas and moisture. This reference strain value was found as 38.74%. Details of sensitivity analysis are given in Table 7.4 through 7.8 and they are briefly discussed in the following sections.

7.5.1 Sensitivity to Landfill Permeability

Landfill permeability used in the predictions was change by ± 50% to see its contribution to the strain. Results are shown in Table 7.4. Even though gas pressure and moisture flow are very sensitive to landfill permeability, a significant difference was not seen in the total strain.

Table 7.4 Variation of Strain with Landfill Permeability

Permeability (m^2)	Strain after 1000 days (%)	Difference (%)
0.5×10^{-13}	38.25	-1.26
1.0×10^{-13}	38.74	0
1.5×10^{-13}	38.97	+0.59

7.5.2 Sensitivity to First Order Decay Constant

Decay constants for all the waste groups were subjected to a change of ± 50% observed difference are given in Table 7.5. Significant difference was observed.

Table 7.5 Variation of Strain with First order Decay Constant

Decay constants ($days^{-1}$)	Strain after 1000 days (%)	Difference (%)
0.5×10^{-3} , 0.5×10^{-4}, 0.5×10^{-5}	35.88	-7.38
1×10^{-3} , 1×10^{-4}, 1×10^{-5}	38.74	0
1.5×10^{-3} , 1.5×10^{-4}, 1.5×10^{-5}	41.95	+8.29

7.5.3 Sensitivity to Compressibility Parameters

This parameter controls the whole process of mechanical compression. Laboratory values used in the predictions were changed only by ± 10% to investigate the influence. A very high variation was observed suggesting that this value has to be selected carefully for accurate modeling.

Table 7.6 Variation of Strain with Compressibility Parameters

Compressibility parameters	Strain after 1000 days (%)	Difference (%)
$0.9C_c^*$ and $0.9C_s^*$	35.20	-9.14
C_c^* and C_s^*	38.74	0
$1.1C_c^*$ and $1.1C_s^*$	42.54	+9.81

7.5.4 Sensitivity to Coefficient of Diffusion

Even though coefficient of gas diffusion is a function of several variables including temperature and porosity of the porous material, it was made a constant to reduce the computational complexity. Results of sensitivity analysis of diffusion coefficient are provided in Table 7.7. Significant difference was not observed.

Table 7.7 Variation of Strain with Diffusion Coefficient

Coefficient of diffusion (m^2/d)	Strain after 1000 days (%)	Difference (%)
0.36	38.98	+0.62
0.40	38.74	0
0.44	38.49	-0.64

7.5.5 Sensitivity to Landfill Temperature

Results of the sensitivity analysis of landfill temperature is given in Table 7.8. As viscosity of gas and water are functions of temperature, hydraulic and gas conductivities are functions of viscosity. But a significant difference was not observed.

Table 7.8 Variation of Strain with Landfill Temperature

Landfill temperature (K)	Strain after 1000 days (%)	Difference (%)
305	38.68	-0.15
315	38.74	0
325	38.80	+0.15

CHAPTER 8

CONCLUSIONS AND RECOMMENDATIONS

8.1 Summary and Conclusions

A comprehensive mathematical model was developed to predict settlements in biocell landfills coupling generation and dissipation of landfill gas and distribution of moisture.

The major mechanisms of waste settlement were identified as mechanical compression and biodegradation-induced strain. Mechanical compression was modeled with the help of laboratory simulations. In the absence of a proper theoretical explanation, laboratory simulations are perhaps the best possible alternative to study the mechanical compression of waste.

To model the settlements due to biodegradation, it was assumed that waste degradation obeys the first order kinetic equation. A phase diagram was introduced to define masses and volumes of each phase. Waste comprises material, which may range from highly degradable to non-degradable solids. Therefore, the use of average material properties could be misleading and also could produce erroneous results. In order to better represent the problem, solid phase was further subdivided into four groups based on the rate of degradability.

To simulate the actual landfill settlement behavior, gas generation and dissipation and moisture distribution were coupled to the settlement. A governing equation was derived to link gas pressure with the varying landfill volume. Richards equation was used to model the moisture movement in the waste mass.

Compaction and compressibility characteristics of solids waste were studied using laboratory compaction and compression tests. A synthetic waste was designed for the

testing purposes based on a typical North American waste composition (USEPA, 1997). The specific gravity of the simulated waste was found to be approximately 1.65. It was found that this waste can be compacted to a maximum dry density of 525 kg/m^3 at 60% water content (gravimetric). This waste also showed a linear stress–strain relationship when logarithmic stress values were used. Unloading followed a shallower, yet another constant slope. These slopes were defined as compression ratio and swell ratio (compressibility parameters of waste). Values of these parameters for fresh waste (simulated waste, which simulated fresh conditions) were found as 0.205 and 0.069, respectively. Based on laboratory experiments, it was also found that the compressibility of waste could decrease with time. Since model results were very sensitive to compressibility parameters, different values were used depending on the state of biodegradation (or age).

A computer model was developed to numerically solve the equations and to predict the settlements using MATLAB. In the absence of a complete set of data, the model was verified for its performance in settlement predictions and gas pressure predictions separately. When the settlement component of the model was tested assuming a constant moisture profile and atmospheric pressure, a satisfactory agreement was observed between modeling results and field observations. Gas pressure part of the model was also tested with a constant moisture profile. Although the agreement between predicted and measured pressure values was not as good as the settlement part, results were satisfactory as far as the trend and the magnitudes are concerned.

Settlement of the City of Calgary Biocell was then predicted using assumed model parameters. Four cases were considered in the settlement analysis: case 1- constant

pressure and moisture profiles; case 2 - variable pressure and constant moisture profiles; case 3 - constant pressure and variable moisture profiles; case 4 - variable pressure and moisture profiles. Settlement profiles generated by all four cases were compared. The model predicts higher strain values, when moisture as well as gas pressure are incorporated in to the simulation. Therefore, it was concluded that modeling settlement without taking gas pressure and moisture into account, could underestimate the total settlement.

Time dependent variation of landfill density was a bonus of the modeling effort. The density values predicted for 25 years are well above 1000 kg/m^3 and matched with those reported in literature.

8.2 Recommendations for Future Research

As modeling of settlement with variable gas and moisture profiles is conceptually new, and has a huge potential for future research. As indicated by the sensitivity analysis, compressibility parameters play a vital role in predicting settlements, yet the current model depends totally on the values of the parameters those were estimated using 'simulated' waste. Compressibility of waste has to be investigated extensively using real waste. Aging of waste is very hard to simulate using simulated waste. Therefore, variation of compressibility parameters has to be well established using laboratory tests of different scales.

Estimation of biodegradation-induced settlements depends on a single bold assumption, which states that waste obeys first order kinetic equation. This has neither been proved nor denied. Even if it was correct, it has to be well defined based on a

carbon balance. Unavailability of proper decay constants is another challenge at the moment. A theatrical value can be computed assuming first order decay equation and using time taken for half-life. But it does not guarantee any degradation if other conditions such as moisture, pH and availability nutrients are not satisfied. If the other variables cannot be linked to decay, at least a term, which defines efficiency of degradation has to be introduced.

Since introduction of variable gas pressure and moisture is new, in the current version of the proposed model both of these variables appear in a loose form. The model uses few theoretical assumptions in estimating gas generation. For simplicity, this model only considers a single gas component. Hence, no opportunity is given to represent characteristics of different landfill gases and their interactions. To be realistic this framework has to be equipped with multi-component gas generation and transport model.

Role of moisture is not well defined in the current version. Most probably it is the weakest link in the model but it is one of the most influential factors determining the total settlement as far as the current results are considered. In the current form of the model, moisture does not engage in any of the activities other than restricting gas flow. This has to be replaced with an efficient water balance technique, which consider of leachate generation.

In the current version of the model, rate of construction was not considered. To indicate effects of staged construction (three lifts) on total settlement, first 50 days and second 50 days were modeled separately to include in the total settlement profile. Therefore, the computational framework has to be modified to accommodate either the rate of construction or delay in construction between two consecutive lifts.

APPENDIX

COMPUTER PROGRAM

The computer program developed using MATLAB to solve the numerical equations is included in this appendix.

```
clc;
close all;
clear all;

% settlement coupled with gas pressure and moisture

%%%%%%%%%%%%%%%%%%%%%%%%%%%%%%%%%%%%%%%%%%%%%%%%
%%%      Copyright © 2005 by Chamil Hiroshan Hettiarachchi      %%%
%%%                  ALL RIGHTS RESERVED                    %%%
%%%%%%%%%%%%%%%%%%%%%%%%%%%%%%%%%%%%%%%%%%%%%%%%

%%% DEFINITION OF PARAMETERS %%%%%%%%%%%%%%%%%%%%%

%%% Geometry related parameters %%%

dZ_i=0.25; % intial layer thickness at the placement(m)
n_l=20; % number of lifts per cell
n_c=3; % number of cells


%%% Time related parameters %%%

dt=1.0; % time step (days)
TT=1000; % total simulation time (days)


%%% Permeability of landfill %%%

K_i=10^-13; % (m2)


%%% Landfill cover %%%

dZ_s=0.5; % thickness of the final cover (m)
DenS=2000; % tensity of the cover material (kg/m3)


%%% Moisture characteristics %%%

mc_i=0.20; % initial moisture content throughout
% mc_i=0.30; % used when the program runs with constant moisture profile
mc_r=0.10; % residual water content
maxm=0.6; % field capacity as a % of saturated moisture content

DenW=1000; % density of water at 315K (kg/m3)
```

```
%%% Leachate recirculation %%%

hT_m=0.1; % max head @ top  (m3/m2/day)
hT_f=0.1; % head @ top after reaching desired saturation (m3/m2/day)

TI=60; % initial period, linear increase till rate reaches max, (days)
TF=1;  % frequency of recirculation , once in how many days (days)


%%% Van Ganutchen parameters %%%

a_VG=26;
n_VG=2.216;
m_VG=1-1/n_VG;
p_VG=0.5;


%%% Gas characteristics %%%

D=0.4; % diffusion coeficient (m2/d)
m=30/1000; % molar mass of the gas mixture:50% CH4; 50% CO2 (kg)
R=8.31477/m; % individual gas constant for methane(J/kg/K)
T=325.0; % temperature(K)

Pr_a=101.0; % atmospheric pressure (kPa)
Pr_i=  0.0; % initial relaive pressure throughout (kPa)

G_i=0.0 ; % initial rate of gas generation  (kg/day/m3)
L0=0.28; % total gas generation potential (m3/kg)
T0=30; % time when the max rate of gas generation occurs(days)

%%% Waste chatracteristics %%%

DenC=500; % initial dry density at the placement (kg/m3)

Cc1=0.205; % compression ratio, for time(days) < 2x10^2
Cc2=0.184; % compression ratio, for 2x10^2 < time(days) < 2x10^3
Cc3=0.174; % compression ratio, for 2x10^3 < time(days) < 2x10^4
Cc4=0.163; % compression ratio, for time(days) > 2x10^4

Cs1=0.069; % swell ratio, for time(days) < 2x10^2
Cs2=0.067; % swell ratio, for 2x10^2 < time(days) < 2x10^3
Cs3=0.064; % swell ratio, for 2x10^3 < time(days) < 2x10^4
Cs4=0.043; % swell ratio, for time(days) > 2x10^4
```

```
fs1=0.35; % initial mass fraction of non degradable solids
fs2=0.25; % initial mass fraction of slowly degradable solids
fs3=0.25; % initial mass fraction of moderately degradable solids
fs4=0.15; % initial mass fraction of rapidly degradable solids

Gs1=3.0; % specific gravities of non degradable solids
Gs2=2.0; % specific gravities of slowly degradable solids
Gs3=1.2; % specific gravities of moderately degradable solids
Gs4=1.0; % specific gravities of rapidly degradable solids

lambda1=0.0000;  % decay constant of non degradable solids
lambda2=0.00001;   % decay constant of slowly degradable solids
lambda3=0.0001;   % decay constant of molderately degradable solids
lambda4=0.001;   % decay constant of rapidly degradable solids


%%% INITIAL CONDITIONS %%%%%%%%%%%%%%%%%%%%%%%%%%%%%

n=(n_l)*(n_c); % number of layers

%%% Initial values of the variables %%%

mc(1:n+1,1)=mc_i; % initial vol. water content
Pr(1:n+1,1)=Pr_i; % initial relative pressure (kPa)
G (1:n+1,1)=G_i ; % initial rate of gas generation  (kg/day/m3)


%%% Initial thickness & porosity of waste layers %%%

for k=1:n,

   %%% Initial thickness
   dZ(k,1)=dZ_i*(1-(Cc1)*log10((n-(k-1))+(DenS*dZ_s)/(DenC*dZ_i)));

   %%% Initial mass within a layer
   Mass(k,1)=(DenC*dZ_i)+DenW*0.5*(mc(k,1)+mc(k+1,1))*dZ(k,1);

   dZs(k,1)=(DenC*dZ_i/DenW)*((fs1/Gs1)*exp(-lambda1*(1-1)*dt)+...
      (fs2/Gs2)*exp(-lambda2*(1-1)*dt)+(fs3/Gs3)*exp(-lambda3*(1-1)*dt)+...
      (fs4/Gs4)*exp(-lambda4*(1-1)*dt));

   dZw(k,1)=0.5*(mc(k,1)+mc(k+1,1))*dZ(k,1);

   dZg(k,1)=dZ(k,1)-dZs(k,1)-dZw(k,1);
```

```
   mc_s(k,1)=1-dZs(k,1)/dZ(k,1); % theoritical saturated moisture content

end

mc_s(n+1,1)=mc_s(n,1); % theoritical saturated moisture content @ top surface


%%% Initial stress distribution %%%

for k=1:n+1,
   SigX=DenS*dZ_s*9.81/1000; % load from the final cover
   for i=k:n,
      SigmaT(k,1)=SigX+Mass(i,1)*9.81/1000; % uncorrected
      SigX=SigmaT(k,1);
   end
   SigmaT(n+1,1)=DenS*dZ_s*9.81/1000; % stress at the top surfce
   SigmaE(k,1)=SigmaT(k,1)-Pr(k,1); % pressure correction added
end

%%% Initial total height %%%

THD=0; % dummy variable to calculate the total height
for k=1:n,
   TH(1)=THD+dZ(k,1);
   THD=TH(1);
end;


%%% Initial height of layers 1 to k (to be used in pressure correction) %%%

for k=1:n+1,
   HKX=0; % dummy variable to calculate height of layers 1 to k at t=1
   for j=2:k,
      HK(k,1)=HKX+dZ(j-1,1);
      HKX=HK(k,1);
   end;
end;


%%% Initial values of Se, h, and Kw %%%

Kws=1.4*(10^12)*K_i; % saturrated hydralic conductivity (m/day)
Kgs=8.0*(10^9)*K_i; % 3.5*(10^10)*K_i; % saturated gas conductivity (m/d)

for k=1:n+1,
   Se(k)=(mc(k,1)-mc_r)/(mc_s(k,1)-mc_r); % effective saturation
```

```
   h(k,1)=-(1/a_VG)*(((Se(k))^(-1/m_VG))-1)^(1/n_VG); % matric potential

   %%% Unsaturated hydraulic conductivity %%%
   Kw(k,1)=Kws*((Se(k))^p_VG)*(1-(1-(Se(k)^(1/m_VG)))^m_VG)^2;

   %%% Unsaturated gAS conductivity %%%
   Kg(k,1)=Kgs*((1-Se(k))^p_VG)*(1-(1-((1-Se(k))^(1/m_VG)))^m_VG)^2;
end;


%%% Initial value of total moisture %%%

hT(1)=0;
QT(1)=0;

TWD1=0; %  dummy variable to calculate initial total moisture
for k=1:n,
   TW(1)=TWD1+dZw(k,1);
   TWD1=TW(1);
end;


%%% COMPUTATIONS %%%%%%%%%%%%%%%%%%%%%%%%%%%%%

TSTS=round(TT/dt); % total number of simulation time steps
for t=1:TSTS


   %% Rates of infiltration and removal of leachate %%%

   if (t*dt)<TI & TW(t) < maxm*(sum(mc_s(1:n+1,t))/(n+1))*(TH(t))
      hT(t+1)=(t*dt/TI)*hT_m; % (m)
   else if rem(t*dt,TF)==0 & TW(t) < maxm*(sum(mc_s(1:n+1,t))/(n+1))*(TH(t))
         hT(t+1)=hT_m; % (m)
      else
         hT(t+1)=hT_f; % (m)
      end;
   end;

   if TW(t) < maxm*(sum(mc_s(1:n+1,t))/(n+1))*(TH(t))
      QB(t+1)=0.0; % volume of leachate removed (m3/m2)
   else
      QB(t+1)=TW(t)-maxm*(sum(mc_s(1:n+1,t))/(n+1))*(TH(t)); % (m3/m2)
   end;
```

```
%%% Correction for the moisture content (multiplier) %%%

for k=1:n+1,
  if t==1
    C_M(k,t)=1;
  else if k==1
      C_M(k,t)=(dZ(k,t-1))/(dZ(k,t));
    else if  k==n+1
        C_M(k,t)=1;
      else
        C_M(k,t)=(dZ(k,t-1)+dZ(k-1,t-1))/(dZ(k,t)+dZ(k-1,t));
      end;
    end;
  end;
end;


%%% Calculation of moisture montent %%%

for k=2:n,
  if k==n,
    mc(k,t+1)=min(mc(k,t)*C_M(k,t)+...
        (dt*(Kw(k,t)+Kw(k-1,t))/(dZ(k-1,t)*(dZ(k-1,t)+dZ(k,t))))*h(k-1)-...
        (dt*(Kw(k,t)+Kw(k-1,t))/(dZ(k-1,t)*(dZ(k-1,t)+dZ(k,t))))*h(k)-...
        (dt*(Kw(k,t)+Kw(k+1,t))/(dZ(k,t)*(dZ(k-1,t)+dZ(k,t))))*h(k)+...
        (dt*(Kw(k,t)+Kw(k+1,t))/(dZ(k,t)*(dZ(k-1,t)+dZ(k,t))))*hT(t)+...
        (dt*(Kw(k+1,t)-Kw(k-1,t))/(dZ(k-1,t)+dZ(k,t))), maxm*mc_s(k,t));

  else if k==2,
      mc(k,t+1)=min(mc(k,t)*C_M(k,t)+...
        (dt*(Kw(k,t)+Kw(k-1,t))/(dZ(k-1,t)*(dZ(k-1,t)+dZ(k,t))))*h(k+1)-...
        (dt*(Kw(k,t)+Kw(k-1,t))/(dZ(k-1,t)*(dZ(k-1,t)+dZ(k,t))))*h(k)-...
        (dt*(Kw(k,t)+Kw(k+1,t))/(dZ(k,t)*(dZ(k-1,t)+dZ(k,t))))*h(k)+...
        (dt*(Kw(k,t)+Kw(k+1,t))/(dZ(k,t)*(dZ(k-1,t)+dZ(k,t))))*h(k+1)+...
        (dt*(Kw(k+1,t)-Kw(k-1,t))/(dZ(k-1,t)+dZ(k,t)))-QB(t), maxm*mc_s(k,t));

    else
      mc(k,t+1)=min(mc(k,t)*C_M(k,t)+...
        (dt*(Kw(k,t)+Kw(k-1,t))/(dZ(k-1,t)*(dZ(k-1,t)+dZ(k,t))))*h(k-1)-...
        (dt*(Kw(k,t)+Kw(k-1,t))/(dZ(k-1,t)*(dZ(k-1,t)+dZ(k,t))))*h(k)-...
        (dt*(Kw(k,t)+Kw(k+1,t))/(dZ(k,t)*(dZ(k-1,t)+dZ(k,t))))*h(k)+...
        (dt*(Kw(k,t)+Kw(k+1,t))/(dZ(k,t)*(dZ(k-1,t)+dZ(k,t))))*h(k+1)+...
        (dt*(Kw(k+1,t)-Kw(k-1,t))/(dZ(k-1,t)+dZ(k,t))), maxm*mc_s(k,t));

    end;
  end;
```

```
end;

mc(1,t+1)=mc(2,t+1); % assumed moisture content @ the bottom
mc(n+1,t+1)=mc(n,t+1); % assumed moisture contnet @ the top surface

%   mc(1:n+1,t+1)=mc(1:n+1,t); % used when program runs with constant moisture


%% Calculation of gas pressure - Formation of the of matrix P  %%%

P=eye(n-1,n-1); %  matrix to calculate coefficients of pressure terms

for j=1:n-1,
  for i=1:n-1,

    if t==1 & i==j % (initial)
      P(i,j)=(1+(log(dZg(i+1,t)/dZg(i+1,t)))+...
        dt*(dZ(i+1,t)/dZg(i+1,t))*2*D/(dZ(i,t)*dZ(i+1,t))); % main diagonal (B)
    else if t==1 & i==j & rem(i, n_l)==0 % (initial, gas extraction points)
        P(i,j)=0; % % elements in the main diagonal (B)
      else if t>1 & i==j % (t>1)
          P(i,j)=(1+(log(dZg(i+1,t)/dZg(i+1,t-1)))+...
            dt*(dZ(i+1,t)/dZg(i+1,t))*2*D/(dZ(i,t)*dZ(i+1,t))); % main dia. (B)
        else if t>1 & i==j & i==n/2+1 % (t>1, gas extraction points)
            P(i,j)=0; % elements in the main diagonal (B)
          else if t>=1 & i==j-1 & rem(i, n_l)==0 % (gas extraction points)
              P(i,j)=0; % elements in the upper diagonal (C)
            else if t>=1 & i==j-1 % (other points)
                P(i,j)=-dt*(dZ(i+1,t)/dZg(i+1,t))*...
                  Kg(i+1,t)/(dZ(i,t)+dZ(i+1,t))+...
                  2*D/((dZ(i,t)+dZ(i+1,t))*dZ(i+1,t))); % upper dia. (C)
              else if t>=1 & i==j+1 & rem(i, n_l)==0 % (gas extraction points)
                  P(i,j)=0; % elements in the lower diagonal (A)
                else if t>=1 & i==j+1 % (other points)
                    P(i,j)=dt*(dZ(i+1,t)/dZg(i+1,t))*...
                      Kg(i+1,t)/(dZ(i,t)+dZ(i+1,t))-...
                      2*D/((dZ(i,t)+dZ(i+1,t))*dZ(i,t)));
                      % lower diagonal (A)
                  else
                    P(i,j)=0;
                  end
                end
              end
            end
          end
        end
      end
```

```
        end
      end
    end % end of i
  end %end of j

  %%% Correction for pressure (has to be added) %%%

  for k=1:n+1,
    if t<=2
      C_P(k,t)=0;
    else if rem(k-1, n_l)==0 % (gas extraction points)
        C_P(k,t)=0;
      else
        C_P(k,t)=(Pr(k-1,t)-Pr(k,t))*(HK(k,t-1)-HK(k,t))/...
          (dZ(k-1,t)-(HK(k,t-1)-HK(k,t)));
      end;
    end;
  end;


%%% Calculation of gas pressure - Construction of the column matrix D  %%%

  DG=zeros(n-1,1); % column matrix D to accomodate constants from each eqn.

  for i=1:n-1,
    if t==1 % modified to avoid complexities from the last term
      DG(i)=(Pr(i+1,t)+C_P(i+1,t))+dt*(dZ(i+1,t)/dZg(i+1,t))*R*T*G(i+1,t)-...
        (Pr_a*1000)*log(dZg(i+1,t)/dZg(i+1,t));
    else % other nodes, pressure from the preveous time step is corrected
      DG(i)=(Pr(i+1,t)+C_P(i+1,t))+dt*(dZ(i+1,t)/dZg(i+1,t))*R*T*G(i+1,t)-...
        (Pr_a*1000)*log(dZg(i+1,t)/dZg(i+1,t-1));
    end
  end

  Pr_c=inv(P)*DG; % Pr_c is the calculated pressure terms at time t+1

  Pr(2:n,t+1)=Pr_c/1000; % assigning pressure to the middle nodes



  %%% pressure at the  gas extraction points %%%

  for k=1:n+1
    if rem(k-1, n_l)==0
      Pr(k,t+1)=Pr(k,t); % pressure at the upper boundary
    end
```

```
    end

%   Pr(1:n+1,t+1)=Pr_i/1000; % used when the program runs with atm. pressure


    %% Calculation of rate of generation of landfill gas %%%

    C0=0.86*L0/(fs2+fs3+fs4); % proportionality constant

    for k=1:n+1,
      if t*dt<=T0 & k==1 % linear increase in rate till t=T0 @ bottom
        G(k,t+1)=C0*((t*dt)/T0)*((1/dZ(k,t))*(DenC*dZ_i)*((fs1*lambda1)*exp(-
lambda1*T0)+...
          (fs2*lambda2)*exp(-lambda2*T0)+(fs3*lambda3)*exp(-lambda3*T0)+...
          (fs4*lambda4)*exp(-lambda4*T0)));
      else if t*dt<=T0 & k==n+1 % linear increase in rate till t=T0 @ top
          G(k,t+1)=C0*((t*dt)/T0)*((1/dZ(k-1,t))*(DenC*dZ_i)*...
            ((fs1*lambda1)*exp(-lambda1*T0)+(fs2*lambda2)*exp(-lambda2*T0)+...
            (fs3*lambda3)*exp(-lambda3*T0)+(fs4*lambda4)*exp(-lambda4*T0)));
        else if t*dt<=T0 % linear increase in rate till t=T0 @ other nodes
            G(k,t+1)=C0*((t*dt)/T0)*(0.5*(1/dZ(k,t)+1/dZ(k-1,t))*(DenC*dZ_i)*...
              ((fs1*lambda1)*exp(-lambda1*T0)+(fs2*lambda2)*exp(-lambda2*T0)+...
              (fs3*lambda3)*exp(-lambda3*T0)+(fs4*lambda4)*exp(-lambda4*T0)));
          else if k==1, % negative exponential rate after t=T0 @ bottom
              G(k,t+1)=C0*(1/dZ(k,t))*(DenC*dZ_i)*...
                ((fs1*lambda1)*exp(-lambda1*(t-T0)*dt)+...
                (fs2*lambda2)*exp(-lambda2*(t-T0)*dt)+...
                (fs3*lambda3)*exp(-lambda3*(t-T0)*dt)+...
                (fs4*lambda4)*exp(-lambda4*(t-T0)*dt));
            else if k==n+1 % negative exponential rate after t=T0 @ top
                G(k,t+1)=C0*(1/dZ(k-1,t))*(DenC*dZ_i)*...
                  ((fs1*lambda1)*exp(-lambda1*(t-T0)*dt)+...
                  (fs2*lambda2)*exp(-lambda2*(t-T0)*dt)+...
                  (fs3*lambda3)*exp(-lambda3*(t-T0)*dt)+...
                  (fs4*lambda4)*exp(-lambda4*(t-T0)*dt));
              else % negative exponential rate after t=T0 @ other nodes
                G(k,t+1)=C0*0.5*(1/dZ(k,t)+1/dZ(k-1,t))*(DenC*dZ_i)*...
                  ((fs1*lambda1)*exp(-lambda1*(t-T0)*dt)+...
                  (fs2*lambda2)*exp(-lambda2*(t-T0)*dt)+...
                  (fs3*lambda3)*exp(-lambda3*(t-T0)*dt)+...
                  (fs4*lambda4)*exp(-lambda4*(t-T0)*dt));
              end
            end
          end
        end
      end
```

```
end;


%%% Calculation of stresses and thicknesses & porosity %%

for k=1:n,
   Mass(k,t+1)=(DenC*dZ_i)*(fs1*exp(-lambda1*(t)*dt)+...
      fs2*exp(-lambda2*(t)*dt)+fs3*exp(-lambda3*(t)*dt)+...
      fs4*exp(-lambda4*(t)*dt))+DenW*0.5*(mc(k,t)+mc(k+1,t))*dZ(k,t);
   dZs(k,t+1)=(DenC*dZ_i/DenW)*((fs1/Gs1)*exp(-lambda1*(t)*dt)+...
      (fs2/Gs2)*exp(-lambda2*(t)*dt)+(fs3/Gs3)*exp(-lambda3*(t)*dt)+...
      (fs4/Gs4)*exp(-lambda4*(t)*dt));
end;
for k=1:n+1,
   SigY=DenS*dZ_s*9.81/1000; % load from the final cover
   for i=k:n,
      SigmaT(k,t+1)=SigY+Mass(i,t+1)*9.81/1000; % uncorrected
      SigY=SigmaT(k,t+1);
   end
   SigmaT(n+1,t+1)=DenS*dZ_s*9.81/1000; % stress at the top surfce
   SigmaE(k,t+1)=SigmaT(k,t+1)-Pr(k,t); % pressure correction added
end;

if (t*dt)<=200
   Cc=Cc1;
   Cs=Cs1;
else if (t*dt)>200 & (t*dt)<=2000;
      Cc=Cc2;
      Cs=Cs2;
   else if (t*dt)>2000 & (t*dt)<=20000;
         Cc=Cc3;
         Cs=Cs3;
      else
         Cc=Cc4;
         Cs=Cs4;
      end
   end
end

for k=1:n,

   if  t*dt<=2*T0
      dZ(k,t+1)=dZ(k,t)-(dZs(k,t)-dZs(k,t+1));
   else if t*dt>2*T0 & SigmaE(k,t+1)>=SigmaE(k,t)
         dZ(k,t+1)=dZ(k,t)-(dZs(k,t)-dZs(k,t+1))-...
            dZ_i*(Cc)*log10(SigmaE(k,t+1)/SigmaE(k,t));
```

```
      else
        dZ(k,t+1)=dZ(k,t)-(dZs(k,t)-dZs(k,t+1))-...
          dZ_i*(Cs)*log10(SigmaE(k,t+1)/SigmaE(k,t));
      end
    end
    dZw(k,t+1)=0.5*(mc(k,t+1)+mc(k+1,t+1))*dZ(k,t+1);
    dZg(k,t+1)=dZ(k,t+1)-dZs(k,t+1)-dZw(k,t+1);
    mc_s(k,t+1)=1-dZs(k,t+1)/dZ(k,t+1); % sat.moisture content (=porosity)
end
mc_s(n+1,t+1)=mc_s(n,t+1); % sat. urated moisture content @ top surface


%%% Calculation of Total Height %%%

THD=0; % dummy variable to calculate the total height
for k=1:n,
    TH(t+1)=THD+dZ(k,t+1);
    THD=TH(t+1);
end;

%%% Initial height of layers 1 to k (to be used in pressure correction) %%%

for k=1:n+1,
    HKY=0; % dummy variable to calculate height of layers 1 to k, at time=t+1
    for j=2:k,
      HK(k,t+1)=HKY+dZ(j-1,t+1);
      HKY=HK(k,t+1);
    end;
end;


%%% Calculation of Se, h, and Kw %%%

for k=1:n+1,
    Se(k)=(mc(k,t+1)-mc_r)/(mc_s(k,t+1)-mc_r); % effective saturation
    h(k,t+1)=-(1/a_VG)*(((Se(k))^(-1/m_VG))-1)^(1/n_VG); % matric potential

    %%% Unsaturated hydraulic conductivity %%%
    Kw(k,t+1)=Kws*((Se(k))^p_VG)*(1-(1-(Se(k)^(1/m_VG)))^m_VG)^2;

    %%% Unsaturated gas conductivity %%%
    Kg(k,t+1)=Kgs*((1-Se(k))^p_VG)*(1-(1-((1-Se(k))^(1/m_VG)))^m_VG)^2;
end;


%%% Calculation of total moisture %%%
```

```
   TWD2=0; % dummy variable to calculate total moisture
   for k=1:n,
      TW(t+1)=TWD2+dZw(k,t+1);
      TWD2=TW(t+1);
   end;


end % end of time loop

% plot(Pr);
% plot(mc);
% plot(mc_s);
% plot(Kw);
% plot(Kg);
% plot(SigmaT);
% plot(SigmaE);
plot(TH);
```

REFERENCES

1. Arigla, S. G, Tsotsis, T. T, Webster, I. A, Yortss, Y. C., and Kattapuram, J. J. (1995). "Gas Generation, Transport, and Extraction in Landfills." *Journal of Environmental Engineering*, 121(01), 33-44.

2. ASTM (2002). "Annual Book of ASTM Standards." West Conshohocken, PA.

3. Benson, C. H., and Wang, X. (1998). "Soil Water Characteristic Curves for Solid Waste." *Environment Geotechnics - Report 98-13*, Environment Geotechnics Program, Department of Civil and Environmental Engineering, University of Wisconsin-Madison. http://www.uwgeotech.org/Old%20Website%20Files/pubs/gr_benson_soil.pdf (October 2004).

4. Bjarngard, A., and Edgers, L. (1990). "Settlements of Municipal Solid Waste Landfills." *Proceedings of the Thirteenth Annual Madison Waste Conference*, Madison,WI.

5. Bleiker, D. E., Farquhar, G., and McBean, E. (1995). "Landfill Settlement and the Impact on Site Capacity and Refuse Hydraulic Conductivity." *Waste Management and Research*, 13, 533-554.

6. Bleiker, D. E., McBean, E. and Farquhar, G. (1993). "Refuse Sampling and Permeability Testing at the Brock West and Keele Valley Landfills." *Proceedings of the Sixteenth International Madision Waste Conference*, Department of Engineering Professional Development, University of Wisconsin-Madison, 548-567.

7. Chunmiao, Z., and Gordon, B. D. (1995). Applied Contaminant Transport Modeling-Theory and Practice, Van Nostrand Reinhold, New York.

8. Chynoweth, D. P., and Pullammanappallil, P. (1996). Anaerobic digestion of Municipal Solid Wastes in Microbiology of Solid Waste (Eds. Palmisano, A. C. and Barlaz, M. A.), CRC Press, 71–114.

9. Edgers, L., Noble J. J., and Williams, E. (1992). "A Biological Model for Long Term Settlement in Landfills," *Environmental Geotechnology*, Useman & Acer (eds), Balkema, Rotterdam, 177-184.

10. Edil, T. B., Ranguette, V. J., and Wuellner, W. W. (1990). "Settlement of Municipal Refuse." *Geotechniques of Waste Fills – Theory and Practice: ASTM STP 1070*, Philadelphia, 225-239.

11. El-Fadel, M., and Al-Rashed, H. (1998a). "Settlement in Municipal Solid Waste Landfills I: Field Scale Experiments." *Journal of Solid Waste Technology and Management*, 25 (2), 89-98.

12. El-Fadel, M., and Al-Rashed, H. (1998b). "Settlement in Municipal Solid Waste Landfills II. Mathematical Modeling." *Journal of Solid Waste Technology and Management*, 25 (2), 99-104.

13. El-Fadel, M., Findikakis, A., and Leckie, J. (1989). "A Numerical Model for Methane Production in Managed Sanitary Landfill." *Waste Management and Research*, 31-42.

14. El-Fadel, M., and Khoury, R. (2000). "Modeling Settlement in MSW Landfills: A Critical Review." *Critical Reviews in Environmental Science & Technology*, 30 (3), 327-361.

15. Farquhar, G. J, and Rovers, F. A. (1973). "Gas Production during Refuse Decomposition." *Water Air and Soil Pollution*, 483-495.

16. Findikakis, A. N., and Leckie, J. O. (1979). "Numerical Simulation of Gas Flow in Sanitary Landfills." *Journal of Environmental Engineering Division*, ASCE, 105(EE5), 927-945.

17. Findikakis, A. N., Papelis, C., Halvadakis, C. P., and Leckie, J. O. (1988). "Modeling Gas Production in Managed Sanitary Landfills." *Waste Management and Research*, 6, 115-123.

18. Florida Department of Environmental Protection (1999). Solid Waste Management Annual Report. http://www.dep.state.fl.us/waste/categories/recycling/pages/99.htm (April 2005).

19. Gabr, M. A., Hossain, M. S., and Barlaz, M. A. (2000). "Solid Waste Settlement in Landfills with Leachate Recirculation." *Geotechnical news*, 28(2), 50-55.

20. Ham, R. K., and Barlaz, M. A. (1987). "Measurement and Prediction of Landfill Gas Quality and Quantity." ISWA International Symposium on Process, Technology, and Environmental Impact of Sanitary Landfill, Cagliari, Sardinia, Italy.

21. Hashimoto, S., and Suzuki, M. (2002). "Vertical Distributions of Carbon Dioxide Diffusion Coefficients and Production Rates in Forest Soils." *Soil Science Society of America Journal* 66, 1151-1158.

22. Hettiarachchi, C. H., Meegoda, J. N., and Hettiaratchi, J. P. A. (2003). "Settlement of Bioreactor Landfills," *Modeling of Settlement Behavior of Bioreactor Landfills: Interim Report*. Department of Civil Engineering, University of Calgary, Alberta, Canada.

23. Hettiarachchi, C. H., Meegoda, J. N., and Hettiaratchi, J.P.A. (2005). "Towards a Fundamental Model to Predict the Settlements in Bioreactor Landfills," *GeoFrontiers Conference (ASCE, Geotechnical Special Publication No. 142)*, Austin, TX.

24. Hettiarachchi, V. C. (2005). Gas, Heat, and Moisture Transport in Methonobifilters. PhD Dissertation, University of Calgary, Canada.

25. Hoffman, J. D. (2001). Numerical Methods for Engineers and Scientists. 2nd edition. Marcel Dekker, Inc., New York, NY.

26. Hossain, M. S., and Gabr, M. A. (2005). "Prediction of Municipal Solid Waste Landfill Settlement with Leachate Recirculation," *GeoFrontiers Conference (ASCE, Geotechnical Special Publication No. 142)*, Austin, TX.

27. Hossain, M. S., Gabr, M. A., and Barlaz, M. A (2003). "Relationship of Compressibility Parameters to Municipal Old Waste Decomposition." *Journal of Geotechnical and Geoenvironmental Engineering*, 129(12), 1151-1158.

28. Jin, Y., and Jury, W. A. (1996). "Characterizing the Dependency of Gas Diffusion Coefficient on Soil Properties." Soil Science Society of America Journal, Vol. 60, 66–71.

29. Kang, S. T., Shin, H. S., Lee, C. Y., and Lee, N. H. (1997). "Relationship between Biological Decomposition and Landfill Settlement at Various Leachate Recirculation Rates." *Proceedings of the 7th KAIST-NTU-KU Tri-Lateral Seminar/Workshop on Environmental Engineering*, Kyoto, Japan, 29-31.

30. Kumar, S. (2000). "Settlement Prediction for Municipal Solid Waste Landfills Using Power Creep Law," *Soil and Sediment Contamination*, 9(6), 579-592.

31. Ling, H. I., Leshchinsky, D., Mohri, Y., and Kawabata, T. (1998). "Estimation of Municipal Solid Waste Landfill Settlement." *Journal of Geotechnical and Geoenvironmental Engineering*, 124(1), 21-28.

32. LMNO Engineering (2003). Gas Viscosity Calculator. http://www.lmnoeng.com/Flow/GasViscosity.htm (April 2005).

33. McBean, E. A., Rovers, F. A., and Farquhar, G. J. (1995). Solid Waste Landfill Engineering and Design. Prentice Hall, Upper Saddle River, NJ, 83-104.

34. Morris, D. V., and Woods, C. E. (1990). "Settlement and Engineering Considerations in Landfill and Final Cover Design." *Geotechniques of Waste Fills – Theory and Practice: ASTM STP 1070*, Philadelphia, PA, 9-21.

35. Nastav, M., Therrien, R., Lefebvre, R., Gelinas, P. (2001). "Gas Production and Migration in Landfills and Geological Materials." *Journal of Contaminant Hydrology*, 52, 187-211.

36. Oweis, I. S., and Khera, R. P. (1986). "Criteria for Geotechnical Construction on Sanitary Landfills." *Proceedings of the Conference of Environmental Geotechnology*, Allentown, PA, 1, 205-223.

37. Oweis, I. S., and Khera, R. P. (1998). Geotechnology of Waste Management. PWS, Boston, MA.

38. Park, H. I., Lee, R. S. (1997). "Long-term Settlement Behavior of Landfills with Refuse Decomposition." *Journal of Solid Waste Technology and Management*, 24 (4), 159-165.

39. Park, H. I., Lee, R. S., and Do, N. Y. (2002). "Evaluation of Decomposition Effect on Long-term Settlement Prediction for Municipal Solid Waste Landfills." *Journal of Geotechnical and Geoenvironmental Engineering*, 128(2), 107-118.

40. Qian, X., Koerner, R. M., Gray, D. H. (2002). "Geotechnical Aspects of Landfill Design and Construction." Prentice Hall, Upper Saddle River, NJ.

41. Rao, S. K., Moulton, L. K., and Seals, R. K., (1977). "Settlement of Refuse Settlements." *Proceedings of the Conference on Geotechnical Practice for Disposal of Solids Waste Materials*, ASCE, 574-598.

42. Reinhart, D. R., Chopra, M. B., and Townsend, T. (2002). Design And Operational Issues Related to the Co-disposal of Sludges and Biosolids in Class I Landfills – Quarterly progress report, University of Central Florida, Orlando, FL.

43. Reinhart, D. R., and Townsend, T. G. (1998). Landfill Bioreactor Design and Operation. Lewis Publishers, New York, NY.

44. Scanlon, B. R., Nicot, J. P., and Massman, J. W. (2002). "Soil Gas Movement in Unsaturated Systems." CRC Press, <http://www.beg.utexas.edu/environqlty/vadose/pdfs/webbio_pdfs/soilphysics companion2002.pdf (October 2004).

45. Schroeder, P. R., Gibson, A. C., and Smolen, M. D. (1984). "The Hydrologic Evaluation of Landfill Performance Model, Volume II," *Documentation for Version II*, USEPA.

46. Sheurs, R. E., and Khera, R. P. (1980). "Stabilization of a Sanitary Landfill to Support a Highway," *Emulsion, Mix Design, Stabilization and Compaction – Transportation Research Record 754*, National Academy of Sciences, Washington, DC.

47. Sowers, G. F. (1973). "Settlement of Waste Disposal Fills." *Proceedings of the 8th International Conference on Soil Mechanics and Foundation Engineering*, Moscow, USSR, Vol. 2, Pt.2, 207-210.

48. Steefel, C. I., and MacQuarie, K. T. B., (1996). "Approaches to Modeling of Reactive Transport in Porous Media." *Reactive Transport in Porous Media - Reviews in Mineralogy*, Lichtner P. C., Steefel C. I., and Oelkers E. H. (ed)., Vol. 34, The Mineralogical Society of America, Washington, DC.

49. Sullivan, P. (2003). "Landfill Gas Aspects of Bioreactor Landfills," *Presentation at Association of State and Territorial Solid Waste Management Officials (ASTSWMO) Annual State Solid Waste Managers' Conference*, Salt Lake City, UT.

50. USEPA (1997), "Characterization of Municipal Solid Waste in United States." http://www.epa.gov/epaoswer/non-hw/muncpl/msw99.htm (October 2004).

51. USEPA (1998), User's Manual Landfill Gas Emissions: Model Version 2.0, *EPA/6000/R/-98/054*, Research Triangle Park, NC.

52. Van Genuchten, M. T. (1980). "A Closed Form Equation for Predicting the Hydraulic Conductivity of Unsaturated Soils." *Soil Science Society of America Journal*, 44, 892-898.

53. Wall, D. K., and Zeiss, C. (1995). "Municipal Landfill Biodegradation and Settlement." *Journal of Environmental Engineering*, 121 (3), 214-224.

54. Warrick, A.W. (2003). Moisture Dynamics. Oxford University Press.

55. Wilshusen, J. H., Hettiaratchi, J. P. A., De Visscher, A., and Saint-Fort, R. (2004). "Methane Oxidation and Formation of EPS in Compost: Effect of Oxygen Concentration." *Environmental Pollution,* 129, 305-314.

56. Yazdani, R. (2003). "Landfill Bioreactor Demonstration underway in Yolo County, CA." *Technology, News and Trends*, USEPA Newsletter, 5, 1-2.

57. Yen, B. C., and Scanlon, B., (1975). "Sanitary Landfill Settlement Rates." *Journal of Geoechnical Engineering Division*, ASCE, 101(5), 45-487.

58. Young, A. (1989). "Mathematical Modeling of Landfill Gas Extraction." *Journal of Environmental Engineering, ASCE*, 115(6), 1073-1087.

59. Zornberg, J. G., Jernigan, B. L., Sanglerat, T. R., and Cooley, B. H. (1999). "Retention of Free Liquids in Landfills Undergoing Vertical Expansion." *Journal of Geotechnical and Geoenvironmental Engineering*, 125, 583-594.